Dissertation

submitted to the

Combined Faculties for the Natural Sciences and Mathematics

of the Ruperto-Carola University of Heidelberg, Germany

for the degree of

Doctor of Natural Sciences

Put forward by

Kher Sham Lim

born in: Pulau Pinang, Malaysia

Oral examination: 5th November 2014

This page is intentionally left blank

New Aspects Of

Scale And Discrete Flavor

Symmetry Breaking

This page is intentionally left blank

Abstract

The Standard Model (SM) of particle physics is complete with the discovery of the Higgs particle. However the SM cannot be a complete theory of nature as it does not explain the origin of neutrino mass, dark matter (DM), dark energy, matter-antimatter asymmetry and smallness of the strong CP parameter. From theoretical point of view we do not understand the origin of the scale separation between the electroweak (EW) and the Planck scale, and also the flavor puzzle. In this work we will tackle the hierarchy problem with scale symmetry and the flavor puzzle with discrete flavor symmetries, charting new symmetry groups and their breaking, while investigating their implied phenomenologies along the way. In the first part we provide two novel mechanisms to explain the origin of the EW scale generated by quantum effects from an anomalous breaking of a classical scale invariant extension of the SM. For the first model we utilize a direct scale transmission from condensation of a scalar, charged under a high representation of QCD, to trigger EW symmetry breaking (EWSB) dynamically. In the second model, we will use the indirect scale transmission approach to generate the EW scale transmitted by a singlet scalar mediator which couples to the SM and a strongly coupled hidden sector. Chiral symmetry in the dark fermion sector is broken spontaneously due to nonperturbative effects of the running coupling in the hidden sector, triggering indirectly EWSB due to dimensional transmutation and providing stable DM candidates in the form of dark pions. In the last part of this work we focus on charting new discrete flavor symmetry groups to obtain experimentally acceptable leptonic and quark mixing patterns. The interesting new discrete groups that we have found are classified mathematically and provide a new starting point for model building in discrete flavor symmetry.

Zusammenfassung

Das Standardmodell (SM) der Elementarteilchenphysik ist komplett mit der Entdeckung des Higgs-Teilchens. Wir wissen aber dass das SM nicht die endgültige Theorie der Natur sein kann; das SM enthält keine Dunkle Materie oder Dunkle Energie, und hat keine Erklärung für Neutrinomassen und die Asymmetrie zwischen Teilchen und Antiteilchen. Von theoretichen Seite, unbefriedigend ist die große Skalenhierarchie zwischen elektroschwache und Planck-Skala, sowie die Herkunft der Flavorparameter im SM. In dieser Arbeit versuchen wir die genannten Probleme mit Hilfe von Symmetrien zu lösen. Im ersten Teil unserer Arbeit geht es um die Erweiterung des SM mit klassicher Skaleninvarianz, und wie die elektroschwache Skala quantenmechanisch durch die anomalen Brechung der klassichen Skaleninvarianz erzeugt wird. Solche Skalenerzeugung lässt sich in zwei Klassen einteilen, entweder durch direkte oder indirekte Skalenübertragung. Bei der direkten Skalenübertragung erweitern wir QCD mit einem Skalar-Teilchen, das ein Kondensat bei der TeV-Skala bildet und elektroschwache Symmetriebrechung verursacht. In einem Modell mit indirekter Skalenübertragung wird die elektroschwache Symmetriebrechung dagegen durch die chirale Symmetriebrechung in einem verborgenen Sektor erzeugt. Ein Stabiler Dunkle Materie-Kandidat ergibt sich durch die Pseudo-Nambu-Goldstone-Bosonen von chiralen Symmetriebrechung. Als letztes konzentrieren wir uns auf das Flavorproblem, und suchen systematisch nach neuen diskreten Symmetriegruppen, welche die experimentell bevorzugten Mischungswinkeln für Leptonen und Quarks vorhersagen können.

This page is intentionally left blank

Contents

Finis Coronat Opus

This page is intentionally left blank

Introduction and Roadmap

The Standard Model (SM) of particle physics, which consists of the Glashow-Weinberg-Salam theory of Electroweak (EW) interactions [1, 2] and Quantum Chromodynamics (QCD) [3–5], has served as a successful low energy description of the subatomic physics for the last forty years. With the Higgs-like particle being found in the ATLAS [6] and CMS [7] detectors, the SM itself is now complete. However we know that the SM is not the full description of our Universe. The neutrinos, for instance, are massless in the SM and hence further extension is required to accommodate the well measured neutrino mass differences in the neutrino oscillation experiments. Furthermore, the SM does not contain candidates to explain the dark matter (DM) and the dark energy, which make up 95% of the energy content of our Universe. Other problems such as the origin of the matter-antimatter asymmetry, the strong CP problem, and the origin of inflation, also require solutions beyond the SM if we demand that the solution is not fine-tuned but *natural*.

From the theoretical point of view, the SM parameters also contain some tantalizing puzzles, which crave for simpler explanations. Aside from experimental observations which deviate from the SM prediction, the theoretical problem of the SM in general can be divided into two aspects: scales separation and flavor puzzles. To provide explanations for these two puzzles under the banner of symmetry is the main focus of this thesis[1]. Let us start by discussing the aspect of scales in fundamental physics. At the moment we only know three fundamental energy scales in the nature, namely

- the QCD scale $\Lambda_{\mathrm{QCD}} \approx 300\,\mathrm{MeV}$, where the QCD physics becomes strong and non-perturbative,

- the EW scale $v = 246\,\mathrm{GeV}$, which generates masses for elementary particles,

- the Planck scale $M_{pl} \approx 10^{19}\,\mathrm{GeV}$, where gravity becomes strong.

Arranging in their strength, one notices that

$$\Lambda_{\mathrm{QCD}} \sim v \ll M_{pl}, \tag{1.1}$$

prompting the so-called *hierarchy problem* of energy scales. At the moment we are not sure whether the Planck scale is something fundamental, or if gravity is some emergent effect which is described by physics beyond Quantum Field Theory (QFT). The hierarchy

---

[1] And also to provide fine selections of red wine.

between the QCD and Planck scale can be understood as a dynamical phenomenon, where the smallness of Λ_{QCD},

$$\Lambda_{\text{QCD}} = M_{pl} \exp\left(-\frac{8\pi^2}{bg_s^2(M_{pl})}\right) \ll M_{pl}, \tag{1.2}$$

is due to the renormalization group effect, with the beta function coefficient b calculated for the QCD coupling g_s. Such an explanation does not apply to the case of the EW scale v. We will give a thorough explanation for the hierarchy problem regarding the EW scale later in Chapter 2. It suffices to say that there is no symmetry in the SM to protect the EW scale against the high energy scale QFT that the SM embedded into, unless a new symmetry is introduced either in the form of supersymmetry or scale invariance. In this thesis we will follow the latter approach, taking classical scale invariance as a new starting point to solve the hierarchy problem. In Chapter 2 we will give an introduction to classical scale invariance and its anomalous breaking, which will generate the EW scale quantum mechanically. We will see that we can generate the EW scale dynamically from this approach, mimicking the success of QCD. The additional fields charged under a non-abelian gauge group form condensates that can trigger EW symmetry breaking (EWSB) either directly or indirectly. We will present one model each for these two different approaches.

In Chapter 3 we will introduce a model based on *direct* scale transmission. An additional scalar field charged under a higher representation of QCD can condense at the TeV regime, generating the Higgs mass via dimensional transmutation. As this new particle is charged under QCD, it can be easily produced at the LHC. Furthermore this new scalar field can alter the production cross section of the SM Higgs, which can be detected or constrained by ATLAS and CMS. The collider phenomenology and the nonperturbative aspects of this new particle will be discussed in detail.

For the second approach based on *indirect* scale transmission, a model along this line will be discussed in Chapter 4. Here additional fermions charged under fundamental representation of a new non-abelian gauge group will be introduced. Similar to QCD, the fermions form condensates when the chiral symmetry is broken by the nonperturbative effect of gauge coupling flow. The chiral symmetry breaking scale is transmitted via a singlet scalar mediator to trigger EWSB indirectly. As an additional bonus, the pseudo Nambu-Goldstone bosons (PNGB) due to this spontaneous chiral symmetry breaking can serve as DM candidates. The DM phenomenology and the detection prospect of this model will be discussed. Furthermore, we will discuss some of the early universe physics of this new sector, particularly the order of the phase transition.

Hierarchy problem aside, the origin of flavor is also one of the important questions of beyond the SM physics. All absolute entries of the lepton mixing matrix, or the Pontecorvo-Maki-Nakagawa-Sakata (PMNS) matrix

$$|U_{\text{PMNS}}| \approx \begin{pmatrix} 0.821 & 0.549 & 0.152 \\ 0.374 & 0.573 & 0.694 \\ 0.382 & 0.567 & 0.684 \end{pmatrix}, \tag{1.3}$$

are of order one. Comparing this to the Cabibbo-Kobayashi-Maskawa (CKM) matrix

$$|U_{\text{CKM}}| \approx \begin{pmatrix} 0.974 & 0.225 & 0.004 \\ 0.225 & 0.973 & 0.041 \\ 0.009 & 0.040 & 0.999 \end{pmatrix} \tag{1.4}$$

of the quark sector whose off-diagonal entries are small [8], the very different form of the PMNS matrix seems to suggest a different leptonic flavor origin. One popular approach to solve the flavor puzzle is to invoke spontaneously broken discrete symmetries to describe the observed patterns, where the leading-order (LO) leptonic mixing angles up to permutations of rows and columns can be determined solely from flavor symmetry breaking. This approach is based on the misaligned remnant symmetries between the charged lepton and neutrino mass matrices. Since the recent discovery of the large reactor mixing angle θ_{13} [9–11], the beloved simplest discrete group A_4 [12–18] that has been utilized to build most of flavor models is strongly disfavored. In Chapter 5 we will perform a systematical scan of discrete symmetry groups up to order of 1536 to determine which discrete groups can generate LO leptonic mixing angles compatible with the experiments. We extend also the discrete group approach in the quark sector to search for groups that can predict the LO Cabibbo angle. The leptonic mixing patterns may have a common origin with the quark mixing angles. If both the quarks and leptonic mixing patterns originate from a common discrete group, they could serve as a new model building approach, which could be embedded in a Grand Unified Theory (GUT). We will also discuss the predictivity of discrete symmetry groups compared to the anarchy approach.

Standard Model and Symmetries

The modern concept of relativistic Quantum Field Theory (QFT) constructed from principle of quantum mechanics, relativistic invariance and cluster decomposition principle, contains three fundamental concepts, namely *dynamics*, *symmetries* and *scales*, which has described different physical systems successfully[1]. By dynamics we mean that QFT is based on field operators whose structure is a result of quantum mechanics, relativistic invariance and cluster decomposition principle. The dynamics of QFT give rise to the physical observable of the theory. Of course with only dynamics, one can construct more general classes of theories which are not as constrained. A QFT of our particular interest, namely the Standard Model (SM) of particle physics, possesses more structures of symmetries, consisting the Poincaré invariance and the internal gauge symmetry $SU(3)_c \times SU(2)_L \times U(1)_Y$. Furthermore, the SM requires the notion of spontaneous symmetry breaking of scalar field and the Higgs mechanism to generate the masses for the elementary fermions and electroweak (EW) gauge bosons. We will provide a quick review of the SM in Sec. 2.2. Perhaps the most characteristic feature of QFT is the applicability to physics of different scales. Physics is about describing laws of nature at a certain scale. The fact that we can describe low energy physics well without knowing much details about the high energy physics is due to the principle of *coarse graining*. Most of the low energy physics will decouple from the high energy modes, with the exception of the scalar mass. As we will discuss later, most of the solutions proposed to solve such a *hierarchy problem* in the SM involve certain types of new physics or energy scales near the TeV regime. In this chapter we will discuss a novel solution that might serve as a good candidate in solving the hierarchy problem, namely classical scale invariance. We will clarify the subtle difference between conformal symmetry and scale/dilatation symmetry, and also explain the form of such symmetries in the classical and quantum regime in more details. We will also highlight the conjectures and problems arise in conformal field theory. A general model building approach along this line of thought will be discussed and we will present two models with different approaches that yield different phenomenologies in Chapter 3 and 4. The current chapter provides an overview of the latest research on solving the hierarchy problem by breaking classical scale invariance anomalously. This chapter is based on the author's understanding of the conceptual issue in the hierarchy problem, scale invariance and attempts to cure the hierarchy problem starting from the principle of classical scale invariance.

---

[1]This classification is often ignored in the modern QFT literature. For a more conceptual approach towards QFT please refer to Ref. [19].

2.1. Symmetries and Conservation Laws

In this section we will give a precise and general way of deriving Noether's first theorem, which states that symmetries of a physical system imply conservation laws. We follow the notation of Refs. [19–21]. Consider a system with n general field variables Φ_a with $a = 1, \ldots, n$. The dynamics of the system is encoded in the action

$$S = \int_{\mathcal{U}} \mathrm{d}^4 x \, \mathcal{L}(x, \Phi, \partial_\mu \Phi), \tag{2.1}$$

with $\mathcal{L}$ being the Lagrangian and $\mathcal{U}$ is a domain bounded by spacelike surfaces Σ_1 and Σ_2 which extend to infinity. The local field variation $\delta\Phi_a$ and total field variation $\Delta\Phi_a$ are defined as

$$\delta\Phi_a = \Phi'_a(x) - \Phi_a(x), \qquad \Delta\Phi_a = \Phi'_a(x') - \Phi_a(x) = \delta\Phi_a + \Delta x^\mu \partial_\mu \Phi_a, \tag{2.2}$$

where the infinitesimal change of coordinates is given by

$$x'^\mu = x^\mu + \Delta x^\mu. \tag{2.3}$$

We differentiate the two cases in Eq. (2.2) because certain symmetry transformations act on coordinate and field representation simultaneously. If we assume that $\mathcal{L}$ is unchanged by the variations in Eq. (2.2) and Eq. (2.3), i.e.

$$\mathcal{L}'(x', \Phi', \partial'_\mu \Phi') = \mathcal{L}(x', \Phi', \partial_\mu \Phi'), \tag{2.4}$$

with $\partial'_\mu = (\partial x / \partial x')_\mu{}^\nu \partial_\nu = \partial_\mu + \mathcal{O}(\partial_\nu \Delta x^\nu \partial_\mu)$, the total variation of the Lagrangian is given by

$$\Delta\mathcal{L} = \mathcal{L}'(x', \Phi', \partial_\mu \Phi') - \mathcal{L}(x, \Phi, \partial_\mu \Phi) = (\partial_\mu \mathcal{L})\Delta x^\mu + \partial_\mu(\pi_a^\mu \delta\Phi_a) + \mathcal{E}_a \delta\Phi_a, \tag{2.5}$$

with $\pi_a^\mu = \partial\mathcal{L}/\partial(\partial_\mu \Phi_a)$ as the momentum conjugate to Φ_a and $\mathcal{E}_a = \partial\mathcal{L}/\partial\Phi_a - \partial_\mu \pi_a^\mu$ the Eulerian for field Φ_a. Now let us investigate the total variation of the action

$$\Delta S = \int_{\mathcal{U}'} \mathrm{d}^4 x' \, \mathcal{L}'(x', \Phi', \partial'_\mu \Phi') - \int_{\mathcal{U}} \mathrm{d}^4 x \, \mathcal{L}(x, \Phi, \partial_\mu \Phi). \tag{2.6}$$

Changing the measure with $\mathrm{d}^4 x' = \det(\partial x'/\partial x)\mathrm{d}^4 x = (1 + \partial_\mu \Delta x^\mu)\mathrm{d}^4 x$ and substituting Eq. (2.5) in Eq. (2.6), we obtain

$$\Delta S = \int_{\mathcal{U}} \mathrm{d}^4 x \, [\partial_\mu(\mathcal{L}\Delta x^\mu + \pi_a^\mu \delta\Phi_a) + \mathcal{E}_a \delta\Phi_a] = Q(\Sigma_2) - Q(\Sigma_1) + \int_{\mathcal{U}} \mathrm{d}^4 x \, \mathcal{E}_a \delta\Phi_a, \tag{2.7}$$

where the Gauss theorem has been applied to the first term with Q given by

$$Q(\Sigma_i) = \int_{\Sigma_i} \mathrm{d}\sigma_\mu \left(\pi_a^\mu \Delta\Phi_a - \Theta^\mu{}_\nu \Delta x^\nu\right), \tag{2.8}$$

with the canonical energy momentum tensor $\Theta_{\mu\nu}$ and σ_μ representing the normal vector to the surface Σ.

Eq. (2.7) serves as a core equation for investigating the dynamics and conservation laws of a system. For instance if we demand that the total field variation vanishes at the boundary Σ_i and the action principle $\Delta S = 0$, the Euler-Lagrange equation $\mathcal{E}_a = 0$ for the field Φ_a is obtained. Let us now investigate Noether's first theorem. We allow the most generic transformation

$$\Delta x^\mu = \omega^\mu{}_k(x)\epsilon^k, \qquad \Delta \Phi_a = R_{ak}(x, \Phi)\epsilon^k, \tag{2.9}$$

on a Lagrangian where $\omega^\mu{}_k$ and R_{ak} being representations of certain group transformations in coordinate space and field space respectively. For an internal symmetry, $\omega^\mu{}_k = 0$, while for spacetime transformations, both $\omega^\mu{}_k$ and R_{ak} are nontrivial. By demanding that the transformation leaves $\Delta S = 0$ and the equation of motion (EOM) is satisfied $\mathcal{E}_a = 0$ in Eq. (2.7), the charge of the transformation is conserved

$$Q_k = \int_\Sigma \mathrm{d}\sigma_\mu \left(\pi_a^\mu R_{ak} - \Theta^\mu{}_\nu \omega^\nu{}_k\right) = \mathrm{const}, \quad k = 1, \ldots, m. \tag{2.10}$$

Noether's first theorem states: Invariance of $\Delta S = 0$ under a continuous transformation of an m parameter group implies m global conservation laws with conserved currents

$$\partial_\mu J_k^\mu \equiv \partial_\mu(\pi_a^\mu R_{ak} - \Theta^\mu{}_\nu \omega^\nu{}_k) = 0, \quad k = 1, \ldots, m. \tag{2.11}$$

If the Lagrangian is invariant up to a surface term $\partial_\mu K^\mu$, the current J_k^μ is modified to be $\pi_a^\mu R_{ak} - \Theta^\mu{}_\nu \omega^\nu{}_k + K^\mu$.

The above derivation is valid for classical field theory. After quantizing the classical field, the validity of classical conservation laws induces the Ward identities

$$\frac{\partial}{\partial y^\mu}\langle \mathcal{T} J^\mu(y)\Phi(x_1)\ldots\Phi(x_n)\rangle = \langle \mathcal{T}\frac{\partial}{\partial y^\mu}J^\mu(y)\Phi(x_1)\ldots\Phi(x_n)\rangle$$
$$- i\sum_j \delta(x_j - y)\langle \mathcal{T}\Phi(x_1)\ldots\Delta\Phi(x_j)\ldots\Phi(x_n)\rangle \tag{2.12}$$

among the Green functions. We remind the reader that the charge Q of a transformation generate the total variation of the field:

$$[Q, \Phi(y)] = \Delta\Phi(y), \quad [J^0(\boldsymbol{x}, t), \Phi(\boldsymbol{y}, t)] = \Delta\Phi(\boldsymbol{y}, t)\delta^3(\boldsymbol{x} - \boldsymbol{y}). \tag{2.13}$$

The surface terms in Eq. (2.12) can lead to so-called *anomalies* in the quantum system even though the classical currents are conserved. We will investigate this property in Sec. 2.4 later.

So far we only concerned ourselves with global symmetry and its implication on conservation law, which only holds when the EOM $\mathcal{E}_a = 0$ is applied. The ϵ_k parameter above is independent of spacetime, however when it is promoted to a local parameter $\epsilon_k(x)$, the situation changes drastically as we would need to introduce additional *gauge* fields to maintain the invariance of the transformation. This is the core of Noether's second theorem: Suppose

that the action is invariant under infinitesimal field internal transformation

$$\Delta\Phi_a = \mathcal{Q}_{ak}(x,\Phi,\partial_\mu\Phi)\epsilon^k(x) + \mathcal{R}^\mu_{ak}(x,\Phi,\partial_\mu\Phi)\partial_\mu\epsilon^k(x), \tag{2.14}$$

where $\mathcal{Q}_{ak}$ and $\mathcal{R}^\mu_{ak}$ are functions of group transformation of kth parameter, then there exist linear relation between Eulerians and their derivatives

$$\mathcal{Q}_{ak}\mathcal{E}_a = \partial_\mu(\mathcal{R}^\mu_{ak}\mathcal{E}_a). \tag{2.15}$$

This equation is often not appreciated (or mentioned) in modern QFT literature albeit its importance. The RHS of Eq. (2.15) usually is contributed by gauge field due to their affine transformation structure in field space. Once the EOM of the gauge field is satisfied, the current continuity equation on the LHS is derived, without the use of EOM from matters. Quantizing the gauge fields however, particularly the non-abelian gauge fields, requires tremendous mathematical machinery. We refer the reader to Ref. [22].

2.2. Quick Review of the Standard Model

In the previous section we have introduced the concept of symmetries and their implications on conservation laws. Let us now investigate the symmetries of the SM. Essentially the SM consists of the gauge group $\mathrm{SU}(3)_c \times \mathrm{SU}(2)_L \times \mathrm{U}(1)_Y$ which dictates the fundamental interactions of elementary particles mediated by the strong force and the EW force. The particle content of the SM consists of the vector gauge bosons in the adjoint representation and the fermionic sector constitutes the left-handed doublets (L and Q) and right-handed singlets (E, U and D)

$$L = \begin{pmatrix} \nu_L \\ e_L \end{pmatrix} \sim (\mathbf{1}, \mathbf{2}, -1/2), \quad Q = \begin{pmatrix} u_L \\ d_L \end{pmatrix} \sim (\mathbf{3}, \mathbf{2}, 1/6), \quad E = e_R \sim (\mathbf{1}, \mathbf{1}, -1),$$
$$U = u_R \sim (\mathbf{3}, \mathbf{1}, 2/3), \quad D = d_R \sim (\mathbf{3}, \mathbf{1}, -1/3), \tag{2.16}$$

in $\mathrm{SU}(3)_c \times \mathrm{SU}(2)_L \times \mathrm{U}(1)_Y$ representation. The SM Lagrangian can be divided into

$$\mathcal{L}_{\mathrm{SM}} = \mathcal{L}_{\mathrm{kin}} + \mathcal{L}_H + \mathcal{L}_{\mathrm{Y}}, \tag{2.17}$$

where the component of the sub-Lagrangian $\mathcal{L}_{\mathrm{kin}}$ contains the kinetic terms of the SM gauge and fermionic fields:

$$\mathcal{L}_{\mathrm{kin}} = -\frac{1}{4}G^\alpha_{\mu\nu}G^{\alpha\mu\nu} - \frac{1}{4}W^a_{\mu\nu}W^{a\mu\nu} - \frac{1}{4}B_{\mu\nu}B^{\mu\nu} + i\bar{L}_j\slashed{D}L_j$$
$$+ i\bar{E}_j\slashed{D}E_j + i\bar{Q}_j\slashed{D}Q_j + i\bar{U}_j\slashed{D}U_j + i\bar{D}_j\slashed{D}D_j, \tag{2.18}$$

where $G^\alpha_{\mu\nu}$, $W^a_{\mu\nu}$ and $B_{\mu\nu}$ are the gauge field strengths of $\mathrm{SU}(3)_c \times \mathrm{SU}(2)_L \times \mathrm{U}(1)_Y$ given in terms of their respective gauge fields G^α_μ, W^a_μ and B_μ and the flavor index j is included.

As the three of the EW gauge fields and the fermions are not massless, the mass terms can be generated by using the Higgs mechanism [23–25] to break $\mathrm{SU}(2)_L \times \mathrm{U}(1)_Y \to \mathrm{U}(1)_{em}$

spontaneously. In the SM we have a Higgs $SU(2)_L$ doublet

$$H = \begin{pmatrix} G^+ \\ \frac{h+iG^0}{\sqrt{2}} \end{pmatrix} \sim (\mathbf{1}, \mathbf{2}, 1). \tag{2.19}$$

The $(G^\pm, G^0)$ are the would-be Nambu-Goldstone modes, while the neutral component h represents the physical Higgs field. The Higgs Lagrangian is given by

$$\mathcal{L}_H = (D_\mu H)^\dagger (D^\mu H) - m^2 H^\dagger H - \lambda_H (H^\dagger H)^2. \tag{2.20}$$

In a well defined QFT, the potential must be bounded from below, i.e. $\lambda_H > 0$. When the mass parameter m^2 is positive, the potential has only a minimum at $\langle H \rangle = 0$. To achieve spontaneous symmetry breaking we have to demand that $m^2 < 0$, i.e. the doublet acquires a non-zero vacuum expectation value (VEV) and we can parameterize its value to be at the neutral component of the doublet

$$\langle h \rangle = v = \sqrt{\frac{|m^2|}{\lambda_H}} = 246 \, \text{GeV}. \tag{2.21}$$

Once the Higgs field acquires a non-zero VEV, EW symmetry is spontaneously broken and three of the EW gauge bosons, $W^\pm$ and Z, acquire masses while the photon A_μ remains massless. The weak mixing angle θ_W with

$$\cos\theta_W = \frac{g_2}{\sqrt{g_1^2 + g_2^2}}, \quad \sin\theta_W = \frac{g_1}{\sqrt{g_1^2 + g_2^2}}, \tag{2.22}$$

parameterizes the mixing between the third component of the $SU(2)_L$ gauge field and the B_μ. The only remaining physical component of the scalar Higgs doublet in unitary gauge after spontaneous symmetry breaking is the real scalar h, and its mass is given by $m_h^2 = 2\lambda_H v^2$. The origin of mass for all the massive particles in the SM stems from the VEV of the SM Higgs field. We see that the SM has only one dimensionful parameter, namely the mass parameter m^2. The SM Lagrangian enjoys an additional classical dilatation symmetry if this parameter vanishes. We will investigate this very interesting possibility and its implied phenomenology later in this chapter.

The last piece of the SM Lagrangian, the Yukawa sector $\mathcal{L}_Y$ is given by

$$\mathcal{L}_Y = -Y_{ij}^E \bar{L}_i H E_j - Y_{ij}^D \bar{Q}_i H D_j - Y_{ij}^U \bar{Q}_i (i\sigma^2 H^*) U_j + h.c. \,, \tag{2.23}$$

where the Yukawa matrix Y_{ij}^s generates a complex 3×3 mass matrix $M_s = vY_s/\sqrt{2}$ for charged fermions $s \in \{E, D, U\}$ after EWSB. By applying the bi-unitary transformation

$$V_s^\dagger M_s W_s = \text{diag}(m_\text{I}, m_\text{II}, m_\text{III}), \tag{2.24}$$

where $\{\text{I}, \text{II}, \text{III}\}$ represents the fermion generation, the mass matrix M_s can be diagonalized. The mixing between different flavors of the quarks is described by the unitary Cabibbo-

Kobayashi-Maskawa (CKM) matrix [26],

$$V_{\text{CKM}} = V_U^\dagger V_D. \tag{2.25}$$

Similar mixing matrix can also be found for the leptonic sector, if neutrinos are not massless, which would require already physics beyond the SM. We will discuss the structure of flavor physics later in Chapter 5.

2.3. Puzzles and Problems of the Standard Model

Despite the success of the SM in describing the subatomic physics that we have observed, there are observations and theoretical puzzles that require an extension of the SM. The observations incompatible with the SM are:

Neutrino Mass

From pure experimental facts, neutrinos are proven to be massive from the oscillation experiments [27, 28], contrary to the SM where neutrinos are treated as massless fields. Until today, we do not know the absolute mass scale of the neutrinos, their mass hierarchy and origin. The bound for the neutrino mass sum obtained from combined analysis of Planck, WMAP and baryon acoustic oscillation [29] is found to be less than $0.23\,\text{eV}$ at 95% C.L., while the future measurement of electron end point energy spectrum from beta decays by KATRIN [30] should improve the neutrino mass scale bound. It is also not known whether neutrinos are Majorana or Dirac particles, therefore neutrinoless double beta decay ($0\nu\beta\beta$) experiments are crucial to determine such a distinction. Recently GERDA [31] has put a lifetime $\tau_{1/2} > 2.1 \times 10^{25}\,\text{yr}$ at 90% C.L. on $0\nu\beta\beta$ decay Germanium $^{76}_{32}\text{Ge}$ isotope, future run of this experiment could provide hints on the nature of neutrinos. We refer the reader to some reviews [32, 33] for the current status of experimental searches for neutrino properties. In this thesis we are interested in the role of discrete symmetry for the leptonic mixing pattern and we will focus on the leptonic mixing structure for both cases when neutrinos are Majorana and Dirac particles in Chapter 5.

Dark Matter

From the cosmic microwave background (CMB) [29] and large-scale structure observation [34], we know that the energy density of the Universe consists of 25% pressureless fluid, which can be explained by dark matter (DM). DM can also explain the flat angular rotation curves of galaxies [35] and some gravitational lensing observations [36]. The SM also does not have a good candidate for explaining the existence of DM, however. For a long time, the weakly interacting massive particle (WIMP) has been a leading candidate in explaining the DM. In the early universe, the WIMP annihilated with each other to produce the SM particles, and this reversible process continued until the expansion rate of the Universe exceeded the annihilation rate, i.e. a freeze-out process for the DM occurred. The remaining thermal relics, acting as DM, served as the seed for structure formations at later stage of our cosmological evolution. Various direct detection experiments with different techniques have

Figure 2.1: This diagram illustrates all the relevant interactions for a thermal DM. For DM annihilation we read the diagram from left to right, while the direct detection experiment for DM can be represented by looking at the diagram from top to bottom. If DM can be produced at collider, we can interpret the process happening from right to left.
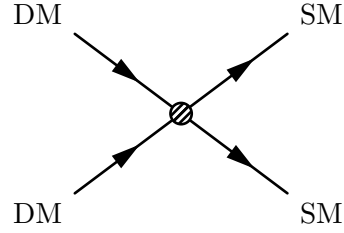
been built and customized to detect the WIMP interaction with the nuclei. The relevant WIMP interaction for calculating the relic abundance, production rate at collider, direct and indirect detection cross section can be compactly summarized in Fig. 2.1. The topic of DM is vast and we cannot cover all its aspects, for a more comprehensive review on DM candidates, direct and indirect detection experiments please refer to Ref. [37]. We will discuss more on the DM candidate proposed in our model and its phenomenologies in Chapter 4.

Baryogenesis

The fact that we exist today and were not annihilated into energetical radiation requires an asymmetry in matter and antimatter. To achieve such a baryon asymmetry it is necessary that the three Sakharov conditions [38], namely baryon number violation, C (charge) and CP (charge-parity) violation, and out of equilibrium dynamics are satisfied. As the CP-violation and the out-of-equilibrium dynamics is not enough to satisfy the Sakharov conditions in the SM. the origin of the matter-antimatter asymmetry demands an explanation beyond the SM. Several proposed solutions for baryogenesis such as Affleck-Dine mechanism [39], EW baryogenesis [40] and leptogenesis [41] have been put forward. We will not discuss this topic further in this thesis, but will briefly touch upon the out-of-equilibrium dynamics described by phase transition in Chapter 4.

Strong CP-problem

The QCD sector in the SM contains the CP violating term

$$\mathcal{L} \supset \frac{\theta_{\text{QCD}}}{32\pi^2} \epsilon^{\mu\nu\rho\sigma} F_{\mu\nu} F_{\rho\sigma} \tag{2.26}$$

in the Lagrangian due to the nontrivial structure of its vacuum. Writing down the most general mass term in the Lagrangian and rotating all the spurious phases away in the SM, one is left with a physical phase in the CKM matrix and an axial phase which induces a similar term like Eq. (2.26). Hence a physical strong CP violating phase

$$\bar{\theta} = \theta_{\text{QCD}} + \arg \det(M_u M_d) \lesssim 10^{-11}, \tag{2.27}$$

is induced which a priori should not be small [42]. The delicate cancellation between the two terms at the RHS of Eq. (2.27) requires extreme fine-tuning, unless there is a new physical mechanism which can explain the reason for such a small value of $\bar{\theta}$. Solutions for

strong CP-problem can be obtained by introducing an axion particle [43] with additional symmetry, or imposing symmetries so that one of the term in RHS of Eq. (2.27) vanishes, e.g. strong CP is spontaneously broken from flavor symmetry [44].

Dark Energy

From the CMB and supernova observations [45, 46] we know that the Universe is expanding, requiring a negative pressure or dark energy. So far we do not know the nature of dark energy, whether it is a constant, some new fields, or due to cosmic inhomogeneity. In this thesis we will not deal with the expansion of the Universe and we refer the interested reader to Ref. [47] for a more complete review.

Theoretical Problems of the Standard Model

From the theoretical point of view, the SM contains some of the puzzles which might hint at the existence of new physics. These problems are not signaling the inadequacy of the SM, rather their appearance has prompted us to rethink the SM and its possible embedding in another perspective. The most interesting theoretical puzzles of the SM consist of the *hierarchy problem* and the *flavor puzzle*. The stabilization of the Higgs mass against the high energy correction in QFT remains one of the most puzzling problem in high energy physics. We will first focus on the conceptual issue in the hierarchy problem in this chapter and will provide our attempts to tackle this problem in Chapter 3 and Chapter 4. On the other hand, the existence of different mass and mixing structure in the quark and leptonic sector seems to crave for simpler explanation. The flavor puzzle and its possible solution will be addressed in Chapter 5. The core of this thesis is to tackle both the theoretical problems and to obtain their interesting phenomenological predictions, which are relevant for explaining the above mentioned discrepancy from the SM prediction. But first let us look at the general attempts to solve any problem in high energy physics.

Problem Solving with Symmetry

In high energy physics we are trained to tackle an issue or a problem from different perspectives. However most of the toolbox can be classified into three categories:

- Symmetry,

- Geometry,

- Dynamics,

where typically one is forced to utilize more than one item in the toolbox. Under dynamics we usually assume some additional field operators that can "align" certain field or vacuum configurations in a desired solution plane. However to engineer such a solution we usually assume that there are some underlying symmetries or geometrical configurations in extra dimension that provide the desired field configuration naturally. The geometrical approach is sometimes not a satisfactory solution, as typically one does not address the reason why certain field configurations are stuck in a certain layer of brane or bulk [48, 49], except just to generate a proper solution set favored by experiments. In this thesis, we instead focus on the

approach based on symmetries and dynamics, where the phenomena and theoretical puzzle that require physics beyond the SM can be addressed with simple reasoning of symmetry and its breaking. Let us now look into the conceptual problem of scales in QFT and its implication for the SM and its possible embedding.

2.3.1. The Hierarchy Problem

With the Higgs boson discovered at the LHC, the SM is complete. At the present all the properties measured for this new boson seem to indicate that the newly discovered scalar boson is SM-like. The SM Higgs field provides a simple mechanism to generate all the masses for the massive elementary particles in the SM, when the Higgs field obtained a nonvanishing vacuum expectation value (VEV). At the moment with all the measured values of other SM couplings, the SM could possibly survive up to the Planck scale by analyzing the renormalization group equation (RGE) [50–55]. In the language of renormalization group (RG), some classes of operators can contribute towards the low energy observables, while some will decouple and become irrelevant for macroscopic phenomenology. Operators that decouple from high energy modes are called *irrelevant operators*, while operators that are always sensitive to the ultraviolet (UV) physics are known as *relevant operators*. Weakly coupled operators with $d = 4$ canonical dimension in a 4-dimensional spacetime are known as *marginal operators* and they may contribute to the macroscopic physics depending on the RGE.

The Higgs mass, being the coupling of the relevant operator ϕ^2, is sensitive to UV physics. Historically, the large separation between the EW scale and the very high energy scale, e.g. M_{pl} is known as the *hierarchy problem*, making it mandatory to *fine-tune* the cancellation between the couplings to obtain the low energy EW mass scale. However, one should be careful with the subtle details involved.

First of all we need to distinguish the difference between the two fine-tuning notion appearing in the scalar field theory, best illustrated by an example. Let us consider two singlet scalar fields that are coupled to each other by potential

$$V = m_1^2 \phi_1^2 + m_2^2 \phi_2^2 + \frac{\lambda_1}{4!} \phi_1^4 + \frac{\lambda_2}{4!} \phi_2^4 + \frac{\lambda_3}{4} \phi_1^2 \phi_2^2, \tag{2.28}$$

where we have imposed a Z_2 parity for each of the scalar fields. Suppose that all the couplings are positive so that spontaneous symmetry breaking does not occur, the one-loop correction for the ϕ_1 mass can be written as

$$\delta m_1^2 \sim C_1 \lambda_1 m_1^2 \ln\left(\frac{m_1^2}{\mu^2}\right) + C_2 \lambda_3 m_2^2 \ln\left(\frac{m_2^2}{\mu^2}\right), \tag{2.29}$$

where C_i represents some pure number coefficients. The parameter μ represents the renormalization scale of our theory. Suppose that $m_1 \ll m_2$, then we would obtain the so-called hierarchy problem between the mass scales. However one can fine-tune the coupling λ_3 such that $\lambda_3 \ll 1$ in order to ameliorate the hierarchy between the two mass scales. Such a delicate cancellation suffers from the *subjective naturalness problem*[2], but it is *technically*

---

[2]Also known as strong naturalness problem, real naturalness problem, bottom-up naturalness problem, Dirac naturalness problem by some authors [56, 57].
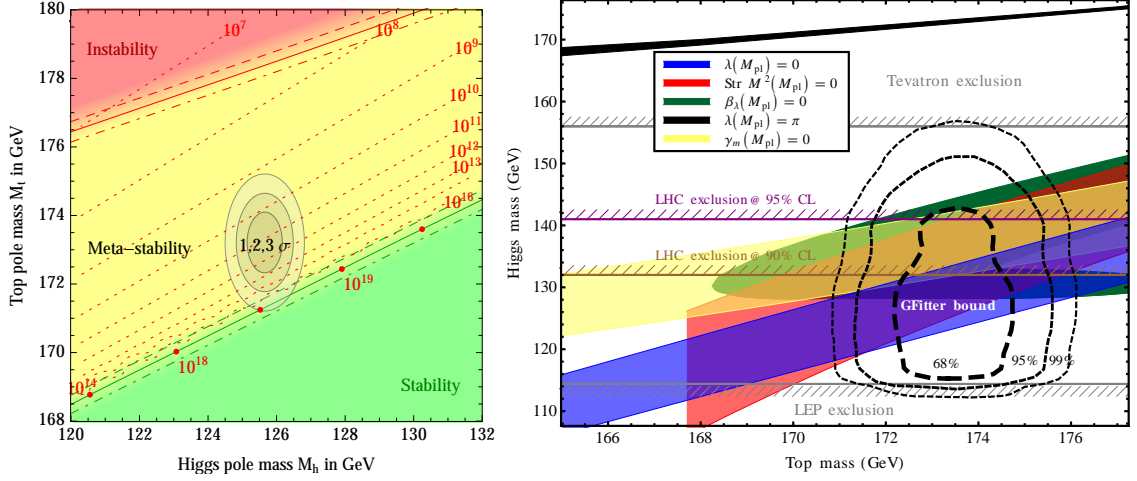
Figure 2.2.: (Left) Phase diagram of vacuum stability/metastability depending on the top and Higgs mass [54]. (Right) Planck scale boundary conditions for the Higgs quartic coupling and their Higgs mass predictions [52].

natural[3] [58], because the beta function for the portal coupling λ_3 is multiplicative

$$\frac{\mathrm{d}\lambda_3}{\mathrm{d}\ln\mu} \sim \lambda_3 g(\lambda_3, \lambda_i), \tag{2.30}$$

and therefore the coupling λ_3 stays small once it is set to be small at a certain energy. The function $g(\lambda_3, \lambda_i)$ contains all the relevant couplings. The theory suffers from subjective naturalness problem as a priori one should not expect the coupling to be so small to cancel out the large contribution of ϕ_2 to the mass of ϕ_1. If the parameter m_1^2 is negative, the field ϕ_1 would obtain a nonvanishing VEV v and trigger spontaneous symmetry breaking. Depending on the renormalization scheme either the mass parameter m_1^2 or the VEV v is sensitive to the correction of m_2^2. Again we could fine-tune the λ_3 parameter to be small such that it is protected by technical naturalness, yet the problem of subjective naturalness remains.

We now like to discuss some of the confusion regarding the subjective naturalness problem in the high energy physics community. The couplings for relevant operators suffer from subjective naturalness problem as they are sensitive to the high energy modes, like our example above. As we know that the SM Higgs doublet undergoes spontaneous symmetry breaking, the Higgs VEV or its mass parameter is sensitive against high energy correction, parameterized by

$$\delta m^2 \sim f(\lambda_i)\Lambda^2 \ln\left(\frac{\Lambda^2}{\mu^2}\right). \tag{2.31}$$

The term Λ in this case represents the sensitivity of new QFT physics scale, and it is not a regulator[4] that can be sent to infinity after renormalization has been carried out. The

---

[3]These two different notions of naturalness have caused so much confusions in the high energy physics community.

[4]In fact we should stop talking about the misleading quadratic divergence from technical cutoff, which is just a regulator and has no meaning.

quantum correction in Eq. (2.31) contributes to the RGE of the Higgs mass

$$\frac{\mathrm{d}m^2}{\mathrm{d}\ln\mu} = m^2\gamma(\lambda_i) + f(\lambda_i)\Lambda^2, \tag{2.32}$$

where we have neglected some irrelevant numerical coefficients. The term γ dictates the running of the Higgs mass if the EW scale is the only scale of nature. If we extend the SM with new physics of scale Λ stemming from high energy QFT physics, one would necessarily run into the subjective naturalness problem. Conventional solution for the subjective naturalness problem is to invoke a new symmetry (supersymmetry) [59] to cancel out the function f or to postulate new structure such as extra dimension [48, 49] or compositeness [60–63] such that the new physics scale Λ is near the scale of m. Applying the argument to the case of the SM, we should observe new physics at TeV scale. However with only the Higgs-like particle discovered and no new particle beyond the SM being found, generally proposed solutions to the hierarchy problem are pushed towards fine-tuned corner. With the current measured Higgs mass and the top quark mass, the SM could even survive up to the Planck scale [53, 64], see Fig. 2.2. It seems that the experimental results so far do not provide any evidence for the conventional solutions of the hierarchy problem and we may ask ourselves whether traditional view of subjective naturalness is correct.

As we have stressed earlier, Λ represents the scale of new heavy QFT modes which couple to the SM Higgs field. From the traditional Wilsonian view of QFT, low energy physics is a remnant of physical degrees of freedom after integrating out the high scale physics. Embedding the SM in another high energy QFT may risk of running into subjective naturalness problem when the m is fine-tuned against the correction of high energy modes. Even the minimal supersymmetric version of the SM suffers from such fine-tuning problem if the supersymmetry breaking scale is large enough. However, the Wilsonian view might not be applicable when the only high scale physics is beyond the concept of QFT, which could be the scenario for quantum gravity as a priori we have no idea what this new physics might be, and the SM might just be a boundary condition of an unknown non-QFT quantum gravity. One might ask, which boundary condition from quantum gravity might be reasonable to explain the SM? Since we do not want a fine-tuning between two widely separated energy scales, then we should perhaps start from a fundamental theory with no explicit energy scale, with the resulting EW scale generated quantum mechanically. That is, we assume that $m(M_{pl}) = 0$. Looking back at the SM Lagrangian, the only explicit mass scale in the Lagrangian is the Higgs bare mass parameter that breaks classical scale invariance and from the observation that $m/M_{pl} \ll 1$, the SM in a full embedded theory with gravity exhibits classical scale invariance from UV perspective due to the smallness of m [65]. Therefore it is possible that the EW scale is generated quantum mechanically via anomalous breaking of the classical scale symmetry. Embedding the SM in a new QFT with very high energy between the EW and Planck scale would invalidate our argument, hence we need to assume that new physics at TeV regime which break classical invariance anomalously in the second term of Eq. (2.32) should be generated radiatively. Why we have a classically invariant Lagrangian as boundary conditions of Planck scale physics, this has to be justified in an UV complete quantum gravity framework. In this thesis we will assume that this is the case, and investigate the implied phenomenologies. This idea is not as far fetched as it

seems as the QCD hadronic length Λ_{QCD} is generated by dimensional transmutation from the dimensionless strong coupling. Perhaps classical scale invariance is a good starting point to rethink about the hierarchy problem, and that the EW scale is generated by quantum phenomenon.

2.4. Scale Invariance Versus Conformal Symmetry

Scale invariance is a special property of an object or a law that preserves its form after a scaling of length or energy is performed, i.e. the object preserves its form when we zoom in or out on it. Since we are dealing with fields in modern high energy physics, a multicomponent field $\Phi(x)$ with d as scale dimension is said to possess *classical* scale invariance if the transformation

$$\Delta_s \Phi(x) = \lambda_s (x^\mu \partial_\mu + d)\Phi(x), \tag{2.33}$$

with λ_s as dilatation parameter, leaves the classical action of the theory invariant. The scale current associated with the above symmetry is defined as

$$J^\mu = x_\nu \Theta^{\mu\nu}, \quad \text{and} \quad \partial_\mu J^\mu = \mathcal{W}, \tag{2.34}$$

with $\mathcal{W}$ as some function of the fields and their derivatives after performing the transformation in Eq. (2.33). The term $\Theta^{\mu\nu}$ is the improved symmetric energy momentum tensor [66]. The classical scale current in Eq. (2.34) is conserved iff $\mathcal{W}$ vanishes

$$\Theta^\mu{}_\mu = \partial_\mu J^\mu = 0. \tag{2.35}$$

Suppose that we restrict ourselves in considering only the scalar, spinor and vector fields with canonical dimension 1, 3/2 and 1 respectively, the quantity $\mathcal{W}$ will only consist of combinations of fields with dimension $d \neq 4$, e.g. $\mathcal{W} = m_\psi \bar{\psi}\psi + m_\phi^2 \phi^2 + \rho\phi^3$ if we write down all the possible renormalizable terms allowed by the symmetry of the theory (we have restricted our dimensionality to $d = 4$ in the Lagrangian). It is clear from the analysis of $\mathcal{W}$ that all terms with dimensionful parameters break classical scale invariance.

What about conformal symmetry? Mathematically speaking conformal symmetry contains scale transformation as its subgroup. The action is classically conformal invariant if it is invariant under the Poincaré transformation, scale transformation and the special conformal transformation

$$\Delta_c \Phi(x) = (2x \cdot \lambda_c x^\nu - x^2 \lambda_c^\nu)\partial_\nu \Phi(x) + 2(x \cdot \lambda_c d - x^\nu \Sigma_{\nu\mu} \lambda_c^\mu)\Phi(x), \tag{2.36}$$

where $\Sigma_{\mu\nu}$ represents the Lorentz rotations on the components of $\Phi(x)$ and λ_c^μ is a special conformal transformation parameter. The conformal group with D conformal transformations is $\mathrm{SO}(D, 2)$. Naively one would think that a classically conformal invariant physical theory is necessary different than classically scale invariant theory. However physical theory may contain more surprises than mathematical intuition. Under some assumptions, scale invariant QFT always seems to be conformal invariant too. It is the dynamic of the theory that promotes the scale invariant QFT to conformal QFT. For $d = 2$ scale invariant QFT,

it has been proven that such QFT possesses the enhanced conformal symmetry, guaranteed by Zamolodchikov-Polchinski theorem [67, 68] under the following assumptions

- unitarity,

- Poincaré invariance,

- discrete spectrum in scaling dimension,

- existence of scale current,

- unbroken scale invariance.

It is conjectured that with the above assumptions, the symmetry enhancement from scale invariant theory to conformal symmetry theory should be also valid for $d = 4$, which up until today, no counter example has been found[5]. We will not distinguish the difference between scale invariance/dilatation symmetry and conformal symmetry in this thesis as most of the models constructed for high energy physics satisfy the required assumptions listed above, but readers should keep in mind the assumptions in play.

2.4.1. Breaking Scale Invariance

In low energy physics, scale invariance must be broken, otherwise particles would have continuous mass spectra or be massless. There are several ways to account for global symmetry breaking. One way is to write down the explicit symmetry breaking term in the Lagrangian with small coupling such that the symmetry is explicitly broken. Another way to achieve symmetry breaking is via spontaneous symmetry breaking, where the ground state of the theory does not respect the original symmetry. Depending on the underlying symmetry, one may obtain Nambu-Goldstone bosons, domain walls or cosmic strings if the symmetry is broken spontaneously. On the other hand, the dynamical equations still possess the desired symmetry and the Ward identities are still valid. Lastly a classical symmetry in a theory can be broken anomalously, where quantum corrections to the classical theory break the underlying symmetry. In this approach, anomalies occur and the quantum correction to the classical theory does not respect the Ward identity (2.12). Scale invariance is interesting as it is possible to achieve the breaking of such symmetry with all the methods mentioned above. For the SM, dilatation symmetry is broken explicitly by the $m^2 H^\dagger H$ term. Suppose that we assume m^2 term is zero at classical level, perturbative quantum corrections will require us to renormalize the theory at a specific energy scale, hence breaking the scale symmetry anomalously. If we insist on breaking scale invariance spontaneously [70], we are not allowed to introduce an energy scale in our renormalized theory, therefore one has to find a method to keep scale invariance at quantum level, and only break the ground state symmetry. A theory with spontaneous broken scale invariance would contain a massless Nambu-Goldstone boson known as dilaton in the spectrum, whereas if scale invariance is broken anomalously, such dilaton particle would not appear. To maintain quantum scale invariance and break it spontaneously, nonrenormalizable terms or some nonperturbative aspects of QFT are usually required and it is not known however if such an approach is

---

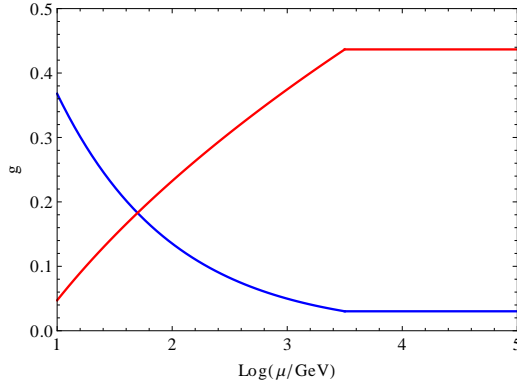[5]See Ref. [69] for more detailed discussions.

Figure 2.3: The running of generic couplings with some generic perturbative boundary conditions. The theory flows to a CFT at around $\mu \sim 5\,\text{TeV}$, where all the generic couplings of a particular theory begin to flow to a set of fixed points. This would solve the hierarchy problem as the VEV of the Higgs only receives contribution at most at the TeV range. No further mass scale exists above the TeV regime.

consistent. We will not pursue model building along this direction in the thesis, and instead focus on breaking scale invariance anomalously.

2.4.2. Anomalies

Depending on how the classical scale invariant theory is defined, i.e. whether it is defined on a curved spacetime or how additional gauge group and representations are introduced, the anomaly from breaking dilatation symmetry anomalously would increase with much complexity. Simply put, the anomalous Ward identity of scale symmetry is badly violated, and even the partially conserved dilatation current (PCDC) in perturbation theory does not exist[6] [71]. The general anomalous Ward identity for the scale/dilatation current can be cast in the following form [69, 72]

$$\langle \Theta^{\mu}{}_{\mu} \rangle = \beta^I \mathcal{O}_I + \mathcal{A} + \mathcal{V}, \tag{2.37}$$

where β^I is the corresponding beta function for operator $\mathcal{O}_I$[7]. We can see that the nonvanishing RHS of Eq. (2.37) can contribute to the violation of dilatation current. The term $\mathcal{A}$ only arises when the theory is defined on curved spacetime, stemming from the Weyl anomaly. We will not discuss the Weyl anomaly as the scale invariant extensions of our models are only defined on a flat spacetime. The term $\mathcal{V}$ contains vector beta functions which describe the RGE for the vector background source. This term is also irrelevant for our discussion. The most important contribution to the anomalous breaking of scale invariance stems from the RGE of the couplings involving the $d = 4$ operators.

There exists a class of theories where the beta functions of the couplings always vanish, which is known as conformal field theory (CFT). For instance the $\mathcal{N} = 4$ Super Yang-Mills theory [73] is a pure CFT due to the cancellation of the terms contributing towards the beta function. Alternatively there is another scenario to restore scale invariance at high energy. A theory is called *asymptotically safe* if the couplings of the theory flow to a set of fixed points at high energy [74, 75], i.e. the beta functions vanish at the UV of the theory, see Fig. 2.3. If this scenario is possible, then scale invariance is restored at the high energy. For a successful implementation of this idea in the case of the SM, the transition scale for a theory to a CFT has to be around the TeV scale in order to avoid the hierarchy problem.

---

[6] Compared to anomalous breaking of axial current in a generic fermionic QFT with flavor chiral symmetry, at least a partially conserved axial current (PCAC) can be defined.

[7] Remember that $\mathcal{W}$ vanishes as we have a classical scale invariant theory from the start.

Model building along this direction so far has been unsuccessful, as it is nontrivial for all the couplings in the SM with extensions to flow towards a set of fixed point. Furthermore, quantum gravity might play a role in the RGE at the Planck scale, potentially spoiling the asymptotic safety scenario.

2.4.3. Boundary Condition or Symmetry?

If we suppose that we have no CFT as our UV completion in our model, at first glance classical scale invariance seems to be a bad symmetry to begin with, as the dilatation current for an interacting theory is anomalous. There is an alternative way to interpret a classically scale invariant theory in another language, namely that all the *renormalized* dimensionful couplings vanish at some high energy scale, i.e. the vanishing renormalized dimensionful couplings at certain high energy scale are just a specific set of boundary conditions for the RGE of the couplings. One might still worry about the fine-tuning problem between the cancellation of Planck scale value to obtain the EW scale. However if quantum gravity is a new concept beyond QFT, then such a Wilsonian view might not apply to the argument on the sensitivity of EW scale against the Planck scale physics. If we accept such an assumption, then classical scale invariance provides a set of special boundary conditions for the RGE of the SM and its extension, which is obtained from the non-QFT physics. This argument also explains the appearance of the dimensionful counterterm in the Lagrangian[8], as one would have naively thought that such terms should not be there due to scale invariance.

The model building with the assumption of scale invariance is hence now straight forward. We will demonstrate how dimensional transmutation is obtained from a concrete ϕ^4 example, starting with a classically scale invariant Lagrangian

$$\mathcal{L} \supset (D_\mu \phi)^\dagger (D^\mu \phi) - \frac{\lambda}{4}(\phi^\dagger \phi)^2, \tag{2.38}$$

where the scalar field ϕ is charged under some gauge group. Next, the effective action with quantum correction taken into account is calculated and depending on the dynamics of the theory, dimensional transmutation can occur perturbatively or via strongly coupled dynamics. The former can be achieved when quantum corrections to the effective potential cause a nonzero VEV to arise[9]

$$V \sim \frac{\lambda}{4!}\phi_c^4 + C\lambda^2 \phi_c^4 \left[\ln\left(\frac{\phi_c^2}{\mu^2}\right) - D\right] + \ldots, \tag{2.39}$$

where the field ϕ_c represents the flat direction of the potential. Notice the appearance of the renormalization scale μ, which breaks the dilatation symmetry due to the renormalization procedure. The renormalized mass appears due to the renormalization conditions and hence one can say that the scale of this theory appears radiatively. This radiative correction as the origin of spontaneous symmetry breaking for the scalar sector is called the Coleman-Weinberg mechanism [76]. Simply put, the anomalous breaking of scale invariance triggers

---

[8]We need the counterterms to obtain renormalized quantities.
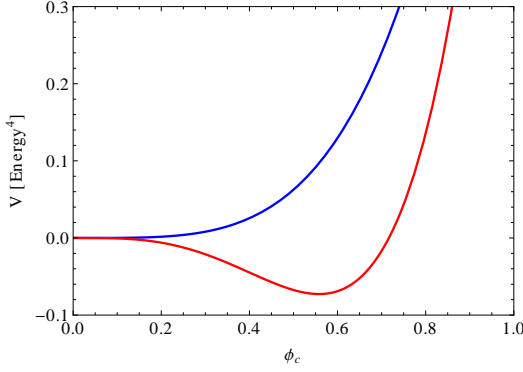[9]There is a saying that log = quantum in QFT folklore.

Figure 2.4: The scalar field ϕ_c obtains a nonzero VEV in the effective potential (red) after quantum correction. The classical potential (blue) is plotted for comparison.

the spontaneous symmetry breaking of the scalar sector, which can be summarized as

$$\langle \Theta^{\mu}{}_{\mu} \rangle \neq 0 \rightarrow \langle \phi_c \rangle \neq 0. \tag{2.40}$$

The effect of mass scale generation by a nonzero VEV in the effective potential can be seen in Fig. 2.4.

On the other hand, dimensional transmutation can also be achieved by strong dynamics. From the example given in Eq. (2.38), suppose that the gauge coupling g of a non-abelian gauge group under which ϕ is charged becomes nonperturbative at some energy scale due to RGE, the theory becomes strongly coupled and a bound state of the scalar field ϕ can be formed due to confinement. The resulting condensate $\langle \phi^{\dagger} \phi \rangle \neq 0$ generates a mass scale of the low energy theory, realizing dimensional transmutation in a nonperturbative way. Again, like the perturbative method explain above, the mass scale generation for the scalar field can be achieved via the anomalous breaking of classically scale invariant theory

$$\langle \Theta^{\mu}{}_{\mu} \rangle \neq 0 \rightarrow \langle \phi^{\dagger} \phi \rangle \neq 0. \tag{2.41}$$

2.5. Scale Invariance and the SM

It is interesting that the SM contains only one dimensionful parameter, namely the mass squared term m^2 in Eq. (2.20). Therefore it is intriguing to extract the SM Higgs mass prediction if the SM possesses classical scale invariance as an additional symmetry. If we accept that classical scale invariance represents a special boundary conditions imposed by quantum gravity beyond QFT, we can extract the SM Higgs mass prediction at low energy, generated by quantum effects. The SM effective potential for the Higgs field is given by

$$V = -\frac{m^2}{2} h^2 + \frac{\lambda}{4} h^4 + \beta_{\lambda} h^4 \ln \left(\frac{h^2}{v^2} \right), \tag{2.42}$$

where we sum over only the EW gauge bosons, the Higgs and the top quark contributions for the beta function β_{λ} of λ. We have chosen the renormalization scale $\mu = v$. From the minimum conditions at $h = v$ and the classical scale invariant condition $m^2 = 0$, the

predicted Higgs mass

$$m_h^2 = \left. \frac{\partial^2 V}{\partial h^2} \right|_{h=v} = 8\beta_\lambda v^2 \tag{2.43}$$

turns out to be imaginary as the beta function for quartic Higgs coupling is negative due to the heavy top quark mass. Therefore classically scale invariant SM is completely ruled out and if classical scale invariance is a boundary condition predicted by quantum gravity, the SM has to be extended.

2.6. Scale Invariant Extension of the SM

With only the SM Higgs like particle discovered and no new particle beyond the SM been found so far, there is no evidence for any of the generally proposed solutions to the hierarchy problem. With the current measured Higgs mass and the top quark mass, the SM could even survive up to the Planck scale [53, 64]. A possible solution to the hierarchy problem is based on classical scale invariance, which is violated at the quantum level and hence a scale is generated. Suppose that we extend the SM with a new classically scale invariant sector, then the EW scale can be generated by the anomalous breaking of dilatation symmetry. Essentially the dimensional transmutation can be achieved in two classes of theories[10]:

- Coleman-Weinberg mechanism [77–94],

- Nonperturbative scale generation in a strongly coupled sector [95–102],

where renormalizability is assumed. Many of these attempts rely on the Higgs portal

$$\lambda_{HS} S^\dagger S H^\dagger H, \tag{2.44}$$

where the additional scalar field S (charged or neutral under a certain gauge group) obtains a VEV either directly or indirectly. It is also possible to generate the EW scale if a condensate of $\langle S^\dagger S \rangle$ is formed due to some underlying strong dynamics [102].

For the case of the Coleman-Weinberg mechanism, the EW scale is generated when the whole effective potential has a global minimum at nonvanishing field value after taking quantum corrections into account. From Eq. (2.42), we see that by minimizing the effective potential at the nonvanishing VEV, the physical Higgs mass with quantum correction has the form of Eq. (2.43). For the SM case, the beta function for λ is negative due to the large top quark contribution. Hence in order to obtain the desired $m_h \approx 125\,\mathrm{GeV}$ [6, 7], extra bosonic degrees of freedom have to be introduced in order to cancel out the top quark contribution. An additional scalar S can accomplish this task and depending on whether the new scalar is charged under certain gauge group or not, one can obtain richer phenomenology in DM or collider searches.

In this thesis we will focus on some other possibilities to generate the EW scale nonperturbatively from a strongly coupled sector. In general a non-abelian gauge sector with some matter representations charged under this gauge group is introduced in order to achieve it.

---

[10]At least up until this thesis was written.

The dimensional transmutation method is similar to QCD, where the strong gauge coupling grows to nonperturbative regime at Λ_{QCD} and subsequently confinement takes place with nontrivial condensates making up the low energy vacuum of QCD. The condensation scale from a strongly coupled sector is transmitted to the EW sector to trigger EWSB, either *directly* or *indirectly*.

2.6.1. Direct Scale Transmission

Consider the Higgs portal term in Eq. (2.44), the difference between direct and indirect scale transmission depends on the role of the scalar field S that couples to the Higgs. In a direct scale transmission scenario, we demand that this additional scalar forms a condensate, generating a scale via dimensional transmutation from a strongly coupled sector and subsequently triggers EWSB. We can consider an additional scalar S charged under a representation of a non-abelian gauge group, which is introduced in addition to the SM. The Higgs portal term always exists as it is a renormalizable term. In general, the condensation of S, i.e. $\langle S^\dagger S \rangle \neq 0$, takes place when

$$C_2(S)\alpha(\Lambda) \gtrsim 1, \tag{2.45}$$

with C_2 representing the quadratic Casimir of the certain representation $\boldsymbol{R}$ of S and α is the gauge coupling of the chosen non-abelian gauge group. Condensation of S takes place when Eq. (2.45) is satisfied, generating a condensation scale $\langle S^\dagger S \rangle = \Lambda_c^2$ which serves effectively as the Higgs mass parameter at low energy

$$\lambda_{HS} S^\dagger S H^\dagger H \to \lambda_{HS} \langle S^\dagger S \rangle H^\dagger H = \lambda_{HS} \Lambda_c^2 H^\dagger H \cong m^2 H^\dagger H. \tag{2.46}$$

This mechanism followed the idea of Eq. (2.41) and we will provide a concrete model in Chapter 3.

2.6.2. Indirect Scale Transmission

Contrary to the direct scale transmission scenario above, the role of the new scalar field in this case is more passive. In general this scalar particle acts as a mediator that transmits a scale from another sector, with the assumption that the new scalar boson couples to both the SM and the additional strongly coupled sector. For example we could insist on using a condensate formed by fermion pair, which is generated by spontaneous chiral symmetry breaking in the hidden sector, to trigger the EWSB. A scalar mediator S, which coupled to both the hidden and SM sector as follows

$$\mathcal{L} \supset yS\bar{\psi}\psi + \lambda_{HS} S^2 H^\dagger H, \tag{2.47}$$

is needed in order to make the theory renormalizable, as the direct coupling

$$\langle \bar{\psi}\psi \rangle H^\dagger H \tag{2.48}$$

requires the nonrenormalizable operator $\bar{\psi}\psi H^\dagger H$. Instead we achieve the scale transmission via an additional scalar field as mediator, where this scalar field S is coupled to the fermions

that form a condensate through the Yukawa interaction. Once the fermionic condensate is formed, the S field obtains a nonzero VEV and subsequently transmits the condensation scale to the EW sector. Schematically this process is summarized as

$$\langle \bar{\psi}\psi \rangle \to \langle S \rangle \to \langle H \rangle, \tag{2.49}$$

where the EW scale generation proceeds as follows

$$\lambda_{HS} S^2 H^\dagger H \to \lambda_{HS} \langle S \rangle^2 H^\dagger H. \tag{2.50}$$

Note that $\langle S^\dagger S \rangle$ is an condensate in Eq. (2.46) while $\langle S \rangle$ represents a VEV in Eq. (2.50). We will discuss a concrete model along this approach in Chapter 4.

2.7. Summary

In this chapter we have provided an explanation for the hierarchy problem and scrutinized it in a detailed way. We have proposed a scale invariant extension of the SM to solve the hierarchy problem. The EW scale is generated quantum mechanically and does not suffer from UV sensitivity, assuming that there is no mass scale in a strict QFT sense between the EW and the Planck scale. As the SM without the mass term could not generate the correct Higgs mass, an extension of the SM is necessary if we assume that classical scale invariance is the right candidate to solve the hierarchy problem. In general there are two ways to generate mass scale from a classically scale invariant theory, either through a perturbative (Coleman-Weinberg) approach or a strongly coupled theory. In this thesis we will focus on the latter and we have classified the general approach to generate mass scale from a strongly coupled sector, either directly or indirectly. In the next two chapters we will show some models on how to implement these core ideas.

Electroweak Symmetry Breaking by QCD

In this chapter we propose a model to trigger electroweak symmetry breaking (EWSB) by the condensation of a scalar charged under the QCD gauge group. We start off with the classically scale invariant Standard Model (SM) plus an additional scalar field which only couples to the Higgs sector. To obtain a condensate at the TeV regime, the scalar field has to be necessarily charged under higher-dimensional representation of $SU(3)_c$. As the scalar field is charged under QCD, it can be produced at the LHC. We will discuss the collider phenomenology relating to the production and decay channels of the QCD scalar field. Additionally the production cross section of the Higgs particle in the gluon fusion channel will also be modified and such deviation can be detected also at the LHC. We will discuss some of the nonperturbative aspects of the model and highlight the challenges that we need to tackle to obtain information in the nonperturbative regime. The structure and results presented in this chapter are based on our work with Jisuke Kubo and Manfred Lindner [102], accepted for publication by *Physical Review Letters*.

3.1. Scale Invariant Extension with Scalar QCD

We would like to explain the electroweak (EW) scale from quantum phenomena, and since the SM alone with $m^2 \to 0$ predicts an incorrect value for the Higgs mass, the SM necessarily needs to be extended. In this chapter we propose a model with an additional scalar field S which is charged under a non-abelian gauge group, forming a condensate when the gauge coupling becomes nonperturbative. As we have mentioned in Sec. 2.6.1, in general the condensation of S, i.e. $\langle S^\dagger S \rangle \neq 0$, occurs when [103–105]

$$C_2(S)\alpha(\Lambda) \gtrsim 1, \tag{3.1}$$

with C_2 representing the quadratic Casimir of a gauge group representation $\boldsymbol{R}$ for S particle, and α is the gauge coupling of a chosen non-abelian gauge group. The important point here is that confinement[1] can occur even if the gauge coupling α is relatively small, provided that the representation of S is large enough to satisfy Eq. (3.1). This important fact is often ignored in the introductory lecture and literature of QCD or strongly coupled QFT. For the case of ordinary QCD, the C_2 of quarks is small due to the fact that it belongs to

---

[1]Though there are subtle differences, we assume that the confinement scale is the same as the condensation scale in this thesis.

the fundamental representation of $SU(3)_c$, and an energy scale of $\mathcal{O}(1\,\text{GeV})$ is generated by the quark condensates. Hence according to Eq. (3.1), QCD can generate much more higher energy condensates in principle, if new colored degrees of freedom charged under a larger representation of QCD exist, One might wonder whether this approach agrees with traditional view of dimensional transmutation, where a gauge coupling is exchanged with a dimensional quantity. We would like to clarify that this view of one-to-one exchange of dimensionless parameter to dimensional quantity is wrong. In fact, dimensional transmutation mechanism can generate different mass scales from a single dimensionless gauge coupling. The crucial point for this situation to occur is the existence of different particles in different representations under a non-abelian gauge group. One can also view the different mass scale generation from a different perspective, where the higher mass scale is generated from the running of the lowest mass scale obtained from the condensates of particles in fundamental representation, with the running dictated by the beta function. Intuitively for the case of QCD we have

$$\Lambda_{\text{QCD}} \to \underbrace{\Lambda_{\text{QCD}} \exp\left(-\int \frac{\mathrm{d}\ln\mu}{\beta_{\text{QCD}+\mathbf{6}}(\mu)}\right)}_{\Lambda_{\mathbf{6}}} \to \underbrace{\Lambda_{\text{QCD}} \exp\left(-\int \frac{\mathrm{d}\ln\mu}{\beta_{\text{QCD}+\mathbf{6}+\mathbf{8}}(\mu)}\right)}_{\Lambda_{\mathbf{8}}} \to \ldots, \quad (3.2)$$

if particles with larger representation such as $\mathbf{6}$ or adjoint exist[2]. Exotic quarks which generate higher energy condensate have been considered before in Refs. [106, 107]. However, most of these exotic fermions which are charged under the EW gauge group cannot generate the correct EW scale without running into large discrepancy with the EW precision tests. The situation will be different if we consider a colored EW singlet scalar field.

The idea presented above works for any arbitrary non-abelian gauge group, for simplicity we would like extend the success of QCD minimally and see whether it is possible to generate the EW scale from QCD condensates. We assume that the SM with a new scalar charged under QCD is classically scale invariant. The EW scale is dynamically generated via the condensation scale of S once Eq. (3.1) is fulfilled. We remind the reader that the strong sector of the SM itself is scale invariant before EWSB, contrary to ordinary QCD with explicit massive quarks after EWSB. The full Lagrangian for our model is given as

$$\mathcal{L} = \mathcal{L}_{\text{SM},m^2\to0} + (D_{\mu,ij}S_j)^\dagger(D^\mu_{ik}S_k) + \lambda_{HS}H^\dagger H S^\dagger S - \lambda_{\mathbf{1}_i}\left[\bar{\boldsymbol{S}}\times\boldsymbol{S}\times\bar{\boldsymbol{S}}\times\boldsymbol{S}\right]_{\mathbf{1}_i}, \quad (3.3)$$

where $D^\mu_{ij} = \delta_{ij}\partial^\mu - ig_s(T_R)^k_{ij}G^\mu_k$ is the covariant derivative of S, and T_R represents the generator for the S field in representation $\boldsymbol{R}$ of $SU(3)_c$. The quartic scalar coupling $\lambda_{\mathbf{1}_i}$ denotes the ith invariant singlet term formed by the contraction of four tensor products in the S representation.

Due to classical scale invariance, quadratic and cubic terms of S do not appear in Eq. (3.3). Hence one can see that the Lagrangian (3.3) exhibits an accidental U(1) symmetry for the S field, which is a priori an accidental global symmetry. This accidental U(1) symmetry for the S sector has very interesting phenomenology if it is identified with the gauged $U(1)_Y$

---

[2]In principle, the scale generated by fermions in fundamental representation of QCD should differ from the gluon condensation scale. The fact that both the scales are of similar order is due to the small difference between the quadratic Casimirs of fundamental and adjoint representations in $SU(3)_c$.

Rep ($\boldsymbol{R}$)	$C_2(\boldsymbol{R})$	$C(\boldsymbol{R})$	Λ (GeV)
3	4/3	1/2	0.3
8	3	3	1
10	6	15/2	20
15	16/3	10	10
15′	28/3	35/2	1000
21	40/3	35	10^5

Table 3.1: Values for the quadratic Casimir and index of certain representations in QCD are listed. We list down the approximate confinement scale Λ for each representation, calculated from Eq. (3.1). Similar table for different gauge groups and representations can be found in Refs. [108, 109].

hypercharge symmetry of the SM, which we will discuss later.

The EWSB triggered by QCD comes with the following steps: First, the strong coupling g_s runs from a finite value fixed at high energy scale (e.g. the Planck scale) to the condensation scale of S. The scalar condensate $\langle S^\dagger S \rangle$ is formed when Eq. (3.1) is satisfied for $\mathcal{O}(1\,\text{TeV})$ where the small value of strong coupling $\alpha_s(\Lambda = 1\,\text{TeV}) \approx 0.09$ is compensated by the large value of C_2 for S in higher representation, say $\boldsymbol{R} = \boldsymbol{15'}$. The condensation scale is fixed once a representation for S is chosen as the strong gauge coupling is well measured and constrained. Table 3.1 shows a list of representations and the order of confinement scale for QCD. The condensate then generates a scale Λ, triggering EWSB dynamically:

$$\lambda_{HS}\langle S^\dagger S \rangle H^\dagger H \to \lambda_{HS}\Lambda^2 H^\dagger H. \tag{3.4}$$

The Higgs mass can be determined from

$$m_h^2 = 2\lambda_{HS}\Lambda^2, \tag{3.5}$$

after EWSB and this subsequently dictates the Higgs quartic coupling λ_H

$$\frac{\lambda_H}{\lambda_{HS}} = \frac{\Lambda^2}{v^2}, \tag{3.6}$$

where $v = 246\,\text{GeV}$ is the Higgs vacuum expectation value (VEV). Note that the coupling λ_{HS} is determined once the condensation scale Λ is set to be any energy value higher than the EW scale, as we require the condensate to form before EWSB. There is no upper limit on Λ in general, except that one would require a larger representation of S to trigger EWSB if λ is larger, as α_s decreases with higher energy and λ_{HS} is getting more fine-tuned in order to match the experimentally observed Higgs mass. The core idea above is to generate the EW scale by direct transmission of condensation scale of a new colored scalar field which couples to the Higgs directly, realizing the radiative EW scale generation by anomalous scale symmetry breaking

$$\langle \Theta^\mu{}_\mu \rangle \neq 0 \to \langle S^\dagger S \rangle \neq 0 \to \langle H \rangle \neq 0. \tag{3.7}$$

Our new additional field does not alter the low energy QCD as the effect of S decouples from the running of strong coupling at low energy. The coupling of S (in higher representation) with the quarks (in fundamental representation) to form a singlet typically requires higher-dimensional operators, therefore the effect of S on hadronic physics is always suppressed. It is crucial to remember that a large C_2 value for larger representation

accomplished two things for us:

- It gives a large contribution to Eq. (3.1) such that condensation can take place at scale of $\mathcal{O}(\mathrm{TeV})$ despite the small coupling of α_s.

- It suppresses the interaction between S and quarks as more quarks fields (higher-dimensional operators) are needed to contract the group indices.

As we can see from Table 3.1, the representation $\mathbf{15'}$ is suitable for EWSB as it generates the desired condensation scale at $\mathcal{O}(1\,\mathrm{TeV})$ naturally without fine-tuning of λ_{HS}. The choice of $\mathbf{15'}$ is unique as smaller representations cannot generate a correct Higgs mass m_h at perturbative level. The coupling λ_{HS} has to be larger than 20 even for the next possibility $\mathbf{10}$, which would render the theory nonperturbative.

3.2. Theoretical Constraints and RGE

Let us discuss the phenomenology of this new colored scalar particle S charged under $\mathbf{15'}$ of the QCD representation. Without imposing some constraints on the parameters based on the experimental measurements, we can first impose some theoretical constraints on the coupling $\lambda_{\mathbf{1}_i}$ and λ_{HS} from the requirement that all the relevant scalar couplings do not destabilize the vacuum or hit a Landau pole. For a $\mathbf{15'}$ representation, three quartic couplings $\lambda_{\mathbf{1}_i}$ exist in the scalar potential as three invariants can be formed from the tensor products

$$\mathbf{15'} \otimes \mathbf{15'} \otimes \mathbf{1\bar{5}'} \otimes \mathbf{1\bar{5}'} = \mathbf{1}_{\mathbf{45}\otimes\mathbf{\overline{45}}} + \mathbf{1}_{\mathbf{60}\otimes\mathbf{\overline{60}}} + \mathbf{1}_{\mathbf{15'}\otimes\mathbf{1\bar{5}'}} + \text{nonsinglet}, \qquad (3.8)$$

where for instance $\mathbf{1}_{\mathbf{45}\otimes\mathbf{\overline{45}}}$ stems from symmetrical tensor product of $\mathbf{45}_s \otimes \mathbf{\overline{45}}_s$. The invariants formed by the tensor products can be calculated by considering all the Clebsch-Gordan coefficients. From there we can calculate the one-loop beta functions for all the scalar quartic couplings [110]. A priori these three $\lambda_{\mathbf{1}_i}$ couplings are independent of each other and one has to perform experiments to obtain them independently. However, since we do not have any prior information about them, and experiments at first stage can only measure the S particle's mass, we have to make some assumptions regarding $\lambda_{\mathbf{1}_i}$. We simplify our calculation by assuming that each $\lambda_{\mathbf{1}_i}$ has roughly the same order, i.e. we normalize $\lambda_{\mathbf{1}_i} \approx \lambda_S/3$ such that the mass m_S of S can be obtained from the Lagrangian. Attentive reader may have noticed already that the bare mass term m_S does not appear in Eq. (3.3) due to scale invariance. The mass of S field is also generated radiatively and can be obtained from self-consistent mean field (SCMF) approximation [111] after $\langle S^\dagger S \rangle$ is formed, where the condensate mean field serves as a backreaction source to the S field. The mass for S is obtained from

$$\frac{\lambda_S}{2}(S^\dagger S)(S^\dagger S) \rightarrow \lambda_S \langle S^\dagger S \rangle S^\dagger S = \lambda_S \Lambda^2 S^\dagger S. \qquad (3.9)$$

The SCMF technique is known as bosonization in condensed matter theory and it is usually applied to the fermionic condensate. We will study SCMF also in Chapter 4 and we refer the reader to Appendix B for more details. We can think of the mass term of S as being sourced by the background vacuum of the $\langle S^\dagger S \rangle$ condensate. Once the dimensional transmutation
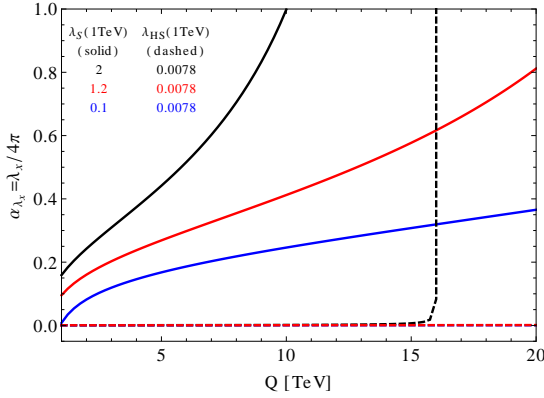
Figure 3.1: The running of scalar couplings with some generic boundary conditions at the scale of $1\,\mathrm{TeV}$. Increasing the mass of S will increase the coupling λ_S, which will drive the theory into the nonperturbative regime at $\mathcal{O}(10)\,\mathrm{TeV}$.

occurs, the coupling λ_S dictates the mass $m_S^2 = \lambda_S \Lambda^2$, while the mixing parameter λ_{HS} determines m_h. As the couplings and the masses are related, our model is very predictive. Note that the large m_S will cancel the negative contribution from λ_{HS} term after EWSB, preventing the S field from obtaining nonzero VEV and hence the $SU(3)_c$ symmetry is not spontaneously broken.

From the RGE analysis we obtain the running of scalar couplings once the condensation scale is set. The resulting RGE for certain generic values of $\lambda_S(\Lambda = 1\,\mathrm{TeV})$ is shown in Fig. 3.1. Remember that the coupling λ_{HS} is set once the condensation scale is fixed, as they are related by the measured Higgs mass m_h. As we demand that theory is perturbative, and since the mass m_S is proportional to λ_S, we cannot tune the mass term to be heavier like most of the beyond the SM extension due to the emergence of Landau pole. The upper bound on m_S is obtained by demanding perturbativity in our simplest scenario, and other more realistic model with additional particles would alter the upper bound significantly. The mass lower bound can be obtained from collider searches, as we will discuss in the next section. The running of λ_{HS} is relatively slow as it is technically nature in the RGE and will become nonperturbative when λ_S hits the Landau pole. The coupling λ_H is subsequently driven to a Landau pole once λ_{HS} and λ_S become nonperturbative.

At the RGE analysis it seems that our model does not solve the hierarchy problem, as we would require new physics at $\mathcal{O}(10)\,\mathrm{TeV}$. We would like to stress that Fig. 3.1 is obtained by our simple assumptions from above, and other RGE scenarios will be obtained if the parameters λ_{1_i} and the confinement scale Λ are varied independently, which is possible as the coupling λ_{1_i} should be a priori independent. In this thesis we have introduced the simplest extension of a QCD scalar boson to achieve EWSB, realistic models which include dark matter (DM) and neutrinos that coupled to the new sector might change the RGE for λ_S substantially. For instance adding new fermions which couple to our colored scalar will decrease the running of λ_S. The existence of Landau pole might be a signal of nonperturbativity, or it might signal the need for more realistic models. We will leave the UV completion issue for the future, and stress that more realistic model building would need to take other physics beyond the SM into account. But we stress that our simple model with minimalistic assumptions and the requirement of low UV scale with the assumption of perturbativity can be tested or ruled out at the LHC.
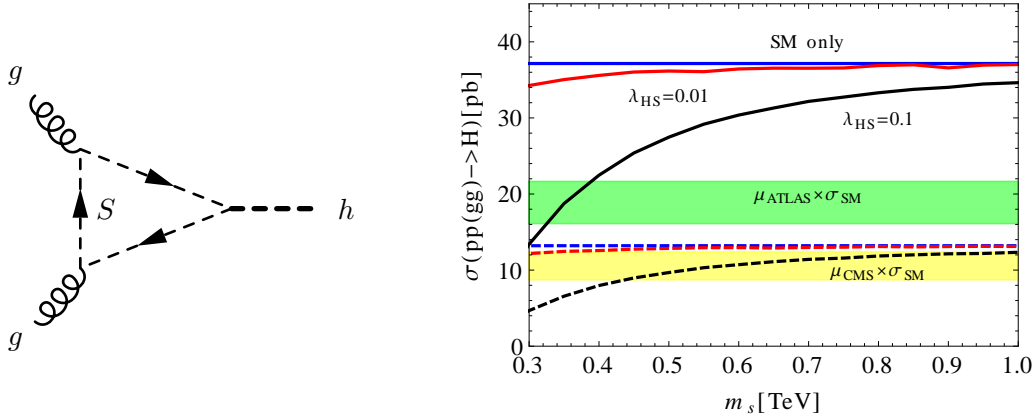
Figure 3.2.: (Left) The contribution of S to the Higgs production in the gluon fusion channel. (Right) The Higgs production cross section from the gluon fusion channel at NLO is calculated for different values of λ_{HS} and m_S. The solid (dashed) curves represent the $\sigma(gg \to h)$ prediction at $\sqrt{s} = 14\,\text{TeV}$ (8 TeV). The combined signal strength μ for ATLAS [112] and CMS [113] is shown where we have assumed a SM-like BR.

3.3. Collider Phenomenology

3.3.1. Higgs Production Cross Section in Gluon Fusion

As the scalar S is coupled to the gluon, it can alter the Higgs production rate in the gluon fusion channel due to Eq. (2.44). We have calculated $\sigma(pp \to h + X)$ to next-to-leading order (NLO) with this additional scalar, with the general formula for the hadronic cross section of the Higgs production via gluon fusion given as

$$\sigma(pp \to h + X) = \sum_{a,b} \int_0^1 \mathrm{d}x_1 \mathrm{d}x_2 \mathrm{d}z \, f_a(x_1, \mu_F^2) f_b(x_2, \mu_F^2) \delta\left(x - \frac{\tau_h}{x_1 x_2}\right) \hat{\sigma}_{ab}(z), \qquad (3.10)$$

with $\tau_h = m_h^2/s$, where s is the center-of-mass energy squared. The term μ_F represents the factorization scale for the parton density function (PDF) $f_{a,b}$. The cross section $\hat{\sigma}_{ab}$ includes all the partonic processes of $ab \to h + X$ at the center-of-mass energy $\hat{s} = x_1 x_2 s$ with $a, b = g, q, \bar{q}$. The additional color scalar S in our model contributes to the Higgs production in gluon fusion via loop, see Fig. 3.2. We followed the calculation of Ref. [114] and utilized the heavy scalar approximation. For the case of the SM, we have checked our calculation against the automated calculation from HDECAY [115], HIGLU [116], and iHixs [117]. The PDF parameterization of MSTW2008 [118] implemented in LHAPDF [119] has been utilized in our computation, where we have set the factorization scale μ_F and the renormalization scale μ_R to be at m_h. The zero-width approximation for the Higgs boson has been utilized to simplify the calculation. The leading-order (LO) partonic cross section of the gluon fusion process depends on the couplings in the following way:

$$\hat{\sigma}_{gg} = \frac{G_\mu \alpha_s^2(\mu_R)}{128\sqrt{2}\pi} \left| C(\boldsymbol{3})\mathcal{G}_t + C(\boldsymbol{S})\frac{\lambda_{HS}v^2}{2m_S^2}\mathcal{G}_S \right|^2, \qquad (3.11)$$

where $C(\boldsymbol{R})$ is the index of the R representation for bosons and fermions listed in Table 3.1. The $\overline{\text{MS}}$ strong coupling α_s is evaluated at the scale of μ_R. We only consider the top quark and S scalar contributions, with their Harmonic Polylogarithms $\mathcal{G}_{S,t}$ given as
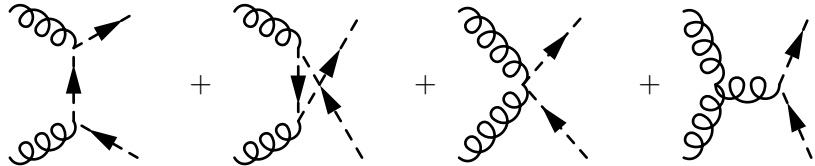
$$
\mathcal{G}_t = -\frac{m_t^2}{m_h^2}\left[8 - 4\left(1 - 4\frac{m_t^2}{m_h^2}\right)\ln^2\left(\frac{\sqrt{1 - 4m_t^2/m_h^2} - 1}{\sqrt{1 - 4m_t^2/m_h^2} + 1}\right)\right],
$$

$$
\mathcal{G}_S = 4\frac{m_S^2}{m_h^2}\left[1 + \frac{m_S^2}{m_h^2}\ln^2\left(\frac{\sqrt{1 - 4m_S^2/m_h^2} - 1}{\sqrt{1 - 4m_S^2/m_h^2} + 1}\right)\right]. \tag{3.12}
$$

For this thesis, we have calculated the Higgs production cross section via gluon fusion up to NLO including the Altarelli-Parisi splitting function. The result is too tedious to be shown and we refer the reader to Ref. [114] for the technical details. The resulting NLO production cross section is shown in Fig. 3.2 (Right).

Since our simplest extension of QCD does not modify the branching ratio (BR) of the SM Higgs[3], the signal strength μ times $\sigma(pp \to h)_{\text{SM}}$ from our model's prediction can be compared to the measurements by ATLAS [112] and CMS [113]. Depending on the coupling λ_{HS} and the mass of S, the S field decreases the Higgs gluon fusion production rate, to almost half the SM rate for large value of λ_{HS} (small Λ) and small m_S. Contrary to the usual color scalar extension of the SM [120], we obtain a suppression of the $gg \to h$ production rate instead of enhancement due to the negative sign of λ_{HS}, which is crucial for EWSB.

3.3.2. Colored Scalar Boson Production

As the LHC is mainly a gluon collider, our colored S boson can be produced at the LHC, with the dominating LO production channel $gg \to S_i^* S_j$ given by

$$\tag{3.13}$$

The LO pair production of colored scalars charged under higher QCD representation in the gluon fusion channel has been calculated in Refs. [121–125] and the relevant result for our case is given by

$$
\sigma(pp \to SS^*) = \int_0^1 \mathrm{d}x_1 \mathrm{d}x_2 \mathrm{d}z\ f_g(x_1, \mu_F^2) f_g(x_2, \mu_F^2) \hat{\sigma}(gg \to SS^*), \tag{3.14}
$$

with the partonic cross section given as

$$
\hat{\sigma}(gg \to SS^*) = \frac{\pi \alpha_s^2(\mu_R)}{96s}\left[y(41 - 31y^2) + (18y^2 - y^4 - 17)\ln\left|\frac{y+1}{y-1}\right|\right], \tag{3.15}
$$

---

[3]The decay $h \to \gamma\gamma$ is modified with the U(1) accidental symmetry which we will discuss later, but this loop induced decay is very small compared to the tree-level decays.

Figure 3.3: The S pair production cross section from gluon fusion channel is calculated for different values of m_S. The 95% confidence level exclusion limit on $\sigma \times$ BR for $\sqrt{s} = 7\,\text{TeV}$ by ATLAS is plotted for the lower mass bound. We assume 100% BR of $\langle S^\dagger S \rangle$ into two jets.
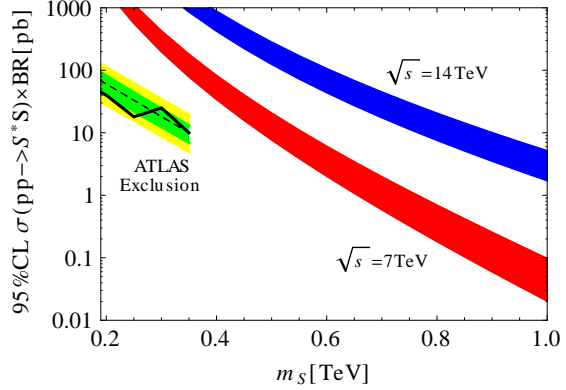
where $y = \sqrt{1 - 4m_S^2/s}$. The resulting two S particles will form a bound state pair each, with each pair decaying predominantly to gg (2 jets) or to Higgs particles. As we demand the condensate $\langle S^\dagger S \rangle$ to trigger EWSB, it has to be heavier than the Higgs, and therefore will decay to Higgs particles or two gluons. For the case when the condensate mixes with the Higgs, the BR of $h \to b\bar{b}$ for the final state dominates. While if $\langle S^\dagger S \rangle$ decays into two gluons, we would expect two jets emerge as final state decay products. Taking both possibilities into account, we would expect almost 70% for $S^* S \to jjjj$ in the total cross section.

The prediction of the production cross section times branching ratio for our model is given in Fig. 3.3. Like in previous section, the `MSTW2008` parameterization of PDF implemented in `LHAPDF` is utilized in our calculation with the factorization scale μ_F and the renormalization scale μ_R set to be at m_S. The width of the color band in Fig. 3.3 represents the theoretical uncertainty on factorization and renormalization scale and the α_s uncertainty from RGE with extra S contribution. Note that we did not consider the bound state and fragmentation study in our analysis, which would require a dedicated study. As every $\langle S^\dagger S \rangle$ bound state will decay predominantly into 2 jets and only events with more than 2 jets will be triggered at the LHC, we can only compare the model's prediction with hadron collider experimental results if we consider the production of more than one condensate. For the simplest case we consider the production of two condensates resulting from the processes in Eq. 3.13. We can impose a lower mass limit on our colored scalar with the ATLAS exclusion limit on pair production of massive colored scalar decaying to four jets [126]. We have assumed 100% BR to four jets for the sake of comparison. From the ATLAS searches, $m_S \lesssim 350\,\text{GeV}$ is excluded at 95% confidence level and serves as our lower bound on m_S. Combining this result with the perturbative upper bound from the triviality bound in Sec. 3.2, the mass parameter of S in our simple model is constrained from both ends, i.e.

$$350\,\text{GeV} \lesssim m_S \lesssim 3\,\text{TeV}, \tag{3.16}$$

which can be probed or ruled out by the LHC.

In principle exotic condensate such as condensate of S and quarks can be formed, it turns out that to contract the $\mathbf{15'}$ index with the fundamental $\mathbf{3}$ to form a singlet, at least four quarks are needed, i.e. $\langle qqqqS^* \rangle$ can be formed. In principle this exotic condensate can be produced at the LHC. However, as the S sector contains an accidental U(1) symmetry
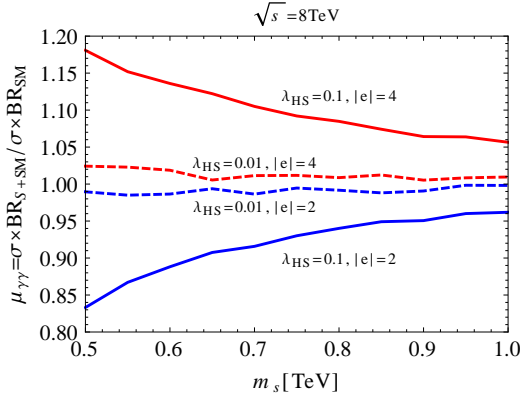
Figure 3.4: The signal strength of $h \rightarrow \gamma\gamma$ branching ratio with the additional colored S contribution relative to the SM prediction are shown for different electric charges e and λ_{HS} for S. The large e has to compensate the suppression of production cross section for $\mu_{\gamma\gamma}$ enhancement.

(see below) and if this global symmetry is not broken, such exotic bound state are required to be pair produced. We therefore expect that the production of this exotic particles is a subleading effect as the exotics are much heavier than the simplest $\langle S^\dagger S \rangle$ state. Let us discuss some other interesting phenomenologies regarding this accidental symmetry.

3.3.3. Accidental Symmetry

The colored S field in Eq. (3.3) possesses an accidental U(1) symmetry

$$S \rightarrow e^{i\theta} S \tag{3.17}$$

due to the absence of a cubic term as classical scale invariance is imposed in the Lagrangian. We can have interesting phenomenology depending on how this accidental symmetry is identified. Let us imagine a scenario where the scalar "proton", i.e. a bound state of $\langle SSS \rangle$ exists. Due to the accidental U(1) symmetry, this particle is stable, and can serve as a good DM candidate. However, like the case of baryon, we need to explain the origin of $\langle SSS \rangle - \overline{\langle SSS \rangle}$ asymmetry, which is usually very involved.

A more interesting possibility for rich collider phenomenology is when the accidental symmetry is identified with the local $U(1)_Y$ of the SM, i.e. the S particle is electromagnetically charged. For instance the $h \rightarrow \gamma\gamma$ decay channel is enhanced by the additional S running in the loop. Enhancement of $h \rightarrow \gamma\gamma$ is obtained due to the minus sign of λ_{HS} [120], contrary to the usual suppression factor obtained in other typical scalar extension with positive coupling between the Higgs and the additional scalar particle [127]. Strong enhancement of the signal strength $\mu_{\gamma\gamma}$ for different values of m_S, λ_{HS} and electric charge can be obtained, with the result normalized to the SM prediction shown in Fig. 3.4. As we have mentioned before in Sec. 3.3.1, the negative sign in the λ_{HS} term suppresses the Higgs production cross section in gluon fusion channel, while enhancing the signal strength $\mu_{\gamma\gamma}$. The combined effect of $\sigma \times$ BR can be only enhanced by increasing the electric charge of S or λ_{HS} to compensate the suppression of production cross section. Comparing to $\mu_{\gamma\gamma} \approx 1.57$ (1.13) reported by ATLAS [112] (CMS [113]) with the average $\mu_{\gamma\gamma} \approx 1.35$, our simplest model would require relatively large electric charge to explain the large $h \rightarrow \gamma\gamma$ anomaly for large m_S. If the accidental symmetry is indeed a local abelian electromagnetic gauge group, the large electric charge provides another possibility to study the S particle production via Drell-Yan processes in a linear collider, which we postpone for future analysis.

3.4. Confinement of Strongly Coupled Scalar Field

In the previous sections we have discussed the perturbative aspects of the colored scalar S. We have restricted the nonperturbative aspect of the model to the upscaling of the gap equation in Eq. (3.1). Note that it is highly nontrivial to obtain the inequality of Eq. (3.1) and it turns out that the condition in Eq. (3.1) is even harder to be proven for the scalar QCD case. But before we highlight the challenges, let us turn to the example of fermionic QCD.

An analytical way to understand confinement of QCD in the quark sector is to calculate the scaling of the gap equation from the Dyson-Schwinger equation (DSE)

$$\text{(3.18)}$$

where simplification with rainbow-ladder approximation has been utilized and only the LO contribution is kept in our analysis, i.e. we have dropped the dressed propagator for the gluon in the last term of Eq. (3.18). Without further simplification, we would require the DSE of the gluon propagator and the three-point function, which would make this equation very hard to solve. We will approximate the one-particle irreducible (1PI) three-point function by the tree level value $-ig_s\gamma^\nu$. Written in full equation

$$iS^{-1}(p) = \not{p} - m - ig_s^2 \int \frac{\mathrm{d}^4k}{(2\pi)^4}\gamma^\mu G_{\mu\nu}(p-k)S(k)\gamma^\nu, \tag{3.19}$$

with the dressed propagator for the quark given as

$$S(p) = \frac{i}{Z(p)\not{p} - \Sigma(p)}. \tag{3.20}$$

The wave function $Z(p)$ and self-energy $\Sigma(p)$ are both scalar functions of momentum. As it turns out, the self-energy $\Sigma(p)$ is the crucial part that determines the effective mass generated by dimensional transmutation of QCD coupling g_s. From the matrix structure of the $\not{p}$, the wave function and the self-energy term can be separately solved. Rearranging Eq. (3.19) and working in Landau gauge, the wave function $Z(p) = 1$ for any self-energy value, while the self-energy becomes

$$\begin{aligned}
\Sigma(p) &= m + 3g_s^2 C_2 \int \frac{\mathrm{d}^4k}{(2\pi)^4}\frac{\Sigma(k)}{(p-k)^2(k^2+\Sigma^2(k))} \\
&= m + \frac{C_2\alpha_s}{2X}\int_0^p \mathrm{d}k\frac{k^3\Sigma(k)}{p^2(k^2+\Sigma^2(k))} + \frac{C_s\alpha_s}{2X}\int_p^\infty \mathrm{d}k\frac{k\Sigma(k)}{k^2+\Sigma^2(k)},
\end{aligned} \tag{3.21}$$

after the angular variables are integrated. The value X is $\pi/3$ in our case, however it is gauge and truncation scheme dependent and different values ranging from 0.6 to $\pi/3$ have been obtained [103–105]. We will keep X to be free in our general analysis. Differentiating Eq. (3.21) and rearranging the terms, we obtain the differential equation

$$p^2\Sigma'' + 3p\Sigma' + \frac{C_2\alpha_s}{X}\frac{p^2\Sigma}{p^2+\Sigma^2} = 0, \tag{3.22}$$

which can be further linearized to a Fredholm integral equation [103, 128, 129] for large p when Σ in the denominator of the last term is neglected. Using the ansatz $\Sigma \sim (p)^a$, we obtain that the power a must satisfy
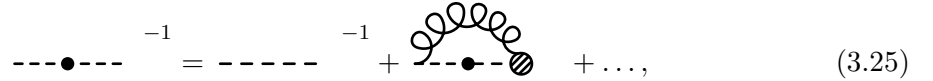
$$a = -1 + \sqrt{1 - \frac{C_2 \alpha_s}{X}}.$$
(3.23)

Within certain truncation scheme, in order to know whether dynamical chiral symmetry is broken and confinement has taken place, we need to obtain the critical value X in

$$C_2(\psi)\alpha(\Lambda) \gtrsim X.$$
(3.24)

Intuitively, if $C_2\alpha(\Lambda) > X$, we can satisfy the finite boundary condition at the UV for the oscillatory differential equation, even if $m \to 0$. For the case of $C_2\alpha(\Lambda) < X$, the boundary condition cannot be satisfied and hence dynamical chiral symmetry breaking is excluded. Now comes the subtlety that one has to be careful in obtaining the exact bound of X as the value X is gauge and truncation scheme dependent. Lowering X will enable us to consider lower representation of S but throughout our analysis in this chapter we have assumed the conservative bound $X > 0.8$. We refer the reader to Refs. [103–105] for more details.

Let us turn to the case of our interest in this thesis, i.e. the nonperturbative aspects of scalar QCD. The DSE for scalar QCD is given as

$$\cdots\bullet\cdots^{-1} = \texttt{-----}^{-1} + \texttt{quark}\cdots\bullet\texttt{-}\diagup\diagdown + \ldots,$$
(3.25)

where we have dropped all the subleading terms without gauge coupling. Written in full equation form

$$Z(p)p^2 + \Sigma^2(p) = p^2 + \frac{3C_2\alpha_s}{2\pi}\left(\int_0^p \mathrm{d}q \frac{q^5}{p^2(Z(q)q^2 + \Sigma^2(q))} + \int_p^\infty \mathrm{d}q \frac{qp^2}{Z(q)q^2 + \Sigma^2(q)}\right),$$
(3.26)

we notice that the wave function and the self-energy term for scalar DSE are not separable as the scalar field does not possess the γ matrix structure in the DSE, contrary to the case for quarks. Furthermore, the scalar DSE integral equation is not linearizable, contrary to the DSE for quark. The main reason for such difficulty is due to the lack of a confinement order parameter for scalar QCD. Comparing to the case of ordinary QCD with fermions, the order parameter for confinement can be related to the degree of chiral symmetry breaking. Although we cannot solve Eq. (3.25), numerical lattice QCD may shed light on the solution, which we leave for the experts.

We instead try to understand confinement from a perturbative perspective. We have utilized the scaling $\Sigma \sim (p)^a$ from Eq. (3.23) to obtain Eq. (3.24) for the case of fermionic DSE. The a parameter is actually the negative part of anomalous dimension $\gamma_{\langle \bar\psi\psi \rangle} = -a$ for the self-energy $\Sigma(p)$ of the quark condensate. From the perturbative calculation, the anomalous dimension of operator $\langle S^\dagger S \rangle$ can be calculated from the wave function renormalization of S

and renormalization of the composite operator $S^\dagger S$:

$$ \tag{3.27} $$

It turns out that when we calculate the anomalous dimension for $\langle \bar{\psi}\psi \rangle$ in the same representation with the scalar case above, both the anomalous dimensions turn out to be the same

$$ \gamma_{\langle \bar{\psi}\psi \rangle} = \gamma_{\langle S^\dagger S \rangle} + \mathcal{O}(\lambda_S). \tag{3.28} $$

up to the correction subleading correction of $\mathcal{O}(\lambda_S)$. Hence we can conjecture that the relevant order parameter $C_2 \alpha_s$ at LO for determining confinement in QCD should be the same for both fermion and scalar in the same representation, which we have assumed throughout the thesis. In fact it has been argued that the scaling property for scalar and quark propagator in the infrared is identical [130] and this result can be verified in lattice QCD.

The QCD coupling α_s also becomes nonperturbative in the TeV regime even though the coupling is pretty small. From the perturbative RGE of α_s, the one-loop beta function guarantees asymptotic freedom for α_s with our additional **15′** scalar field. However at two-loop order, the asymptotic freedom is lost. This comes from the large C_2 value which is responsible for high energy condensation and as a consequence, the exact evolution of strong coupling cannot be perturbatively calculated in the TeV regime. One has to rely on nonperturbative methods such as Functional Renormalization Group (FRG) [131] or lattice QCD to obtain the running of α_s. The strong coupling may become perturbative again for sufficiently small α_s or with additional vector bosons charged under QCD at high energy such that perturbative asymptotic freedom is restored. A similar conclusion was made also in Ref. [107]. On the other hand, measuring α_s at high energy will provide another independent test for our model, and the plan of the LHC is to probe α_s up to $2\,\mathrm{TeV}$.

3.5. Summary

In this chapter we have introduced a minimalistic classically scale invariant extension of the SM to trigger EWSB radiatively by the condensation of a new scalar charged under QCD. The condensation scale of the colored scalar particle, which is obtained by the running of strong coupling, generates the EW scale dynamically. As the LHC is essentially a gluon collider, this new colored scalar particle can be pair produced and can be probed by ATLAS and CMS. With the theoretical and experimental constraints imposed, the mass of this scalar particle should be in the range of $350\,\mathrm{GeV}$ to $10\,\mathrm{TeV}$. Additionally, the production cross section of the SM Higgs particle in gluon fusion channel will be modified if such a colored scalar boson exists. We have seen that the model proposed in this chapter generates the EW scale from a direct condensation scale transmission. In the next chapter, we will discuss another model based on indirect scale transmission.

Scale Invariance and Dark Sector

In this chapter we will introduce an indirect scale transmission mechanism to trigger electroweak symmetry breaking (EWSB) radiatively from a classically scale invariant extension of the Standard Model (SM). We will introduce a classically scale invariant model with a strongly coupled hidden sector, mimicking the success of QCD. Additional fermions charged under this hidden gauge group, which are invariant under the additional continuous flavor symmetry, will undergo spontaneous chiral symmetry breaking when the hidden gauge coupling evolves to nonperturbative regime. The breaking scale is then transmitted to the SM Higgs sector, triggering the EWSB. The model contains dark matter (DM) candidates, which are pseudo Nambu-Goldstone bosons (PNGB) resulting from spontaneous chiral symmetry breaking. The phase transition in the dark and electroweak (EW) sector will be discussed. This chapter follows the original works [100, 101] resulted from collaboration with Martin Holthausen, Jisuke Kubo, and Manfred Lindner. As the results of Ref. [100] precede those in Ref. [101], this chapter will contain more accurate analysis and we will present only the updated plots, leaving those which are obsolete. All the relevant plots and results are reproduced from Refs. [100, 101] with reprint permission.

4.1. A Scale Invariant Hidden Sector Extension of the SM

As we have mentioned in Sec. 2.6, the key to transmit the scale of chiral symmetry breaking from a dark sector to the Higgs sector is the Higgs portal term

$$\mathcal{L} \supset \lambda_{HS} S^\dagger S H^\dagger H, \tag{4.1}$$

where S could be a real or complex scalar, charged or neutral under certain gauge groups. For simplicity we only consider a real singlet S field which is the only field that communicates between the SM (via Higgs portal) and the dark sector. We propose a model with a hidden $SU(3)_H$ gauge sector coupled to the SM via this real singlet scalar S, similar to Refs. [96–98]. Our work goes beyond Refs. [96–98] as the Nambu-Jona-Lasinio (NJL) [132] method is utilized throughout this work to calculate the mass spectrum of the relevant fields and the couplings in a coherent and consistent manner. The work in Refs. [96–98] used the effective field theory (EFT) approach to describe the low energy interactions of the new particles, resulting in more low energy parameters which are free and in general not restrictive. The scarcity of parameters in our approach allows us to relate and exclude certain low energy

EFT parameters in Refs. [96–98].

The hidden sector Lagrangian is given by

$$\mathcal{L}_H = -\frac{1}{2} \operatorname{Tr} F^2 + \operatorname{Tr} \bar{\psi}(i\gamma^\mu D_\mu - yS)\psi \ , \tag{4.2}$$

where the hidden sector fermion ψ transforms under fundamental representation of $\mathrm{SU}(3)_H$ and possesses a chiral $\mathrm{SU}(3)_L \times \mathrm{SU}(3)_R$ symmetry. The F term is the usual kinetic term for the hidden $\mathrm{SU}(3)_H$ gauge field. The trace is taken over the flavor and hidden color indices with or without spinor indices, which should be clear from the context. The covariant derivative is defined as $D_\mu = \partial_\mu - ig_4\lambda^a G^a_\mu$ and λ^a are the usual SU(3) Gell-Mann matrices. The total Lagrangian $\mathcal{L}_T = \mathcal{L}_H + \mathcal{L}_{SM+S}$ consists of the hidden sector and the SM interactions, along with the modified scalar potential

$$V_{SM+S} = \lambda_H (H^\dagger H)^2 + \frac{1}{4}\lambda_S S^4 - \frac{1}{2}\lambda_{HS} S^2 (H^\dagger H), \tag{4.3}$$

where H is the SM Higgs doublet field defined in Eq. (2.19). No mass term and dimensionful parameter appears in the classical Lagrangian above due to the requirement of classical scale invariance, which itself is anomalous. This symmetry is violated at quantum level by the nonperturbative effect of dynamical chiral symmetry breaking, which generates a condensation scale. This scale is transmitted to the SM sector by the singlet S and subsequently a mass term in the Higgs potential is generated. The whole scale generation process can be summarized as

$$\langle \bar{\psi}\psi \rangle \to \langle S \rangle \to \langle H \rangle. \tag{4.4}$$

The EWSB scale is dynamically generated. After spontaneous chiral symmetry breaking, the dark pions exist in the form of PNGB and have the mass scale of the order of the condensation scale, close to the EW scale. As we have nonvanishing Yukawa interaction between ψ and S, a hidden Yukawa coupling y breaks the chiral $\mathrm{SU}(3)_L \times \mathrm{SU}(3)_R$ symmetry of ψ explicitly to the diagonal $\mathrm{SU}(3)_V$, and hence only PNGBs are obtained instead of massless Nambu-Goldstone particles. The dark pions are stable due to the unbroken $\mathrm{SU}(3)_V$ symmetry and they could serve as DM candidates. Unlike most of the DM models, no additional discrete symmetry is required to guarantee the stability of dark sector in our model. The scale tumbling mechanism described above provides a good motivation on the common origin for the EW and DM scale, which is largely motivated by the WIMP miracle. Note that in our model we have chosen a gauge group of $\mathrm{SU}(3)_H$ and 3 flavors of hidden sector fermions charged under the fundamental representation of this non-abelian gauge group, this is because we can rescale the NJL parameters from ordinary QCD to fit our model in order to analyze some nonperturbative aspects such as confinement, condensation and chiral symmetry breaking without utilizing nonperturbative calculations. In principle other non-abelian gauge groups with a different number of fermions charged under different representation can also be used to construct models for explaining the origin of the EW and DM scale, however one would require to calculate the NJL parameters nonperturbatively. Our simple model, which mimics the success of QCD, serves as a prototype of EW scale generation via an indirect scale transmission from a strongly coupled hidden sector.

4.1.1. NJL Treatment of the Low Energy Hidden Sector

Dynamical chiral symmetry breaking can be analyzed with the NJL approach

$$\mathcal{L}_{\text{NJL}} = \text{Tr}\,\bar{\psi}(i\gamma^\mu\partial_\mu - yS)\psi + 2G\,\text{Tr}\,\Phi^\dagger\Phi + G_D(\det\Phi + h.c.), \tag{4.5}$$

which we will use as a low-energy approximation for Eq. (4.2) similar to QCD, where

$$\Phi_{ij} = \bar{\psi}_i(1-\gamma_5)\psi_j = \frac{1}{2}\lambda_{ji}^a\,\text{Tr}\,\bar{\psi}\lambda^a(1-\gamma_5)\psi,$$

$$(\Phi^\dagger)_{ij} = \bar{\psi}_i(1+\gamma_5)\psi_j = \frac{1}{2}\lambda_{ji}^a\,\text{Tr}\,\bar{\psi}\lambda^a(1+\gamma_5)\psi, \tag{4.6}$$

and λ^a are the Gell-Mann matrices with $\lambda^0 = \sqrt{2/3}\,\mathbb{1}$. The second term in Eq. (4.5) describes four-fermion interactions while the last term describes six-fermion interactions, which breaks the axial $U(1)_A$ symmetry [133–135]. We refer the reader to Appendix B for a quick relevant review of the NJL approach. For a more thorough review please refer to Refs. [111, 136–139]. The essence of NJL is as follows, the chiral symmetry in the dark sector is spontaneously broken due to nonperturbative effects of strongly interacting dark sector, dictated by the renormalization group of the hidden gauge coupling. The vacuum of the dark sector becomes nontrivial and subsequently the scalar condensates are formed. The dark fermion constituent mass is also dynamically generated. Also due to the explicit breaking of chiral symmetry by the Yukawa coupling y, PNGBs are obtained. All of this relevant physics happen simultaneously in the NJL model. Note that however NJL does not describe confinement.

Let us investigate the relevant parameters in the NJL approach for our model in more details. The effective Lagrangian $\mathcal{L}_{\text{NJL}}$ possesses four parameters, $y\,[0], G\,[-2], G_D\,[-5]$, and the cutoff $\Lambda\,[1]$, with the canonical mass dimension for each parameter given in the bracket. The parameters G, G_D and Λ are not independent as $\mathcal{L}_H$ has only two independent parameters and can be related by the NJL approach, typically

$$G^{1/2}\Lambda \sim |G_D|^{1/5}\Lambda \sim \mathcal{O}(1). \tag{4.7}$$

In principle G, G_D, Λ can be calculated from lattice QCD or Dyson-Schwinger equation (DSE), which is highly nontrivial for arbitrary gauge group with different fermionic representation. Instead, as we utilize a SU(3) gauge group for our hidden sector with 3 flavors of fermions, we can use the relations from observed hadron physics in QCD to scale up G, G_D, Λ to obtain the NJL parameters for our model. This allows us to circumvent the nonperturbative calculation.

To obtain the condensates from Eq. (4.5) we will use a self-consistent mean field (SCMF) approximation [111, 136, 137] to calculate the hadron spectrum in QCD. In essence, SCMF approach is a trick to integrate out the heavy modes of the fermions to obtain the bosonic condensate, while leaving the interaction between the condensates and heavy fermions intact. SCMF is known as bosonization approach in condensed matter physics or Hartree-Fock approximation in many-body physics. We refer the reader to the Appendix B for a quick review of relevant tools in bosonization in the NJL approach. Here we briefly outline this approximation method.

As the coupling g_4 becomes nonperturbative in the infrared (IR) region, a chiral symmetry breaking condensate

$$\langle \bar{\psi}_i \psi_j \rangle \equiv \widehat{\bar{\psi}_i \psi_j} = -\frac{1}{4G} \text{diag}(\sigma, \sigma, \sigma), \tag{4.8}$$

is generated by the dynamics of our theory. This condensate is a CP-even classical field $\sigma(x)$. The contraction denoted by $\widehat{}$ is defined w.r.t. the nontrivial mean field vacuum $|\text{VAC}\rangle = |[\sigma, \phi_a]\rangle$, which one can think of as the bosonic bound state of the fermion pair. The CP-odd effective field counterparts are given by the dark pions

$$\phi_a = -2iG \ \widehat{\bar{\psi}\gamma_5 \lambda^a \psi}, \tag{4.9}$$

normalized with the constant G such that ϕ has a proper mass dimension. We collect the relevant mean fields in

$$\widehat{\Phi} \equiv \varphi = -\frac{1}{4G} \left(\text{diag}(\sigma, \sigma, \sigma) + i(\lambda^a)^T \phi_a \right), \tag{4.10}$$

ignoring the analogous η or ρ mesons in our theory, and systematically normal order each fermion pair in Eq. (4.5) (see Appendix B) until the whole equation is divided into the sum

$$\mathcal{L}_{\text{NJL}} = \mathcal{L}_0 + \mathcal{L}_I, \tag{4.11}$$

where $\mathcal{L}_0$ represents the mean field dynamics which is of interest to us, and $\mathcal{L}_I$ describes the fluctuations. For consistency we require $\langle \text{VAC}|\mathcal{L}_I|\text{VAC}\rangle = 0$, i.e. we need to average out the fluctuations w.r.t. $|\text{VAC}\rangle$. Once the normal ordering is completed, we find the mean field Lagrangian to be

$$\begin{aligned}
\mathcal{L}_0 = &i \, \text{Tr} \, \bar{\psi}\gamma^\mu \partial_\mu \psi - \left(\sigma + yS - \frac{G_D}{8G^2}\sigma^2 \right) \text{Tr} \, \bar{\psi}\psi - i \, \text{Tr} \, \bar{\psi}\gamma_5 \phi \psi - \frac{1}{8G} \left(3\sigma^2 + 2\sum_{a=1}^{8} \phi_a \phi_a \right) \\
&+ \frac{G_D}{8G^2} \left(-\text{Tr} \, \bar{\psi}\phi^2 \psi + \sum_{a=1}^{8} \phi_a \phi_a \, \text{Tr} \, \bar{\psi}\psi + i\sigma \, \text{Tr} \, \bar{\psi}\gamma_5 \phi \psi + \frac{\sigma^3}{2G} + \frac{\sigma}{2G}\sum_{a=1}^{8} (\phi_a)^2 \right). \tag{4.12}
\end{aligned}$$

with the notation

$$\phi = \sum_{a=1}^{8} \phi_a \lambda^a. \tag{4.13}$$

Note that the trace acts on the dark color space, the spinor indices as well as the flavor structure, e.g. a full form of $\text{Tr} \, \bar{\psi}\psi$ is written as $\text{Tr} \, \bar{\psi}\psi = \bar{\psi}_{\alpha ia}\psi_{\alpha ia}$ with α representing the spinor index, i the dark color index, and a the flavor index. The Lagrangian (4.12) determines the dynamics of the effective condensate fields and their interaction with the heavy fermions. The bosonic fields have to be considered as propagating fields, even though they lack proper kinetic terms. This is because they are the physical degrees of freedom in low energy regime after bosonization. Eq. (4.12) determines all the coupling necessary for computing the mass spectrum for the bosons and serves as a starting point for us to calculate all the relevant effective couplings for DM interactions.

4.1.2. The Effective Potential and Symmetry Breaking

Now let us study the condensation in the hidden sector due to dimensional transmutation. We integrate out the fermion fields in $\mathcal{L}_0$ given in Eq. (4.12) to obtain the one-loop effective potential:

$$V_{\text{NJL}}(\sigma, S) = \frac{3}{8G}\sigma^2 - \frac{G_D}{16G^3}\sigma^3 - 3n_c \int \frac{\mathrm{d}^4 k}{i(2\pi)^4} \ln \det(\not{k} - M), \tag{4.14}$$

where the "constituent mass" M is given by[1]

$$M = \sigma + yS - \frac{G_D}{8G^2}\sigma^2. \tag{4.15}$$

The first two terms in Eq. (4.14) are obtained from "tree level" effective Lagrangian (4.12), while the last term encodes the one-loop contribution of the heavy fermion to the effective potential. See Appendix B for a short introduction to path integral bosonization approach. In this thesis we evaluate all the loop integrals with four-dimensional momentum cutoff Λ, in contrast to the three-dimensional momentum cutoff introduced in Refs. [111, 136, 137]. The potential is asymmetric in σ due to the anomaly term (the determinant) in Eq. (4.5). The full effective potential for our model is

$$V = V_{\text{SM}+S} + V_{\text{NJL}}, \tag{4.16}$$

which gives a full picture of how the scale transmission from chiral symmetry breaking to EWSB really works. The σ condensate formed by spontaneous chiral symmetry breaking influences the potential by shifting the S field in last term of Eq. (4.14). Hence S obtains a nonzero vacuum expectation value (VEV) and subsequently the Higgs field undergoes EWSB. As a consistency check, the spontaneous chiral symmetry breaking scale is not transmitted for $y \to 0$, as the scalar mediator S will not feel the shift in Eq. (4.14). In this case, the dark pions remains massless as they are true Nambu-Goldstone bosons.

The dimensionless parameters in our theory, $y, \lambda_H, \lambda_{HS}, \lambda_S$, remain as primary free parameters in our effective NJL theory. Once their values are given, the form of the effective potential is determined and the global minimum of the potential can be obtained. The vacuum subsequently determines the amount of scaling required for the dimensionful quantities G, G_D, Λ with the constraint that $\langle h \rangle = 246 \, \text{GeV}$. The parameters G, G_D and the phenomenological cutoff Λ for our models are determined from rescaled QCD values[2]

$$(G^{\text{QCD}})^{-1/2} = 461 \, \text{MeV}, \quad (-G_D^{\text{QCD}})^{-1/5} = 437 \, \text{MeV}, \quad \Lambda^{\text{QCD}} = 924 \, \text{MeV}, \tag{4.17}$$

according to their dimensions as

$$G = f^{-2}G^{\text{QCD}} \, , \; G_D = f^{-5}G_D^{\text{QCD}} \, , \; \Lambda = f\Lambda^{\text{QCD}}, \tag{4.18}$$

by a common rescaling factor f. We scale up all the dimensional parameters w.r.t. a fixed Higgs VEV. Again we stress that G, G_D, Λ are not free parameters in our theory. Once the

---

[1] M is the constituent dark fermion mass when all the bosonic fields obtain their VEVs.

[2] For the determination of QCD parameters we refer the reader to Refs. [100, 111, 136, 137].

dimensionless parameters are specified and the absolute minimum of the effective potential is determined, the mass spectrum of particles in the model can be calculated. At low energy we have three CP-even scalars h, S, σ, and eight CP-odd DM ϕ_a. The former mix with each other, and the SM Higgs-like particle with $m_h \approx 125\,\text{GeV}$ has to be identified with one of the mass eigenstates of the CP-even particles.

We remind the reader that h and S are propagating fields already at tree-level, but the bosonized fields, e.g. σ and ϕ_a, only become dynamical at one-loop order. The bosonized σ and ϕ do not have canonically normalized kinetic terms in the lowest order, therefore we can only determine the masses from the poles of the propagators $\Delta_{ij}(p^2) = i(\Gamma^{-1})_{ij}(p^2)$. At one-loop order the contributions to the inverse propagators Γ_{ij} $(i, j = h, S, \sigma)$ are determined via

$$
\begin{aligned}
\Gamma_{hh}(p^2) =& p^2 - 3\lambda_H \langle h \rangle^2 + \frac{1}{2}\lambda_{HS}\langle S \rangle^2, \quad \Gamma_{hS} = \lambda_{HS}\langle h \rangle \langle s \rangle, \quad \Gamma_{h\sigma} = 0, \\
\Gamma_{SS}(p^2) =& p^2 - 3\lambda_S \langle S \rangle^2 + \frac{1}{2}\lambda_{HS}\langle h \rangle^2 - 3n_c y^2 \int \frac{\mathrm{d}^4 k}{i(2\pi)^4} \frac{\text{Tr}(k+M)(\slashed{k} - \slashed{p} + M)}{(k^2 - M^2)((k-p)^2 - M^2)}, \\
\Gamma_{S\sigma}(p^2) =& -3n_c y \left(1 - \frac{G_D \langle \sigma \rangle}{4G^2}\right) \int \frac{\mathrm{d}^4 k}{i(2\pi)^4} \frac{\text{Tr}(k+M)(\slashed{k} - \slashed{p} + M)}{(k^2 - M^2)((k-p)^2 - M^2)}, \\
\Gamma_{\sigma\sigma}(p^2) =& \frac{3G_D \langle \sigma \rangle}{8G^3} - \frac{3}{4G} - 3n_c \left(1 - \frac{G_D \langle \sigma \rangle}{4G^2}\right)^2 \int \frac{\mathrm{d}^4 k}{i(2\pi)^4} \frac{\text{Tr}(k+M)(\slashed{k} - \slashed{p} + M)}{(k^2 - M^2)((k-p)^2 - M^2)} \\
& + 3n_c \frac{G_D}{G^2} \int \frac{\mathrm{d}^4 k}{i(2\pi)^4} \frac{M}{(k^2 - M^2)},
\end{aligned}
\tag{4.19}
$$

where the constituent mass M is determined from Eq. (4.15) with all the bosonic fields obtaining their VEVs. The integrals in Eq. (4.19) have to be regulated with a cutoff, which can be further simplified with the cutoff version of Passarino-Veltman functions [140], see Appendix C for more details. Once the propagators are diagonalized, the physical mass spectrum from the poles $\tilde{m}_1^2$, $\tilde{m}_2^2$ and $\tilde{m}_3^2$ can be obtained, and the corresponding eigenvectors $\xi^{(i)}$ can be computed from

$$
\Gamma_{ij}(\tilde{m}_k^2)\, \xi_j^{(k)} = 0,
\tag{4.20}
$$

which can be used to rotate the flavor eigenstates (h, S, σ) to the mass eigenstates (s_1, s_2, s_3)

$$
\begin{pmatrix} h \\ S \\ \sigma \end{pmatrix} = \begin{pmatrix} \xi_1^{(1)} & \xi_1^{(2)} & \xi_1^{(3)} \\ \xi_2^{(1)} & \xi_2^{(2)} & \xi_2^{(3)} \\ \xi_3^{(1)} & \xi_3^{(2)} & \xi_3^{(3)} \end{pmatrix} \begin{pmatrix} s_1 \\ s_2 \\ s_3 \end{pmatrix}.
\tag{4.21}
$$

Once we have rotated the fields to the mass basis, the wave function renormalization Z for each field can be calculated as

$$
Z_i^{-1} = \left. \frac{\mathrm{d}\Gamma_i(p^2)}{\mathrm{d}p^2} \right|_{p^2 = m_i^2}.
\tag{4.22}
$$

As we have argued in Sec. 2.6, we requires that any scale invariant extension of the SM needs to survive up to the Planck scale, should classical scale invariance be the solution to the hierarchy problem. This requirement restricts a sizable amount of parameter space in
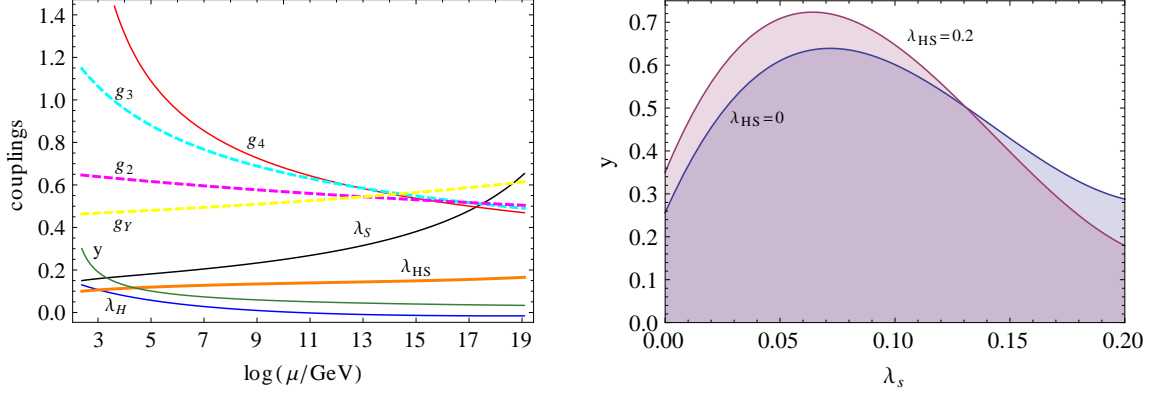
Figure 4.1.: (Left) The RG running for $g_4^2 = 4\pi$, $\lambda_H = 0.13$, $\lambda_S = 0.15$, $\lambda_{HS} = 0.1$, $y = 0.3$ with the boundary conditions given at $\mu = 1\,\text{TeV}$ are shown. We also show the running of the SM gauge couplings $g_Y = \sqrt{5/3}g_1$, g_2 and g_3. (Right) The allowed parameter regions for λ_S and y ($\mu = 1\,\text{TeV}$) for a given value of λ_{HS}.

low energy EFT approach of Refs. [96–98]. We require that all parameters do not destabilize the scalar potentials, and all the couplings do not hit a Landau pole up to the Planck scale in accordance to the RGE, i.e.

$$0 < \lambda_H < 4\pi, \quad 0 < \lambda_S < 4\pi, \quad 4\lambda_H\lambda_S - \lambda_{HS}^2 > 0. \tag{4.23}$$

These theoretical considerations restrict the parameter regions of λ_H, λ_S, λ_{HS} and y massively. We have calculated the relevant one-loop RGE for our model:

$$16\pi^2\beta_{\lambda_H} = \lambda_H(-9g_2^2 - 3g_1^2 + 12y_t^2) + 24\lambda_H^2 + \frac{3}{4}g_2^4 + \frac{3}{8}(g_1^2 + g_2^2)^2 - 6y_t^4 + \frac{1}{2}\lambda_{HS}^2,$$

$$16\pi^2\beta_{\lambda_{HS}} = -2\lambda_{HS}\left(2\lambda_{HS} - 3\lambda_S + \frac{9}{4}g_2^2 + \frac{3}{4}g_1^2 - 3y_t^2 - 6\lambda_H - 18y^2\right),$$

$$16\pi^2\beta_{\lambda_S} = 2\lambda_{HS}^2 + 18\lambda_S^2 + 72y^2\lambda_S - 18y^4,$$

$$16\pi^2\beta_y = 3y(7y^2 - 4g_4^2),$$

$$16\pi^2\beta_{g_4} = -9g_4^3. \tag{4.24}$$

The remaining SM RGEs are unchanged.

We can go beyond the perturbativity and vacuum stability requirement and restrict some boundary conditions based on theoretical reasoning. Since g_4 becomes nonperturbative at the vicinity of $\mu \approx 1\,\text{TeV}$, we demand that $g_4(\mu = 1\,\text{TeV}) \approx \sqrt{4\pi}$ for simplicity. Next we fix λ_H and λ_{HS} from the experimental Higgs mass measurement [6, 7]. Lowering $\lambda_H(\mu = 1\,\text{TeV}) < 0.13$ will make the Higgs vacuum unstable before Planck scale while increasing $\lambda_H(\mu = 1\,\text{TeV}) > 0.15$ will require a larger mixing with the S field to generate the correct Higgs mass, this scenario is strongly constrained [112, 113]. Therefore we restrict $\lambda_H(\mu = 1\,\text{TeV}) \in (0.13, 0.14)$ in our analysis. The λ_{HS}, λ_S and y couplings are restricted by the requirement of perturbativity and vacuum stability. At one-loop order, the RG evolution of the Yukawa coupling y is only influenced by the value of y and g_4. Hence with the boundary condition of g_4 fixed as mentioned above, the range of y valid up to Planck scale is naively

determined to be $y(\mu = 1\,\text{TeV}) \in (0, 0.6)$, as shown in Fig. 4.1 (right). As for the quartic S coupling, $\lambda_S(\mu = 1\,\text{TeV}) \in (0, 0.2)$ is sufficient to guarantee the running of coupling up to the Planck scale, without violating the vacuum stability and perturbativity constraint. Lastly once the range of λ_S is known, it is easy to determine the range of λ_{HS} from the last vacuum stability condition in Eq. (4.23), which typically has the same parameter space as λ_S. In Fig. 4.1 (left) the running of the relevant couplings are shown for some generic boundary conditions imposed within the discussed allowed range. The gauge coupling g_4 for the dark sector possesses a similar value to the SM QCD gauge coupling g_3 at the Planck scale. This observation is intriguing if we assume that both the strongly coupled sectors possess a common origin at the Planck scale, as this might explain why

$$\Lambda_{\text{QCD}} \sim \Lambda \ll M_{pl}, \tag{4.25}$$

which can be traced back to the different running of strong couplings due to a different number of fermions charged under the hidden gauge group. The strong hidden sector coupling g_4 grows nonperturbative at a higher scale than QCD due to the smaller number of flavors. This observation is also fascinating for the DM phenomenology, as the similarity for both strongly coupled sectors could explain the similar magnitude of relic abundance

$$\Omega_c \hat{h}^2 \sim \Omega_b \hat{h}^2, \tag{4.26}$$

for the DM and baryons. Once the parameter space is fixed from the constraints above, the masses and couplings for the scalars can be calculated as described in the previous section and furthermore, the properties of our DM candidate can be determined, which we now describe.

4.2. Dark Pions as Dark Matter Candidates

Before we move on to calculate the relevant interaction for the DM, let us briefly discuss the folklore of the theoretical limit imposed on strongly interacting DM and how such naive estimation could be misleading. In general the leading-order (LO) relic abundance of the DM from thermal production can be approximated to be

$$\Omega_c h^2 \sim \frac{m_{\text{DM}}}{\langle \bar{v}\sigma \rangle T_f}, \tag{4.27}$$

where T_f denotes the freeze out temperature and m_{DM} denotes the mass of the DM particle. The quantity $\langle \bar{v}\sigma \rangle$ represents the velocity-averaged annihilation cross section of the DM particles into the SM particles.

There exist a common folklore in the DM model building community that strongly interacting DM will require that the mass of such DM candidate to heavier than $\sim 20\,\text{TeV}$ [141] in order to produce the correct relic abundance. This is because the DM, in a form of bound state, generally has $m_{\text{DM}} \sim \Lambda$ and the cross section $\langle \bar{v}\sigma \rangle \sim \Lambda^{-2}$ from naive dimensional analysis. One can compare the case of proton and its self interaction in the QCD case. The mass and the annihilation cross section of the DM determine the relic abundance directly and there is no way to escape the estimation that $\Lambda \sim 20\,\text{TeV}$. This conclusion is however

incorrect, if the strongly interacting DM is a PNGB [142]. In this case, the mass of the DM particle is separated from the annihilation cross section, enabling us to have more freedom to obtain a TeV scale DM in a very natural way. The lightness of the PNGB DM is due to the approximate chiral symmetry of the fermionic sector and the coupling that determines the annihilation cross section is determined by the nonperturbative confinement scale Λ. As a comparison, one observes that the QCD pions are significantly lighter than the baryonic counterparts.

One might worry that it is difficult to build a model with interacting dark pions as DM candidates. As we have learned from QCD, the QCD pions can decay into two photons and hence are not stable over cosmological evolution. However, one has to be careful on the type of PNGB in a certain model. If the PNGB is a condensate of chiral fermions charged under a certain gauge group, the only possibility to assure the DM stability is by imposing a discrete parity or by demanding a gauge group that has real or pseudo-real representations [142]. For vectorial fermions, life is much more simpler, as we do not have an anomaly that generates the decay of pions to two photons, which is the case for our model.

As our DM consists of mesonic bound states, one would think that hidden sector baryons could also be stable due to hidden baryon number conservation, and can contribute additionally to the DM abundance. However, like the ordinary SM scenario, one would also need to explain the excess of dark baryons over their antiparticles. With the assumption of no such asymmetry in our model, let us estimate the hidden baryon abundance by using the strongly coupled cross section for the hidden sector $\sigma_{hb} \sim 4\pi/m_{hb}^2 \sim 5 \times 10^{-7}\,\mathrm{GeV}^{-2}$ for a $5\,\mathrm{TeV}$ hidden baryon mass. The relic hidden baryon density is estimated to be $\Omega_{hb}\hat{h}^2 \sim 10^{-4}$, too small to explain the cold DM relic abundance on its own. Hence we will neglect the dark baryons in our work.

4.2.1. Dark Matter Mass and Couplings

As we have mentioned above, our DM candidates, i.e. the dark pions, are CP-odd particles. Like the bosonized σ field discussed in Sec. 4.1.2, the DM ϕ_a do not contain tree-level kinetic terms. The DM mass is generated at one-loop level and is defined as the solution of the inverse propagator:

$$\Gamma_{\mathrm{DM}}(p^2) = -\frac{1}{2G} + \frac{G_D\langle\sigma\rangle}{8G^3} + \frac{G_D n_c}{G^2}\int\frac{\mathrm{d}^4 k}{i(2\pi)^4}\frac{M}{(k^2 - M^2)}$$
$$+ 2n_c\left(1 - \frac{G_D\langle\sigma\rangle}{8G^2}\right)^2\int\frac{\mathrm{d}^4 k}{i(2\pi)^4}\frac{\mathrm{Tr}\left[(\slashed{k} - \slashed{p} + M)\gamma_5(\slashed{k} + M)\gamma_5\right]}{((k-p)^2 - M^2)(k^2 - M^2)}, \qquad (4.28)$$

where the constituent fermion mass M is given in Eq. (4.15) with all the scalar fields obtaining VEVs. The DM mass m_{DM} and the wave function renormalization Z_{DM}

$$\Gamma_{\mathrm{DM}}(m_{\mathrm{DM}}^2) = 0 \ , \ \ Z_{\mathrm{DM}}^{-1} = \left.\frac{\mathrm{d}\Gamma_{\mathrm{DM}}(p^2)}{\mathrm{d}p^2}\right|_{p^2 = m_{\mathrm{DM}}^2}, \qquad (4.29)$$

can be calculated from the inverse propagator in Eq. (4.28).

The DM mass m_{DM} vanishes for $y \to 0$ as the chiral symmetry is not explicitly broken in this limit (pure Nambu-Goldstone bosons are obtained). To imitate the success of NJL
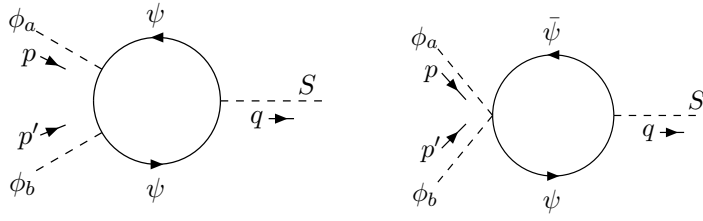
Figure 4.2.: Relevant one-loop contributions to the effective $\phi\phi S$ coupling are shown.

in describing hadron physics, we take $m_{\mathrm{DM}} < 2M$. The fermion modes are not allowed to be integrated out if the constituent mass M is lighter. The DM mass will develop an imaginary part in the one-loop amplitude when $M < m_{\mathrm{DM}} < 2M$. The imaginary part of the two-point function is related to the real part due to dispersion relation

$$\mathrm{Re}\,\Gamma(p^2) = \frac{1}{\pi}\mathcal{P}\int_0^\infty \mathrm{d}s\,\frac{\mathrm{Im}\,\Gamma(s)}{p^2 - s} + \text{subtractions}, \tag{4.30}$$

where we only take the principal part of the integral [111, 136]. This requirement of $m_{\mathrm{DM}} < 2M$ will constrain our parameter space for y later.

Before we calculate the annihilation cross section of our DM, we need to know how it communicates with the SM sector. The dark pion is connected to the SM sector only through loop-suppressed interactions, with the S and σ particles acting as messenger fields, which mix with the SM Higgs. The σ field is very heavy for our allowed parameters and can be ignored. The dominating channel of DM interaction which is relevant for calculating the relic abundance and the direct detection cross section is contributed by $\phi\phi S$ and $\phi\phi SS$ interactions. The $\phi\phi S$ coupling is generated from the one-loop diagrams shown in Fig. 4.2, where the three-point vertex function is given by

$$\Gamma_{\phi\phi S}(p,p',M) = 4n_c y\left(1 - \frac{G_D\langle\sigma\rangle}{8G^2}\right)^2 I_a(p,p',M) + n_c y\frac{G_D}{4G^2}I_b(p,p',M), \tag{4.31}$$

where the integrals

$$I_a(p,p',M) = \int \frac{\mathrm{d}^4k}{i(2\pi)^4}\frac{\mathrm{Tr}\left[(\slashed{k}+M)\gamma_5(\slashed{k}-\slashed{p}+M)(\slashed{k}+\slashed{p}'+M)\gamma_5\right]}{((k-p)^2-M^2)(k^2-M^2)((k+p')^2-M^2)},$$
$$I_b(p,p',M) = \int \frac{\mathrm{d}^4k}{i(2\pi)^4}\frac{\mathrm{Tr}\left[(\slashed{k}-\slashed{p}'+M)(\slashed{k}+\slashed{p}+M)\right]}{((k-p')^2-M^2)((k+p)^2-M^2)}, \tag{4.32}$$

can be recast in the cutoff version of Passarino-Veltman integrals (Appendix C). For the calculation of the relic abundance of DM and its interaction cross section with matter, we require $\Gamma_{\phi\phi S}(p,p',M)$ for $p = p' = (m_{\mathrm{DM}},\mathbf{0})$ and for $p = -p'$:

$$\Gamma_a^s = I_a(p,p',M)\big|_{p=p'=(m_{\mathrm{DM}},\mathbf{0})}, \qquad \Gamma_a^t = I_a(p,p',M)\big|_{p=-p',p^2=m_{\mathrm{DM}}^2},$$
$$\Gamma_b^s = I_b(p,p',M)\big|_{p=p'=(m_{\mathrm{DM}},\mathbf{0})}, \qquad \Gamma_b^t = I_b(p,p',M)\big|_{p=-p',p^2=m_{\mathrm{DM}}^2}, \tag{4.33}$$
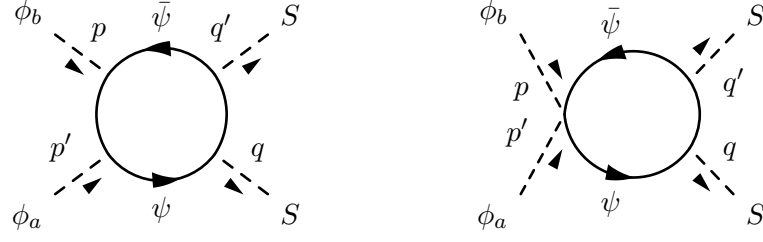
Figure 4.3.: One-loop contributions to the $\phi\phi SS$ coupling.

which after performing the integration, the effective $\phi\phi S$ couplings

$$\kappa_s \equiv n_c y \left[4 \left(1 - \frac{G_D \langle \sigma \rangle}{8G^2} \right)^2 \Gamma_a^s + \frac{G_D}{4G^2} \Gamma_b^s \right], \tag{4.34}$$

$$\kappa_t \equiv n_c y \left[4 \left(1 - \frac{G_D \langle \sigma \rangle}{8G^2} \right)^2 \Gamma_a^t + \frac{G_D}{4G^2} \Gamma_b^t \right], \tag{4.35}$$

are obtained

Next we consider the four-point vertex function which, depending on the dimensionless parameters, can be dominant effect for the relic abundance. This channel only contributes to the direct detection cross section as subleading effect due to t-channel suppression. The four-point vertex function $\phi\phi SS$ is given as

$$\Gamma_{\phi\phi SS} = 2 n_c y^2 \sum_{\substack{i \notin \text{Equiv} \\ \{p,p',q,q'\}}} \left[\left(1 - \frac{G_D \langle \sigma \rangle}{8G^2} \right)^2 I_c^i(p,p',q,q',M) + \frac{G_D}{4G^2} I_d^i(p,p',q,q',M) \right], \tag{4.36}$$

where we sum over all the topologically inequivalent loop diagrams shown in Fig. 4.3 by taking the crossing symmetry into account. The integral I_c represents the loop integral in left figure while I_d the right one. We only need the four-point vertex function in computing the relic abundance of DM, hence we only consider the case for $p = p' = (m_{\text{DM}}, \mathbf{0})$

$$\Gamma_c^s = \sum_{\substack{i \notin \text{Equiv} \\ \{p,p',q,q'\}}} I_c^i(p,p',M) \Big|_{p=p'=(m_{\text{DM}},\mathbf{0})}, \quad \Gamma_d^s = \sum_{\substack{i \notin \text{Equiv} \\ \{p,p',q,q'\}}} I_d^i(p,p',M) \Big|_{p=p'=(m_{\text{DM}},\mathbf{0})}, \tag{4.37}$$

and denote the effective $\phi\phi SS$ vertex coupling as

$$\varkappa_s = 2 n_c y^2 \left[\left(1 - \frac{G_D \langle \sigma \rangle}{8G^2} \right)^2 \Gamma_c^s + \frac{G_D}{4G^2} \Gamma_d^s \right]. \tag{4.38}$$

The effective $\varkappa_s$ only contributes significantly to the DM annihilation cross section when the Yukawa coupling y becomes large and $m_S < m_{\text{DM}}$. In this parameter region, the one-loop diagrams contain an imaginary part, which is not a pathological problem in the NJL approach as it can be related to the real part via Eq. (4.30). The inclusion of the imaginary part for the calculation has proven to be a successful approach in the NJL approach for QCD [111, 136, 137]. In our previous paper [100], this channel was ignored and as a consequence, a fine-tuned parameter space was needed in order to explain the relic abundance of the DM.
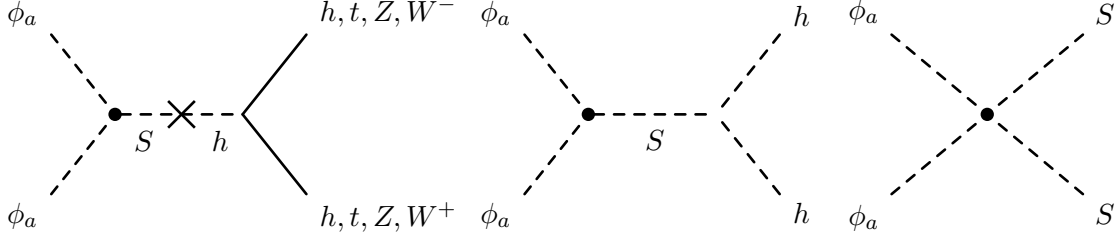
Figure 4.4.: Relevant annihilation modes of DM into the SM particles in calculating the DM relic density. The relevant s-channel $\phi\phi S$ (left and middle) coupling is κ_s given in Eq. (4.34), while $\phi\phi SS$ coupling (right) given as $\varkappa_s$ is obtained from Fig. 4.3.

The inclusion of $\varkappa_s$ provides a more experimentally accessible phenomenology, which we will discuss below.

4.2.2. Dark Matter Relic Abundance and its Direct Detection

We will now focus on the DM annihilation to the SM particles, predominantly to the Higgs particle, the top quark, the S particle, and the EW gauge bosons in the early universe. We utilize the approximation for calculating the relic density [143]

$$\Omega_c \hat{h}^2 = 8 \times \frac{3.8 x_f s_0}{\sqrt{g_*} M_{pl} \langle \bar{v}\sigma \rangle \rho_c} \hat{h}^2, \tag{4.39}$$

where $s_0 = 2970 \,\mathrm{cm}^{-3}$ is the entropy density at present, $\rho_c = 1.05 \times 10^{-5} \hat{h}^2 \,\mathrm{GeV/cm}^3$ is the critical density with $\hat{h} \approx 0.7$ the dimensionless Hubble parameter and $g_* = 115.75$ is the number of the effectively massless degrees of freedom at the freeze-out temperature. The prefactor 8 in Eq. (4.39) stems from the fact that we have eight DM pions in the model due to spontaneous chiral symmetry breaking. Furthermore $x_f = m_{\mathrm{DM}}/T_f$ at the freeze-out temperature T_f can be obtained from [143]

$$x_f = \ln \left(\frac{0.1 M_{pl} \langle \bar{v}\sigma \rangle m_{\mathrm{DM}}}{\sqrt{g_* x_f}} \right). \tag{4.40}$$

The next task is to obtain the annihilation cross section $\langle \bar{v}\sigma \rangle$ from our theory.

In Fig. 4.4 we show the effective diagrams for DM annihilation into the SM particles. The leading effect in DM annihilation is given by the s-channel interaction, as the t-channel contributions are small due to two κ_t coupling insertions with ϕ propagating in between, which can only dominate if the total four-momentum of the incoming DMs is approximately the mass of the DM. Hence they are typically negligible compared to the dominant channel in Fig. 4.4.

Let us consider first the s-wave contribution to the thermal average $\langle \bar{v}\sigma \rangle$, as shown in Fig. 4.4. Since our DM candidates are cold relics, we can utilize the low velocity approximation of the annihilation cross section

$$\langle \bar{v}\sigma \rangle \approx \frac{Z_{\mathrm{DM}}^2}{32\pi m_{\mathrm{DM}}^3} \Big[(m_{\mathrm{DM}}^2 - m_W^2)^{1/2} a_W + (m_{\mathrm{DM}}^2 - m_Z^2)^{1/2} a_Z + (m_{\mathrm{DM}}^2 - m_t^2)^{3/2} a_t$$
$$+ (m_{\mathrm{DM}}^2 - m_h^2)^{1/2} a_h + (m_{\mathrm{DM}}^2 - m_S^2)^{1/2} |\varkappa_s|^2 \Big], \tag{4.41}$$
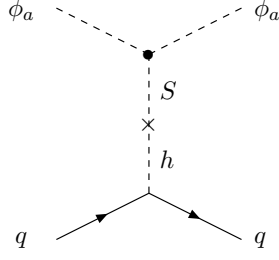
Figure 4.5: Relevant diagram contributing to the direct detection of DM in our model. The $\phi\phi S$ coupling is κ_t, which is given in Eq. (4.35).

where Z_{DM} is given in Eq. (4.29) and

$$
\begin{aligned}
a_W &= 4\,|\Delta_{hs}|^2\,m_W^4 \left(\frac{\kappa_s}{v}\right)^2 \left(3 + 4\frac{m_{\text{DM}}^4}{m_W^4} - 4\frac{m_{\text{DM}}^2}{m_W^2}\right), \\
a_Z &= 2\,|\Delta_{hs}|^2\,m_Z^4 \left(\frac{\kappa_s}{v}\right)^2 \left(3 + 4\frac{m_{\text{DM}}^4}{m_Z^4} - 4\frac{m_{\text{DM}}^2}{m_Z^2}\right), \\
a_t &= 24 \left(\frac{\kappa_s}{v}\right)^2 |\Delta_{hs}|^2\,m_t^2, \\
a_h &= \frac{1}{2}\left(\frac{\kappa_s m_W}{vg}\right)^2 \left| 24\lambda_H \Delta_{hs} - 4\lambda_{HS}\frac{\langle S\rangle}{v}\Delta_{ss}\right|^2,
\end{aligned}
\tag{4.42}
$$

with $v = 246$ GeV and

$$
\begin{aligned}
\Delta_{hs} &= \frac{\xi_2^{(2)}\xi_1^{(2)}}{4m_{\text{DM}}^2 - m_S^2 + i\gamma_S m_S} + \frac{\xi_2^{(1)}\xi_1^{(1)}}{4m_{\text{DM}}^2 - m_h^2}, \\
\Delta_{ss} &= \frac{\xi_2^{(2)}\xi_2^{(2)}}{4m_{\text{DM}}^2 - m_S^2 + i\gamma_S m_S} + \frac{\xi_2^{(1)}\xi_2^{(1)}}{4m_{\text{DM}}^2 - m_h^2}.
\end{aligned}
\tag{4.43}
$$

Here κ_s and $\xi's$ are given in Eq. (4.34) and Eq. (4.21), respectively, $g \simeq 0.63$ is the SU(2)$_L$ gauge coupling, and

$$
\gamma_S = \frac{\lambda_{HS}^2 \langle S\rangle^2}{8\pi m_S^2}\sqrt{\frac{m_S^2}{4} - m_h^2}
\tag{4.44}
$$

is the decay width of S. For $y \gtrsim 0.4$, the annihilation cross section is dominated by $\phi\phi SS$ interactions. This channel was previously ignored in our paper [100] as we have imposed that $M < m_{\text{DM}}$, which is too restrictive. In later publication [101], we restore the $\phi\phi SS$ as in this parameter region, we have $M < m_{\text{DM}} < 2M$ and the $\varkappa_s$ effective coupling is no longer negligible. The $M < m_{\text{DM}} < 2M$ constraint is valid, as this also occurs in ordinary QCD (compared the constituent mass of strange quark and the η' meson mass).

If we assume that the DM is thermally distributed in our galaxy with a certain profile, we can in principle detect its interaction with ordinary matter with a DM direct detection experiments. The DM direct detection is a very rich subject and we refer the reader to Ref. [144] for a review. The thermal DM can propagate to the detector and scatter off a nuclei, leaving its imprint in the form of nuclear recoil. We can compute the interaction cross section of our DM candidate with nuclei. The spin-independent elastic scattering cross
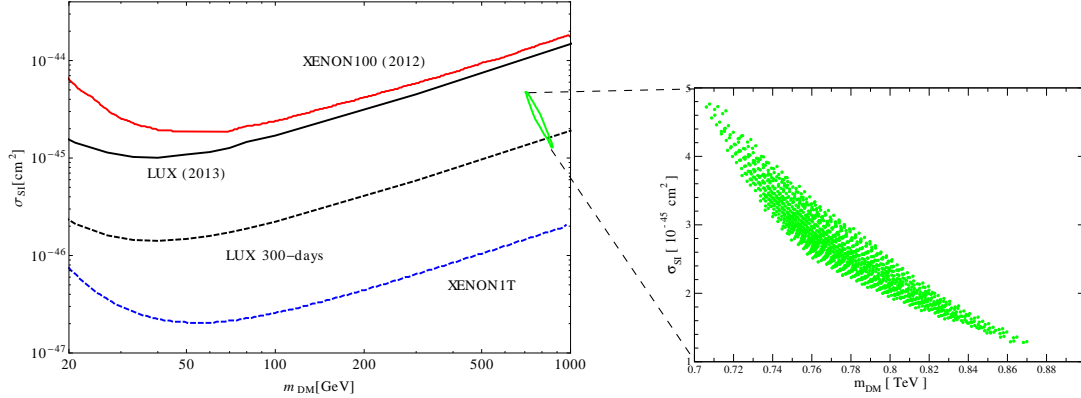
Figure 4.6.: The DM mass $m_{\rm DM}$ against the spin-independent cross section σ_{SI} with the relevant satisfying additional constraints are shown. The XENON100 limit [147] and the LUX limit [148] is $\sim 10^{-44}\,{\rm cm^2}$ for $m_{\rm DM} \sim 700\,{\rm GeV}$. The XENON1T [149] and the LUX 300 days run [150] will probe or exclude the natural parameter space of our model.

section off the nucleon σ_{SI} shown in Fig. 4.5 is calculated to be [145]

$$\sigma_{SI} = \frac{Z_{\rm DM}^2}{\pi} \left[\frac{\kappa_t \hat{f} m_N}{2 v m_{\rm DM}} \left(\frac{\xi_2^{(2)} \xi_1^{(2)}}{m_S^2} + \frac{\xi_2^{(1)} \xi_1^{(1)}}{m_h^2} \right) \right]^2 \left(\frac{m_N m_{\rm DM}}{m_N + m_{\rm DM}} \right)^2 , \qquad (4.45)$$

where κ_t is the effective $\phi\phi S$ coupling is given in Eq. (4.35), m_N represents the nucleon mass, and $\hat{f} \sim 0.3$ stems from the nucleonic matrix element [146]. Before we scan for parameter space for our DM that can yield sizable spin-independent elastic cross section, we need to constrain the parameters from relic abundance of DM $\Omega_c \hat{h}^2 \approx 0.119$ from cosmological observation [29].

We are ready to scan the parameter space for our model. We impose that all the dimensionless parameters y, λ_S, λ_H and λ_{HS} satisfy the theoretical bounds described in Sec. 4.1.2 and experimental constraints $v = 246\,{\rm GeV}$, $m_h = 125.9\,{\rm GeV}$, $\Omega_c \hat{h}^2 \approx 0.119$, and $|\xi_1^{(1)}| \gtrsim 0.9$, and allow the uncertainties up to 3σ. The phenomenology of our model is very promising as the spin independent annihilation cross section is just below the XENON100 [147] and LUX [148] constraints and above the XENON1T sensitivity [149], see Fig. 4.6 for more details. The mass of the DM shift towards $700 - 900\,{\rm GeV}$ region and can be probed with future XENON1T experiment or LUX 300 days run [150]. The annihilation cross section is mainly contributed by the $\phi\phi SS$ interaction for large Yukawa coupling y. The allowed natural region on the $\sigma_{SI} - m_{\rm DM}$ plane is restricted to a small strip due to the very constraining parameters imposed by experiments, e.g. Higgs masses, relic density, etc., and also by theoretical constraints such as vacuum stability and triviality bound. As we are not allowed to utilize NJL approach for $M_{\rm DM} > 2M$, we obtain an upper bound for the DM mass. The lower bound of DM mass comes from $y \gtrsim 0.4$, while lowering y would require very fine-tuned parameter $m_S \simeq 2 m_{\rm DM}$ to satisfy the correct relic abundance. Therefore with the restrictive natural parameter space, our model is very predictive and easily probed or excluded by future direct detection experiments.
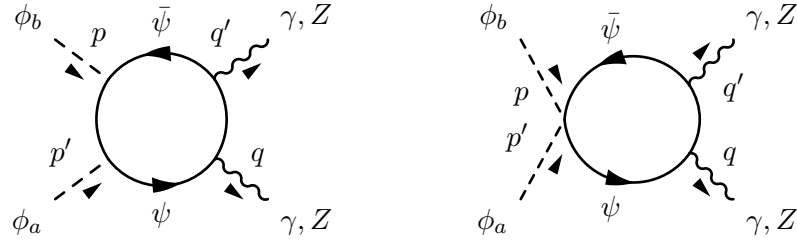
Figure 4.7.: DM annihilation to two photons or two Z bosons in addition to the annihilation channel in Fig. 4.3.

4.2.3. Electromagnetically Charged Dark Fermions and Gamma-ray Line

Our simple model described so far should be viewed as a prototype for model building along the direction of indirect scale transmission. We have scaled up the known QCD values to simplify some calculations. There are many possible ways to extend the classically scale invariant model which contain richer phenomenology. One possible way to extend the model is by introducing another value of n_f and n_c, which would yield different spectrum and constraints of the model, but comes with the disadvantage that one is not allowed to scale up the known QCD values and must determine the NJL parameters by solving the DSE. Another possible interesting extension of our model is to assign a $U(1)_Y$ hypercharge Q to the hidden sector fermions so that they are electrically charged

$$\mathcal{L}_{\mathrm{H}} = -\frac{1}{2}\operatorname{Tr} F^2 + \operatorname{Tr} \bar{\psi}(i\slashed{\partial} + g_4\lambda^a\slashed{G}^a + g_Y Q\slashed{B} - yS)\psi. \tag{4.46}$$

Strictly speaking the hidden sector is not dark anymore due to the electric charge assignment. The coupling is vector-like and hence does not break the $U(1)_Y$ after dynamical chiral symmetry breaking has taken place. The changes to the $\mathcal{L}_{\mathrm{NJL}}$ are minimal, as only the first term in Eq. (4.12) is augmented with extra covariant derivative of $U(1)_Y$. The $U(1)_Y$ does not contribute to the effective potential, hence the mass spectrum of the CP-even scalar and DM remain the same at lowest order.

The additional $U(1)_Y$ provides an interesting phenomenology, particularly in astroparticle physics. After EWSB has taken place, the neutral component of the $SU(2)_L$ mixes with the $U(1)_Y$, hence the DM could annihilate into γ-rays or Z bosons via a one loop process, see Fig. 4.7 for more details. The annihilation cross section of DM into γ-rays or Z bosons can be calculated as

$$\langle \bar{v}\sigma \rangle_{\phi\phi ab} = \frac{\alpha^2 Q^4 Z_{\mathrm{DM}}^2}{16\pi^3 m_{\mathrm{DM}}^2}\mathcal{A}^2(\gamma\gamma) \times \begin{cases} & a\ b \\ (1/2) & \text{for} \quad \gamma\ \gamma \\ t_W^2(1 - m_Z^2/4m_{\mathrm{DM}}^2) & \text{for} \quad \gamma\ Z \\ (3/4)t_W^4(1 - m_Z^2/m_{\mathrm{DM}}^2)^{1/2} & \text{for} \quad Z\ Z \end{cases}, \tag{4.47}$$

where $t_W = \tan\theta_W$ and $\mathcal{A}(\gamma\gamma)$ contains the sum of all topologically nonequivalent loop integrals in Fig. 4.7. The structure of $\mathcal{A}$ is highly nontrivial, because we need a renormalization prescription to restore gauge invariance, as NJL method introduces a cutoff that breaks gauge invariance explicitly. We propose a new renormalization procedure within the framework of NJL to restore gauge invariance, which we call *least subtraction procedure*. This method is developed by one of our collaborators, J. Kubo, and we refer the reader

to our paper [101] for a step-by-step introduction to this new approach. This procedure is crucial to describe our DM annihilation into γ-rays or Z bosons within the NJL framework. Note that in principle the annihilation modes in Fig. 4.7 are required to be included in the relic abundance calculation in Sec. 4.2.2. However, as the annihilation cross section to SS is proportional to y^4 while the annihilation cross section to $\gamma\gamma$, γZ and ZZ is only a function of $\alpha^2 Q^4$, the latter will only contribute significantly if the charge $Q \gtrsim 1$. We will consider an example with $Q = 1/3$ and calculate the annihilation cross section of the DM to γ-rays.

The γ-rays produced from DM annihilation can be detected by the Fermi LAT [151] and the H.E.S.S. experiments [152]. The energy E_γ of a γ-ray line produced in the annihilation into γZ is given by $m_{\text{DM}}(1 - m_Z^2/4m_{\text{DM}}^2)$. The finite detector energy resolution usually cannot distinguish this line from the line obtained from $\phi\phi \to \gamma\gamma$, hence both cross sections are added

$$\langle \bar{v}\sigma \rangle_{\gamma\gamma+\gamma Z} = \langle \bar{v}\sigma \rangle_{\phi\phi\gamma\gamma} + \langle \bar{v}\sigma \rangle_{\phi\phi\gamma Z}. \tag{4.48}$$

We take the electric charge $Q = 1/3$ and we scan for viable parameter space in the $\langle \bar{v}\sigma \rangle_{\gamma\gamma+\gamma Z} - m_{\text{DM}}$ plane, taking the constraints mentioned in Sec. 4.2.2 into account. Note that one can scale up our result to obtain the cross section for another charge by including a factor of $(3Q)^4$. The result is shown in Fig. 4.8 (right) and can be compared to the H.E.S.S. limit (left). As we have mentioned in Sec. 4.2.2, our model predicts a DM mass in the range of $700 - 900\,\text{GeV}$ due to the tight theoretical and experimental constraints on the dimensionless couplings. For $Q = 1/3$ the majority of the predicted $\langle \bar{v}\sigma \rangle_{\gamma\gamma+\gamma Z}$ lies around $10^{-27}\,\text{cm}^3/\text{s}$. Increasing the strength of the charge Q will yield a larger cross section than $10^{-27}\,\text{cm}^3/\text{s}$ and is already disfavored by H.E.S.S. limit. We have not included the annihilation modes into $\gamma\gamma, \gamma Z, ZZ$ in calculating the relic abundance in our $Q = 1/3$ example, as such annihilation modes are negligible compared to the $\phi\phi \to SS$ channel. Therefore the information on the annihilation cross section producing the γ-ray spectrum of DM in our example can be obtained independently, provided that the electric charge is small. Once $Q \gtrsim 1$, the annihilation channel to photons and Z will start to contribute significantly to the relic abundance calculation and one would need to do a thorough analysis.

The analysis of the differential γ-ray flux

$$\frac{d\Phi}{dE_\gamma} \propto \langle \bar{v}\sigma \rangle_{\gamma\gamma} \frac{dN^{\gamma\gamma}}{dE_\gamma} + \langle \bar{v}\sigma \rangle_{\gamma Z} \frac{dN^{\gamma z}}{dE_{\gamma Z}} \simeq \langle \bar{v}\sigma \rangle_{\gamma\gamma+\gamma Z} \; \delta(E_\gamma - m_{\text{DM}}) \tag{4.49}$$

has not been carried out, however the prospects of observing such a line spectrum is discussed in detail in Refs. [153, 154]. Observations of γ-ray lines of energies between $700 - 900\,\text{GeV}$ not only fix the charge of the hidden sector fermion, but would also yield a first experimental hint on the hidden sector for our model.

4.3. Phase Transition at Finite Temperature

So far there are no direct evidence that temperature above $\mathcal{O}(1)\,\text{MeV}$ existed in the early universe. The observation probe for early universe so far only confirms the physics of our Universe up to the epoch of Big Bang Nucleosynthesis (BBN). However, it is natural to
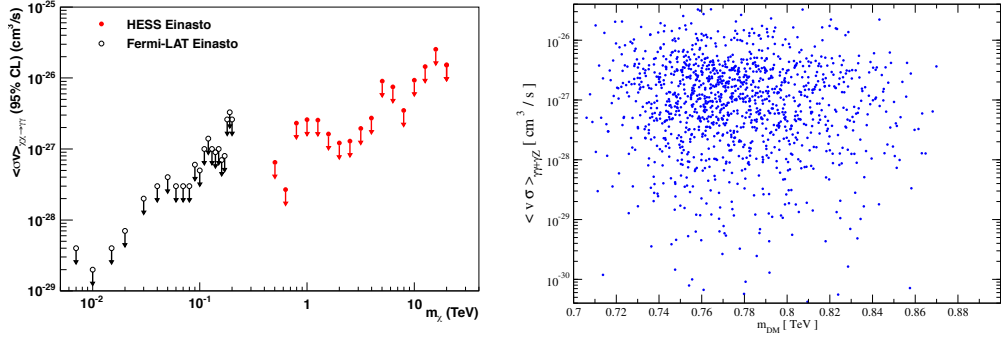
Figure 4.8.: (Left) The Fermi LAT [151] (black) and H.E.S.S. [152] (red) upper bounds on the velocity-averaged DM annihilation cross section for monochromatic γ-ray lines. (Right) the velocity-averaged DM annihilation cross section $\langle \bar{v}\sigma \rangle_{\gamma\gamma+\gamma Z}$ as a function of m_{DM} with $Q = 1/3$, where $\Omega_c \hat{h}^2 = 0.1187 \pm 0.005(3\sigma)$ [29] is imposed.

assume that the Universe had much higher temperature in its history, i.e. the Universe had different phases (ground state configurations) at different epoch. As the temperature of the Universe cooled down to $T \sim \Lambda_{\mathrm{QCD}}$ and below, the QCD chiral symmetry is spontaneously broken [155] with a phase transition from quark-gluon plasma to hadronic matters expected to occur.

At a certain finite temperature of $\mathcal{O}(1)\,\mathrm{TeV}$, the chiral symmetry for our dark sector is expected to be restored, and hence the EW symmetry must be restored above the critical temperature as our model relates both symmetry breaking. The nature of the EWSB could be related to baryon asymmetry in the Universe [156–159] and it is interesting to find out whether the allowed parameter space in Sec. 4.2.2 can generate a strong first order phase transition, which would be natural if it can be realized without extra fine-tuning. A strong first order phase transition is a crucial ingredient for EW baryogenesis and we would like to know whether the chiral symmetry breaking and the EWSB process are highly nonequilibrium as the temperature decreases, which could leave an imprint in the thermal history of the universe.

We continue our analysis with the NJL approach and include the quantum effects at a finite temperature. An effective potential at a finite temperature consists of five components

$$V_{\mathrm{EFF}}(\phi_c, T) = \underbrace{V_{\mathrm{SM}+S}(\phi_c)}_{\text{Tree level}} + \underbrace{V_{\mathrm{NJL}}(\phi_c) + V_{\mathrm{CW}}(\phi_c)}_{\text{Quantum correction}} + \underbrace{V_{\mathrm{FT}}(\phi_c, T) + V_{\mathrm{Ring}}(\phi_c, T)}_{\text{Finite temperature}}, \qquad (4.50)$$

is obtained, where ϕ_c represents a collection of the classical scalar fields h, S and σ. We have followed the calculation in Refs. [160–163]. The term $V_{\mathrm{SM}+S}(\phi_c)$ is the tree-level contribution given in Eq. (4.3), $V_{\mathrm{NJL}}(\phi_c)$ is the one-loop effective potential in Eq. (4.14) when the heavy dark fermions are integrated out. $V_{\mathrm{CW}}(\phi_c)$ is the effective potential (Coleman-Weinberg potential) with one-loop quantum corrections from the relevant fields at $T = 0$. The finite temperature contribution consists of V_{FT} from bosonic and fermionic contributions while V_{Ring} is the ring contribution or plasmon contribution for the bosons, which can be treated as thermal mass contribution sourced by the heat bath. At the one-loop order they are

Figure 4.9: The temperature dependence of $\langle h\rangle/T$ near the critical temperature is analyzed for the allowed parameter space. The SM phase transition (in red) is plotted for comparison. Weak first order phase transition for the allowed parameters occurs around $T = 150\,\mathrm{GeV}$.
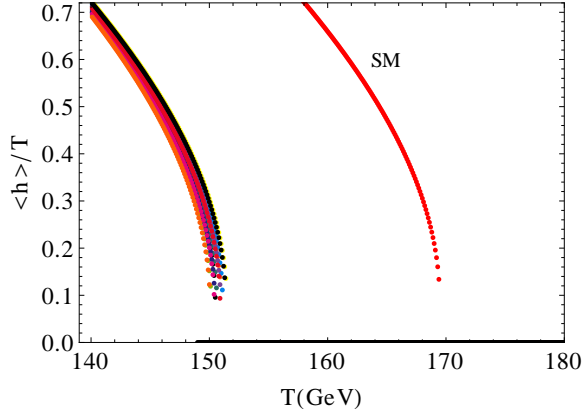
given by

$$V_{\mathrm{CW}}(\phi_c) = \frac{1}{64\pi^2}\sum_i n_i \left\{ m_i^4(\phi_c)\left(\ln\left[\frac{m_i^2(\phi_c)}{m_i^2(\langle\phi_c\rangle)}\right] - \frac{3}{2}\right) + 2m_i^2(\langle\phi_c\rangle)m_i^2(\phi_c)\right\}, \quad (4.51)$$

$$V_{\mathrm{FT}}(\phi_c, T) = \frac{T^4}{2\pi^2}\left(\sum_i n_i^B J_B(m_i^2(\phi_c)/T^2) + \sum_i n_i^F J_F(m_i^2(\phi_c)/T^2)\right), \quad (4.52)$$

$$V_{\mathrm{Ring}}(\phi_c, T) = -\frac{T}{12\pi}\sum_i n_i^B\left[(M_i^2(\phi_c, T))^{3/2} - (m_i^2(\phi_c))^{3/2}\right], \quad (4.53)$$

where $n_i^B = 1$ for a real scalar, $n_i^B = 3$ for a vector boson, and $n_i^F = -4$ for a Dirac fermion. Note that we include only the relevant contributions from the top quark, the $W^\pm, Z$ gauge bosons and the scalars h and S in the Coleman-Weinberg potential and the ring correction. Contributions from Nambu-Goldstone bosons and the rest of the SM particles are negligibly small. The relevant tree level field dependent masses $m_i^2(\phi_c)$ are given as

$$m_W^2(h) = \frac{g_2^2}{4}h^2, \quad m_Z^2(h) = \frac{g_2^2 + g_1^2}{4}h^2, \quad m_t^2(h) = \frac{y_t^2}{2}h^2, \quad (4.54)$$

while the masses for $m_h^2(h, S)$ and $m_S^2(h, S)$ are given in Eq. (4.19).

The crucial part of the potential for a phase transition to occur stems from the finite temperature contribution V_{FT} and V_{Ring}. For a strong first order phase transition to occur, the parameter $\langle\phi\rangle/T$ has to be larger than 1. The relevant thermal functions J_B and J_F are defined as

$$J_B(r^2) = \int_0^\infty \mathrm{d}x\, x^2 \ln\left(1 - e^{-\sqrt{x^2 + r^2}}\right), \qquad J_F(r^2) = \int_0^\infty \mathrm{d}x\, x^2 \ln\left(1 + e^{-\sqrt{x^2 + r^2}}\right), \tag{4.55}$$

where we have also utilized the high temperature expansion to simplify our calculation. Essentially the most important term determining whether phase transition could happen stems from J_B, as we require the odd polynomial term in T to have a bump in the effective potential. An additional contribution from the hidden constituent quark is also present in the V_{FT} potential, where the fermions in the hidden sector is integrated out and we obtain
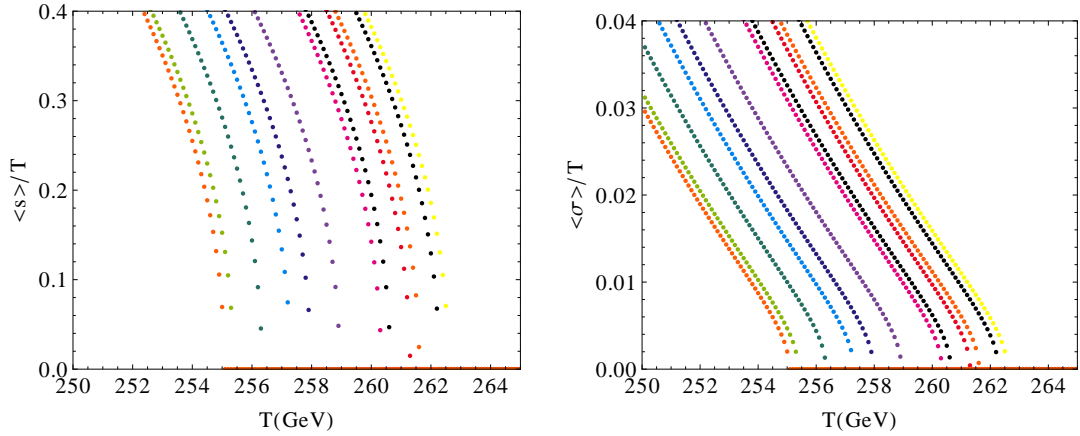
Figure 4.10.: The temperature dependence of $\langle S \rangle / T$ (left) and $\langle \sigma \rangle / T$ (right) near the critical temperature for the allowed parameter region. In this parameter space, only second order phase transition is obtained with critical temperature ranging from $T = 254\,\mathrm{GeV}$ to $262\,\mathrm{GeV}$.

the contribution to

$$V_{\mathrm{FT}} \supset -6n_c \frac{T^4}{\pi^2} J_F(M^2/T^2) \simeq 3n_c \frac{T^2}{12} M^2 + \frac{3n_c}{16\pi^2} \left[M^4 \ln \left(\frac{M^2}{\pi^2 T^2 e^{3/2 - \gamma_E}} \right) \right], \qquad (4.56)$$

where the constituent mass M is given in Eq. (4.15). The ring contributions are usually small, but we will include them for completeness. In addition to the field dependent mass $m_i^2(\phi_c)$, the ring contributions also require the thermal mass $M_i^2(\phi_c, T)$ for i boson [164]:

$$M_{W_L/Z_L}^2(h, T) = m_{W/Z}^2(h) + \frac{11}{6} g_2^2 T^2,$$

$$M_{hh}^2(h, S, T) = m_{hh}^2(h, S) + \left(\frac{3g_2^2}{8} + \frac{\lambda_H}{2} + \frac{y_t^2}{4} - \frac{\lambda_{HS}}{24} \right) T^2,$$

$$M_{SS}^2(h, S, T) = m_{SS}^2(h, S) + \left(\frac{\lambda_S}{4} - \frac{\lambda_{HS}}{6} \right) T^2,$$

$$M_{hS}^2(h, S, T) \approx m_{hS}^2(h, S). \qquad (4.57)$$

We have ignored the contribution from Nambu-Goldstone bosons and $U(1)_Y$ as they are negligibly small. The mass eigenstates for M_{hh}^2, M_{SS}^2 are given by

$$M_{1,2}^2(h, S, T) \approx \frac{1}{2} \left(M_{hh}^2 + M_{SS}^2 \mp \sqrt{(M_{hh}^2 - M_{SS}^2)^2 - 4M_{hS}^2} \right), \qquad (4.58)$$

where only the longitudinal part of $W^\pm, Z$ contributes to their thermal masses.

The temperature dependence of $\langle h \rangle / T$ near the critical temperature for the parameter space that predicts acceptable relic abundance is shown in Fig. 4.9. The EW phase transition for the SM (in red) is plotted for comparison. From the parameter space that predicts acceptable relic abundance, the EW phase transition is weakly first order and that the critical temperature of the present model is around $150\,\mathrm{GeV}$. The shift of critical temperature from the SM is caused by the nonnegligible value of λ_{HS}. We can conclude that our model cannot account for EW baryogenesis, which would require a strong first order phase transition of

$\langle h \rangle / T > 1$. A nonperturbative calculation is required for a more accurate analysis however.

What about the chiral phase transition in the dark sector? The temperature dependence of $\langle S \rangle / T$ and $\langle \sigma \rangle / T$ is shown in Fig. 4.10. The phase transition in the dark sector occurs at around $T \sim 250\,\text{GeV}$ and all of them are of the second order type. No bubble nucleation can occur during the thermal expansion of the universe. However, we would like to stress that our result is based on the NJL approach. Nonperturbative analysis could alter the result.

4.4. Summary

In this chapter we have presented a model where a scale generated via dimensional transmutation in a classically scale invariant hidden sector is transmitted to the SM sector indirectly via a scalar mediator coupled to the SM Higgs. The indirect scale transmission from a TeV scale hidden sector triggers the EWSB radiatively. The origin for such a dimensional transmutation stems from spontaneous chiral symmetry breaking in the hidden fermion sector, which also provides the PNGB as DM candidates. We have utilized the NJL approach to calculate all the relevant scalar mass spectrum and their couplings. In this approach, most of the couplings are interrelated and the parameter space for generating experimentally allowed observations is very restrictive. The predicted DM direct detection cross section can be probed or excluded by the future XENON1T and LUX experiment. Furthermore, we have extended our model to include electrically charged hidden fermions, which could provide striking monochromatic γ-ray line signature in indirect detection experiments. Our model serves as a prototype for model builders who would like to construct more interesting models involving classically scale invariant extensions of the SM and indirect scale transmission.

Discrete Flavor Symmetry

In this chapter we will leave the domain of scale invariance and the electroweak (EW) sector and discuss another type of symmetry, namely the discrete flavor symmetry, which could provide a solution to the flavor puzzle in the quark and leptonic sector. We will first review the flavor puzzle, e.g. comparing and contrasting the mixing structure between the quark and leptonic sector. We will introduce the idea of utilizing a discrete group, broken in a specific vacuum alignment, to explain the mixing pattern for both quarks and leptons. We will introduce an algorithm and implementing it inside the computer algebra program GAP [165–168] to systematically scan all the finite discrete groups up to the order of 1536 which can generate leading-order (LO) mixing patterns that are experimentally favored with the assumption that neutrinos are Majorana particles. The search is then extended to the case when neutrinos are Dirac particles and also to the quark sector. A mathematical classification will be introduced to categorize all the predictive finite discrete groups. Finally we will develop a method to quantify the predictivity of discrete symmetry groups and test their goodness-of-prediction against flavor anarchy. The results and presentation in this chapter follow Refs. [169, 170] stemming from a collaboration with Martin Holthausen and Manfred Lindner. All the relevant plots and results are reproduced with reprint permission.

5.1. Motivation and Introduction

The origin of flavor structure for the Standard Model (SM) fermions is one of the puzzle that requires solutions beyond the SM. Neutrinos, which are massless in the SM, necessary require extension of the SM to explain their mass terms and mixing with the flavor eigenstates. From the mass spectrum point of view, neutrinos have very tiny masses compared to the quarks. Their mass hierarchy is not as obvious as the quarks, as only the mass square difference between the neutrino masses are known. The absolute ordering of the masses, whether the hierarchy is normal ($m_3^2 > m_2^2 > m_1^2$) or inverted ($m_2^2 > m_1^2 > m_3^2$), is still currently unknown. From the mixing pattern perspective, i.e. how the different flavors between quarks or the leptons mix with each other, all the absolute entries of the lepton mixing matrix or the Pontecorvo-Maki-Nakagawa-Sakata (PMNS) matrix

$$|U_{\mathrm{PMNS}}| \approx \begin{pmatrix} 0.821 & 0.549 & 0.152 \\ 0.374 & 0.573 & 0.694 \\ 0.382 & 0.567 & 0.684 \end{pmatrix}, \tag{5.1}$$

Leptonic Mixing Angles				Quark Mixing Angles			
$\sin^2\theta_{12}$ $[10^{-1}]$	$\sin^2\theta_{23}$ $[10^{-1}]$	$\sin^2\theta_{13}$ $[10^{-2}]$	δ $[\pi]$	$\sin^2\theta_{12}$ $[10^{-2}]$	$\sin^2\theta_{23}$ $[10^{-3}]$	$\sin^2\theta_{13}$ $[10^{-5}]$	δ $[10^{-1}\pi]$
$3.20^{+.16}_{-.17}$	$6.13^{+.22}_{-.40}$	$2.46^{+.29}_{-.28}$	$0.8^{+1.2}_{-.8}$	5.09 ± 0.04	1.72 ± 0.09	1.23 ± 0.14	3.8 ± 0.3

Table 5.1.: (Left) Global fit of neutrino oscillation parameters for the case of normal ordering of neutrino masses with the 1σ error adapted from Ref. [171]. There are two nearly degenerate minima at $\sin^2\theta_{23} = 0.430^{+.031}_{-.030}$ in the global fit. (Right) The quark mixing parameters converted to $\sin\theta_{ij}$ format, which will be useful later [8].

are of order one. Compared to the quark mixing matrix, or the Cabibbo-Kobayashi-Maskawa (CKM) matrix [8]

$$|U_{\text{CKM}}| \approx \begin{pmatrix} 0.974 & 0.225 & 0.004 \\ 0.225 & 0.973 & 0.041 \\ 0.009 & 0.040 & 0.999 \end{pmatrix}, \tag{5.2}$$

whose absolute off-diagonal entries are small, we can see that neutrinos mix strongly unlike the case for quarks. The different mixing patterns between these two sectors at first would naively let us to conjecture that both sectors have different origin, which is usually the case for most of the models proposed to explain the flavor structure. This assumption is naive, as both the different structures of quarks and leptons could have a common origin, which we will see later.

Before we start to discuss the different approaches to tackle the flavor problem, let us first define a convention to parameterize the mixing pattern. Both the U_{PMNS} and U_{CKM} matrices can be parameterized as

$$U_{\text{mix}} = \begin{pmatrix} 1 & 0 & 0 \\ 0 & c_{23} & s_{23} \\ 0 & -s_{23} & c_{23} \end{pmatrix} \times \begin{pmatrix} c_{13} & 0 & s_{13}e^{-i\delta_{\text{CP}}} \\ 0 & 1 & 0 \\ -s_{13}e^{i\delta_{\text{CP}}} & 0 & c_{13} \end{pmatrix} \times \begin{pmatrix} c_{12} & s_{12} & 0 \\ -s_{12} & c_{12} & 0 \\ 0 & 0 & 1 \end{pmatrix}, \tag{5.3}$$

where $c_{ij} = \cos\theta_{ij}$ and $s_{ij} = \sin\theta_{ij}$ describe the mixing between ith and jth fermion generations. The Dirac CP phase is parameterized by δ_{CP}. If neutrinos are Majorana particles, additional phase matrix $P = \text{diag}(e^{i\alpha}, e^{i\beta}, 1)$ is multiplied to the RHS of Eq. (5.3). The best fit result for neutrino oscillation parameters from global fit [171–173] and the experimentally measured quark mixing parameters are given in Table 5.1.

For the leptonic mixing angles, the $s_{12} \approx 1/\sqrt{3}$ is measured from the solar neutrino oscillation [28] while $s_{23} \approx 1/\sqrt{2}$ represents the amplitude of atmospheric neutrino mixing flux [174]. Until year 2012 the reactor angle s_{13} was not measured but only limited by CHOOZ experiment [27]. It was thought that the reactor mixing angle is small, possibility zero. This has spark a lot of interest in the high energy physics community to build model based on A_4 [12–18] and $\mathcal{S}_4$ [175–177] discrete symmetries that can lead to the tri-bimaximal

mixing pattern (TBM)

$$U_{\text{PMNS}} \sim U_{\text{HPS}} \equiv \begin{pmatrix} \sqrt{\frac{2}{3}} & \frac{1}{\sqrt{3}} & 0 \\ -\frac{1}{\sqrt{6}} & \frac{1}{\sqrt{3}} & \frac{1}{\sqrt{2}} \\ -\frac{1}{\sqrt{6}} & \frac{1}{\sqrt{3}} & -\frac{1}{\sqrt{2}} \end{pmatrix}, \tag{5.4}$$

proposed by Harrison, Perkins and Scott [178, 179]. It is only until recently that the reactor mixing angle is measured by DAYA BAY [9], RENO [10] and DOUBLE CHOOZ [11], with the value $s_{13} \approx 0.15$. For the quarks mixing patterns, most of the mixing angles are determined from decays of mesons and they have been measured very precisely compared to the leptonic sector. For a thorough review of the quark mixing patterns and how they are measured please refer to the PDG review [8].

In general the ansatz to explain the flavor structure can be classified into two categories:

- Symmetry based approach,

- Anarchy based approach [180–182].

For the latter the occurrence of mixing pattern consists of random variables drawn from the distribution of U(3) Haar measure

$$\mathrm{d}\boldsymbol{V} = \mathrm{d}c_{13}^4 \mathrm{d}s_{12}^2 \mathrm{d}s_{23}^2. \tag{5.5}$$

The crucial hypothesis here is that there is no underlying symmetry in the flavor structure, and nature chooses a specific point in the mixing angle space from the above probability distribution. We would not pursue this idea further in this thesis, except that we will provide a test of goodness-of-prediction for flavor symmetry against anarchy to see how predictive both the approaches are.

We assume that the underlying Yukawa matrices and mixing patterns in the leptonic and quark sectors result from certain symmetries. In general, in order to build a flavor model, one needs to explain the mass hierarchy between the fermions and also the mixing patterns. This is typically done by spontaneous symmetry breaking by certain flavon fields charged differently under a symmetry group. All the approaches to solve the flavor problem using symmetry groups require flavon fields, whether in the form of additional scalar fields or multi-Higgs fields[1]. To explain the mass hierarchy one typically requires mass matrices with certain *texture zeros*, which are motivated by flavor symmetry groups. In the simplest scenario, a U(1) group is utilized with the charges of left-handed and right-handed fermions chosen in an appropriate way to generate mass hierarchy[2]. The small Yukawa coupling/mass term of certain generations are generated from higher-dimensional operators, when the flavon fields obtain a certain configuration of vacuum expectation value (VEV). This approach is known as Froggatt-Nielsen mechanism [184] and is only useful to generate the mass hierarchical structure. To obtain the nontrivial mixing pattern, non-abelian symmetry groups are typically assumed to provide the vacuum alignment of the flavon fields. Continuous non-abelian symmetry such as U(2) [185], SO(3) [186] and SU(3) [187] have

---

[1]By Higgs field we mean scalar field charged under the EW gauge symmetry.
[2]For a good introduction to this approach please refer to Ref. [183].

been studied extensively to explain the nontrivial mixing patterns, however they are generally complicated as additional auxiliary symmetries are required to suppress undesired operators. These problems can be solved in a simpler approach when a discrete non-abelian symmetry is chosen as a starting point, which is the main focus of this chapter. For a more comprehensive review on discrete flavor symmetries and model building in this direction we refer the reader to Refs. [188–190].

With so many flavor parameters to be explained, the actual model building regarding discrete flavor symmetry is very involved. Let us look at the prototype model building for leptonic sector with an A_4 discrete group [12–18] , which is the smallest group that contains a 3-dimensional representation. Rather than writing out a specific A_4 model explicitly, we just want to present the idea and model building approach in flavor symmetry. Let us assign the EW singlet leptons, $\{e_R, \mu_R, \tau_R\}$ with the following representations $\{\mathbf{1_1}, \mathbf{1_{1'}}, \mathbf{1_{1''}}\}$ with $\mathbf{1_1}$ as the trivial representation of A_4. For simplicity let us introduce two real scalar fields χ and ϕ charged under 3-dimensional representation $\mathbf{3}$, under which also the EW lepton doublet L are charged. The LO lepton mass operators are given by

$$\mathcal{L} \supset -\frac{y_e \chi \bar{L} H e_R}{\Lambda} - \frac{y_\mu \chi \bar{L} H \mu_R}{\Lambda} - \frac{y_\tau \chi \bar{L} H \tau_R}{\Lambda} - \frac{x \phi \overline{L^c} \tilde{H}^* \tilde{H}^\dagger L}{\Lambda^2} + h.c, \qquad (5.6)$$

with $\tilde{H} = i\sigma^2 H^*$ and notice that the LO charged mass Lagrangian consists of dimension 5 operators while Majorana neutrino mass matrix is described by dimension 6 operators. Once all the flavon fields obtain their VEVs and break the discrete flavor symmetry, the LO mass matrices for the leptons are obtained. After diagonalizing the mass matrices with the flavor rotation matrices, the mixing matrix U_{PMNS} can be obtained. Now comes the crucial point, if the VEV configurations are random and have no specific structure, we have no predictions of the mixing patterns. This is clear as we did not solve anything with the additional flavon fields, but rather just reparameterizing the Yukawa couplings in another way. This argument changes if the mass matrices contain certain structures. For our example let us assume that the scalar field χ obtains a VEV in direction $\langle \chi \rangle \sim v'(1, 1, 1)^T$. Notice that with this VEV configuration, there is a Z_3 *residual* exchange symmetry of the charged lepton VEVs. Similarly we can work out an interesting VEV configurations for the neutrino sector, say $\langle \phi \rangle \sim u(1, 0, 0)^T$ and we notice that we have a Z_2 symmetry for the two zeros. The residual symmetry of the VEV implies the same residual symmetry of the mass matrices for the leptons. Why we emphasize so much on the nontrivial residual symmetry of the broken flavor group? As the PMNS matrix is determined from the product of unitary and orthogonal rotation matrix that diagonalizes the charged leptons and neutrinos mass matrices, the residual symmetries remain invariant after diagonalizing the mass matrices, and the mismatch amongst them dictate the PMNS matrix up to permutations of rows and columns. The mixing matrix can be determined *solely* from a given discrete flavor symmetry group and its breaking to the residual subgroups. The crucial ingredient to obtain the mixing patterns without looking at the dynamics of the model depends on the representations of the fields in a certain discrete group and the structure of mass matrix which preserves the residual symmetry.

Let us be more precise with this approach. We start with a finite discrete flavor group G_f, under which the left-handed fermion (lepton or quark) doublets transform under a
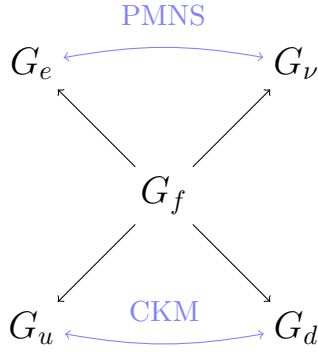
Figure 5.1: Sketch of remnant symmetry approach in this thesis. The flavor group G_f is broken down to different remnant symmetries of the different mass matrices, with the CKM and PMNS matrices generated by the mismatch of the subgroups.

faithful unitary 3-dimensional representation. Assuming that the flavons obtain their VEVs in such a way that the misaligned remnant symmetries between the charged lepton (u-type quark) and neutrino (d-type quark) mass matrices emerge, we can obtain a LO prediction for the leptonic (quark) mixing patterns. The crucial point is that G_f is broken to discrete subgroups G_e and G_ν for the leptonic sector, with the mass matrices of charged leptons and neutrinos respecting the symmetries of the subgroups G_e and G_ν respectively. Similarly the u-type and d-type quark mass matrices still enjoy the remnant symmetry of G_u and G_d respectively in the quark sector. The mismatch between G_e and G_ν generates the leptonic mixing patterns while misalignment between G_u and G_d creates the CKM matrix, see Fig. 5.1 for a clear sketch of the idea. We abbreviate the idea above as *remnant symmetry approach* [169, 170, 175–177, 191–193]. Of course the flavor group G_f in the leptonic sector can be different from the quark sector, and we can treat those two flavor groups independently. However it turns out that most of the interesting flavor groups that we will encounter later can yield both experimentally favored CKM and PMNS matrices at LO. The spirit of this chapter is to find common discrete groups that can explain leptonic and quark mixing patterns simultaneously.

In the leptonic flavor sector, the small discrete flavor symmetry groups such as A_4 and $\mathcal{S}_4$ were popular approaches in model building as they predict the TBM mixing pattern at LO. With the recent nonzero reactor mixing angle θ_{13} measured (see Table 5.1), TBM is strongly disfavored and one needs to rethink the discrete flavor symmetry approach to explain lepton flavor. In general there are two possibilities to reconcile the discrepancy. One possibility is to construct models which can lead to LO TBM structure and allow for large next-to-leading order (NLO) corrections, which usually involves breaking some of the remnant symmetry groups and severely limits the predictivity of the models. Another alternative approach is to start with new (larger) discrete groups that can predict a different type of mixing pattern at LO. In this thesis, we will pursue the second route and give a model independent list of discrete groups that can generate mixing patterns for leptons and quarks at LO. But before that let us first define our conventions and some basic notations in group theory which will be useful for classifying the relevant discrete groups.

5.2. PMNS and CKM Matrices from Remnant Symmetries

As we have seen in Fig. 5.1, lepton mixing can be obtained from the breaking of a discrete flavor symmetry group to some remnant symmetries in the charged lepton and neutrino

masses respectively. Analogously the CKM matrix can be derived in similar way where the remnant symmetries remain for the u-type and d-type quarks mass matrices. The spontaneous symmetry breaking is usually achieved in concrete models with the relevant flavon fields obtaining VEVs in some vacuum alignment configurations, as we have seen above. The actual models to achieve such symmetry breaking with specific vacuum configuration will not be considered in this thesis, but rather we want to search for discrete symmetry groups containing relevant residual symmetry groups which can predict acceptable LO PMNS and CKM matrices, i.e. we need to find discrete flavor groups that can be broken down to some nontrivial residual subgroups for the mass matrices. We first assume that neutrinos are Majorana particles, and will generalize our approach later to include Dirac neutrinos.

The mass matrices for the fermions are defined as

$$\mathcal{L} = -\overline{e_L}M_e e_R - \frac{1}{2}\nu^T M_\nu \nu - \overline{d_L}M_d d_R - \overline{u_L}M_u u_R, \tag{5.7}$$

after EW symmetry breaking (EWSB). Here we do not assume any specific mechanism to generate the Majorana neutrino mass. The PMNS and CKM matrices

$$U_{\text{PMNS}} = V_e^\dagger V_\nu, \qquad U_{\text{CKM}} = V_d^\dagger V_u \tag{5.8}$$

are obtained from the product of the unitary matrices V_s and V_ν which diagonalize the mass matrices

$$V_s^\dagger M_s M_s^\dagger V_s = \text{diag}(m_\text{I}^2, m_\text{II}^2, m_\text{III}^2), \qquad V_\nu^T M_\nu V_\nu = \text{diag}(m_1, m_2, m_3). \tag{5.9}$$

We denote the symbol $s \in \{e, d, u\}$ as the type of matrix and the numeral I, II and III as the fermion's generation for charged leptons, u-type and d-type quarks. For the case where neutrinos are Dirac particles, $s \in \{e, d, u, \nu\}$, i.e. neutrino mass matrix can be diagonalized like the LHS of Eq. (5.9).

In this thesis we follow the notations in Refs. [169, 170, 175–177, 191–193]. We assume a discrete symmetry group G_f in the leptonic sector, under which the left-handed lepton doublets $L = (\nu, e)^T$ transform under a faithful unitary 3-dimensional representation $\rho : G_f \to GL(3, \mathbb{C})$:

$$L \to \rho(g)L, \quad g \in G_f. \tag{5.10}$$

Similarly for the quarks we assume that there is a discrete symmetry group G_Q under which the left-handed quark doublets $Q = (u, d)^T$ transforms:

$$Q \to \rho(g)Q, \quad g \in G_Q. \tag{5.11}$$

In general the discrete group G_f for leptonic sector is not the same as G_Q and we can classify the different cases for G_f and G_Q into two settings:

- G_f and G_Q are independent, in this case we treat the both the discrete groups as separate starting point to obtain PMNS and CKM matrices independently. The leptonic discrete group G_f is broken into remnant symmetry subgroups $\{G_e, G_\nu\}$ for charged lepton and neutrino sectors. Analogously the argument applies for $G_Q \to \{G_u, G_d\}$.

- $G_Q \subset G_f$ or $G_Q \supset G_f$, which we can identify the larger group to be a common discrete group that can simultaneously yield the LO PMNS and CKM matrix, following the idea in Fig. 5.1.

For the first scenario we focus only on the breaking of $G_f \to \{G_e, G_\nu\}$ and classify all the discrete groups that predict experimentally favored LO leptonic mixing patterns. For the latter, as all the quark and lepton masses are different, the flavor symmetry group is required to be broken into two set of different subgroups, i.e. $\{G_d, G_u\}$ for the quark and $\{G_e, G_\nu\}$ for the leptonic sector. In general the generators of G_d and G_u only generate the group G_Q, which is a proper subgroup of G_f, if we assume that G_f is larger. Since we would like to find a unified discrete symmetry group G_f which can predict the LO PMNS and CKM matrix simultaneously, we will only consider a direct breaking $G_f \to \{G_d, G_u\}$, i.e. we look for groups G_f that can be broken into discrete subgroups $\{G_e, G_\nu, G_u, G_d\}$.

As all lepton masses are unequal and the mixing amongst all three mass eigenstates are nontrivial, the discrete flavor symmetry group G_f cannot be a global symmetry of the Lagrangian but has to be broken to different subgroups G_e and G_ν (with trivial intersection) in the charged lepton and neutrino sectors respectively, and to nonequal subgroups G_u and G_d in the u-type and d-type quark sectors. Subgroups from different subgroup set, e.g. G_e and G_d can have nontrivial intersection. An intersection of two subgroups contains the same elements. Note that within a set of the residual leptonic subgroups $\{G_e, G_\nu\}$, the intersection between subgroups in each set has to be trivial as we would like to predict three different mixing angles in the leptonic sector. However, this condition is relaxed for subgroups $\{G_d, G_u\}$ in the quark sector as we do not find any group that can predict three different quark mixing angles at LO. For the quark mixing patterns, all the interesting discrete groups can only predict the LO Cabibbo angle.

As a consequence of the breaking of $G_f \to \{G_e, G_\nu\}$ and $G_f \to \{G_u, G_d\}$, the mass matrices have to fulfill

$$\rho(g_s)^\dagger M_s M_s^\dagger \rho(g_s) = M_s M_s^\dagger \qquad \text{and} \qquad \rho(g_\nu)^T M_\nu \rho(g_\nu) = M_\nu, \qquad (5.12)$$

where $g_s \in G_s$ and $g_\nu \in G_\nu$. The transformation matrix $\rho(g_s)$ only acts on the flavor space of the respective left-handed fermion. Choosing non-abelian subgroups for $G_{s,\nu}$ will lead to degenerate mass spectrum, as representations of non-abelian groups cannot be decomposed into three inequivalent 1-dimensional representations of $G_{s,\nu}$. This scenario is not compatible with the experiments as all three neutrinos and charged fermions are distinguishable. We therefore restrict the subgroups $G_{s,\nu}$ to the abelian case. So what are the constraints on the subgroups $G_{s,\nu}$? As the charged leptons and quarks are distinguishable, the G_s group cannot be smaller than Z_3, i.e. all abelian subgroups of G_f with $|G_s| \geq 3$ can serve as good remnant symmetry group. This also applies for neutrinos if they are of Dirac nature. For the case when neutrinos are Majorana particles, we cannot have complex eigenvalues from the matrix $\rho(g_\nu)$, and therefore $\rho(g_\nu)^2 = 1$ has to be satisfied. We can further choose $\det \rho(g_\nu) = 1$ and by requiring all three Majorana neutrinos to be distinguishable, the group G_ν is restricted to be the Klein group $Z_2 \times Z_2$. In fact the Klein group is the only unique group that satisfy Eq. (5.12) for three distinguishable 1-dimensional representation of G_ν. Higher Z_2^n ($n > 2$) product groups are redundant as the Klein group is the maximal group

to accommodate three inequivalent generations of neutrinos.

Once the generators of all the residual subgroups are specified for a given representation, the mixing patterns of quark and leptonic sector can be determined from the product of the unitary matrices Ω_s and Ω_ν satisfying

$$\Omega_{s,\nu}^\dagger \rho(g_{s,\nu})\Omega_{s,\nu} = \rho(g_{s,\nu})_{\text{diag}}. \tag{5.13}$$

The unitary matrices Ω_s and Ω_ν are determined up to permutation matrices $P_{s,\nu}$ and a diagonal phase matrix $K_{s,\nu}$, i.e.

$$\Omega_{s,\nu} \to \Omega_{s,\nu} K_{s,\nu} P_{s,\nu}. \tag{5.14}$$

The PMNS and CKM matrix up to the permutations of rows and columns can be obtained from

$$U_{\text{PMNS}} = \Omega_e^\dagger \Omega_\nu \,, \quad U_{\text{CKM}} = \Omega_d^\dagger \Omega_u. \tag{5.15}$$

The Dirac CP phases of the PMNS and CKM matrices can also be determined from this method. However the Majorana phases cannot be determined from the remnant symmetry approach. We stress that it is not possible to obtain the unique mixing matrix in the remnant symmetry approach, but only up to the permutations of rows and columns as it is not possible to predict lepton masses. In this sense, the remnant symmetry approach allows us to obtain a manifold of mixing pattern configurations independent of the explicit mass matrices.

5.2.1. Simple Example for Leptonic Mixing Patterns

We will now apply the machinery above to some interesting cases by focusing on the leptonic mixing pattern only. Again we assume in this section that neutrinos are Majorana particles. As we have argued above that the smallest residual symmetry in the charged lepton sector is given by a $G_e = \langle T | T^3 = E \rangle \cong Z_3$. The bracket notation represents the *presentation* of a group generated by the element inside. For a relevant introduction to group theory particularly in discrete groups we refer the reader to Refs. [189, 194]. Next we need to specify the basis for the generators. As it will turn out to be useful later, we assume that $G_e = Z_3$ is in a basis where the generator in 3-dimensional representation is given by

$$\rho(T) = T_3 \equiv \begin{pmatrix} 0 & 1 & 0 \\ 0 & 0 & 1 \\ 1 & 0 & 0 \end{pmatrix}. \tag{5.16}$$

We denote ρ for a general representation, and T_3 for this special 3-dimensional matrix. The matrix $\rho(T)$ is diagonalized by

$$\Omega_e^\dagger \rho(T)\Omega_e = \text{diag}(1, \omega^2, \omega) \qquad \text{with} \qquad \Omega_e = \Omega_T \equiv \frac{1}{\sqrt{3}} \begin{pmatrix} 1 & 1 & 1 \\ 1 & \omega^2 & \omega \\ 1 & \omega & \omega^2 \end{pmatrix}, \tag{5.17}$$

and $\omega = e^{i2\pi/3}$. For the Klein group G_ν, one of the generator S of G_ν, satisfying $\rho(S)^2 = 1$ and $\det \rho(S) = 1$, is given by

$$\rho(S) = S_3 \equiv \begin{pmatrix} 1 & 0 & 0 \\ 0 & -1 & 0 \\ 0 & 0 & -1 \end{pmatrix}. \qquad (5.18)$$

Due to the degenerate eigenvalues (-1), we still have a two-parameter freedom in the matrix Ω_ν. It turns out to be useful for classifying our result later if we rotate the diagonal matrix $\rho(S)$

$$\Omega_\nu^\dagger \rho(S) \Omega_\nu = \mathrm{diag}(-1, 1, -1) \qquad \text{with} \qquad \Omega_\nu = \Omega_U U_{13}(\theta, \delta), \qquad (5.19)$$

where

$$\Omega_U = \begin{pmatrix} 0 & 1 & 0 \\ \frac{1}{\sqrt{2}} & 0 & -\frac{i}{\sqrt{2}} \\ \frac{1}{\sqrt{2}} & 0 & \frac{i}{\sqrt{2}} \end{pmatrix} \qquad \text{and} \qquad U_{13}(\theta, \delta) = \begin{pmatrix} \cos\theta & 0 & e^{i\delta}\sin\theta \\ 0 & 1 & 0 \\ -e^{-i\delta}\sin\theta & 0 & \cos\theta \end{pmatrix}. \qquad (5.20)$$

The degeneracy of the eigenvalues appears because the S generator only generates a Z_2 group with the degeneracy parameterized by a rotation θ in the 1-3 space. As we require three distinguishable Majorana neutrinos, we need the subgroup G_ν to be the Klein group, which requires additional generator U with

$$\rho(U) = U_3 \equiv -\begin{pmatrix} 1 & 0 & 0 \\ 0 & 0 & 1 \\ 0 & 1 & 0 \end{pmatrix}, \quad \text{with} \quad \Omega_U^\dagger \rho(U) \Omega_U = \mathrm{diag}(-1, -1, 1). \qquad (5.21)$$

This fixes the value of θ to zero. The discrete group $\mathcal{S}_4 = \langle S_3, T_3, U_3 \rangle$ with S_3, T_3 and U_3 given in our example above generates the famous TBM pattern

$$U_{\mathrm{PMNS}} = \Omega_e^\dagger \Omega_U = U_{\mathrm{HPS}}, \qquad (5.22)$$

introduced in Eq. (5.4). Until very recently, this pattern gave a good LO description of the leptonic mixing matrix. However the recent measurements of a nonvanishing θ_{13} have strongly disfavored the TBM pattern and to reconcile with this discrepancy, three general approaches are considered within the flavor physics community:

- Give up on flavor symmetry, which would imply flavor anarchy. We will not discuss flavor anarchy in details, but rather we will test its goodness-of-prediction against flavor symmetry in Sec. 5.4.

- Take TBM as starting point and break some residual symmetries with higher order corrections. This approach will not determine the full mixing pattern, but only partial mixing angles with certain sum rules. For instance if the remnant symmetry in the neutrino sector G_ν is taken to be $G_\nu = \langle S \rangle \cong Z_2$, i.e. U generator is broken, then the leptonic mixing matrix is given by $U_{\mathrm{PMNS}} = U_{\mathrm{HPS}} U_{13}(\theta, \delta)$ [195–201]. This mixing pattern leads to $\sin^2\theta_{12} > 1/3$ and is known as tri-maximal pattern TM2 [196, 202–

204]. Similarly we would obtain different sum rules if T generator is broken. This approach however only predicts a partial set of mixing angles but can accommodate the experimental results more easily. A group scan based on this assumption has been performed in Ref. [193].

- Start with new discrete symmetry group. Instead of breaking the residual symmetries and losing some predictivities of flavor symmetry group, we start with a (larger) new discrete symmetry group that generates experimentally allowed LO leptonic mixing angles. This idea can be generalized to the quark sector and we can chart new territories of possible interesting discrete groups. Utilizing this approach is the spirit of this chapter.

5.3. Charting New Discrete Flavor Symmetries

We will now survey a large group of discrete flavor groups that predict acceptable LO mixing patterns. First we will focus solely on the leptonic mixing pattern with the assumption that neutrinos are Majorana particles in Sec. 5.3.1. We then move on to apply our technique to search for discrete symmetry groups that simultaneously predict LO CKM and PMNS structure allowed by experimental measurements in Sec. 5.3.2. In Sec. 5.3.3 we will assume that neutrinos are Dirac particles and perform a scan of discrete groups that predict acceptable leptonic and quark mixing patterns.

To perform such a large survey we would require the computer algebra program called GAP [165] with the additional packages such as REPSN [166] to construct representations for finite groups, and SmallGroups [167] for accessing the subgroups of discrete groups. The procedure to perform and speed up such a group scan is laid out as follows:

1. We fix the relevant G_{s_1} and G_{s_2} where $s_i \in \{e, u, d, \nu\}$ and look for groups which contain these two subgroups. For instance if we want to find discrete groups that explain the leptonic mixing pattern when neutrinos are Majorana particles, $G_{s_1} = G_e = Z_3$ and $G_{s_2} = G_\nu = Z_2 \times Z_2$ are good candidates, as mentioned previously.

2. As all the discrete groups (for our purpose) are known and classified, we systematically look for a group G_f that contains G_{s_1} and G_{s_2} as its subgroups in a certain order, starting with the smallest. In general there are more than one group with the same order, and for simplicity we follow the ordering of SmallGroups in GAP. For example we loop from $\cdots \to [11,1] \to [12,1] \to [12,2] \to \ldots$, with the first number represents the order of the group while the second represents the identification of a certain group in this order. Every discrete group (up to order 1536) in SmallGroups is labeled in this way.

3. Some group theoretical result can be exploited to speed up the scanning process. For instance the Lagrange theorem can be used to skip over groups with order which is not divisible by $|G_{s_1}|$ and $|G_{s_2}|$, while the dimension theorem can be utilized to discard groups with order not divisible by 3. This is because we only consider groups which possess at least one irreducible 3-dimensional representation of the group generators.

For our example we skip over groups with order that is not divisible by 4 (order of Klein group) and 3 (order of Z_3).

4. For a specific group, all the 3-dimensional representations for the generators $\{\rho_{s_1}(S_j)\}$ and $\{\rho_{s_2}(S_k)\}$ are then recorded. The unitary matrices, Ω_{s_1} and Ω_{s_2} that diagonalize the generators are then being multiplied to obtain the desired mixing patterns as shown in Eq. (5.15). All the matrices with permutations of rows and columns for the mixing matrices were recorded. In the example, all the 3-dimensional representations $\rho(U)$, $\rho(S)$ and $\rho(T)$ for generators U, S (Klein group) and T (Z_3 group) are recorded. With each set of generators for the Klein group, we determine the unitary matrix Ω_ν which simultaneously diagonalizes both $\rho(S)$ and $\rho(U)$. In the same representation, a unitary matrix Ω_e that diagonalizes the $\rho(T)$ matrix is obtained. The corresponding Ω_ν and Ω_e will be multiplied to obtain a PMNS matrix. We repeat the process for all the different combinations of Ω_ν and Ω_e obtained from different sets of $\{\rho(U), \rho(S)\}$ and $\rho(T)$ respectively.

5. We then repeat process (2) for the next group G_f.

5.3.1. Leptonic Mixing Patterns for Majorana Neutrinos

In Sec. 5.2 we have shown that in order to (up to permutations of rows and columns) determine the leptonic mixing patterns from pure group theory approach, the most crucial ingredients are the unbroken remnant symmetries in the neutrino and charged lepton mass matrices. It is also important that there are three inequivalent 1-dimensional representations for each sector, such that we have no degeneracy among the generations. As we have argued above, we require that the neutrino sector possesses a Klein group symmetry $Z_2 \times Z_2$, as we require three distinguishable generations of Majorana neutrinos. For the charged lepton sector we require an abelian group. We first consider the smallest relevant Z_3 group, and generalize our search to general finite abelian groups later.

For the case of $G_\nu = Z_2 \times Z_2$, $G_e = Z_3$

We first assume that the charged lepton sector has a Z_3 symmetry while the neutrino sector has a $Z_2 \times Z_2$ symmetry, and perform a scan for all discrete groups of size smaller than 1536 using the algorithm above. The total number of 1336749 finite discrete groups (with an additional group of $\Delta(6 \cdot 16^2)$) has been scanned, and only groups which contain the Klein group and Z_3 as their subgroups are kept. All the permutations of rows and columns for the corresponding PMNS matrices are generated and we order the PMNS matrices with the smallest 1-3 entry and an additional condition such that the 1-1 entry is larger or equal to 1-2 entry. This sorting algorithm removes a huge amount of irrelevant and duplicated matrices.

The flavor mixing angles are extracted from the resulting PMNS matrices and the results are plotted as black circles in Fig. 5.2. From over one million finite discrete groups that we have scanned, only three finite discrete groups up to the order of 1535 including $\Delta(6 \cdot 16^2)$ can generate the leptonic mixing angles allowed by the experimental values up to 3σ. The strongest constraint comes from the recently measured reactor mixing angle θ_{13}. We observe

n	G	n	G	n	G	n	G
4	$\Delta(6 \cdot 4^2)$	9	$(Z_{18} \times Z_6) \rtimes \mathcal{S}_3$	13	$\Delta(6 \cdot 26^2)$	18	$(Z_{18} \times Z_6) \rtimes \mathcal{S}_3$
5	$\Delta(6 \cdot 10^2)$	10	$\Delta(6 \cdot 10^2)$	14	$\Delta(6 \cdot 14^2)$	24	$Z_3 \times \Delta(6 \cdot 8^2)$
7	$\Delta(6 \cdot 14^2)$	11	$\Delta(6 \cdot 22^2)$	15	$Z_3 \times \Delta(6 \cdot 10^2)$		
8	$\Delta(6 \cdot 8^2)$	12	$Z_3 \times \Delta(6 \cdot 4^2)$	16	$\Delta(6 \cdot 16^2)$		

Table 5.2.: Interesting groups generated by T_3, S_3 and $U_3(n, k = 1)$ that predict acceptable leptonic mixing structures. The number n defines the $U_3(n, k = 1)$ generator for generalized Klein group. We observe that only groups of $(Z_n \times Z_{n'}) \rtimes \mathcal{S}_3$ generate leptonic mixing structure that are favored by the experiments.

that many of the discrete finite groups with $G_e = Z_3$ and $G_\nu = Z_2 \times Z_2$ predict leptonic mixing patterns that lie on a parabola in the mixing angle plane. Note that Fig. 5.2 is a zoom-in plot where we have ignored mixing angles that lie beyond the plotted region. The mixing angles lying outside the zoom-in region will be shown in Fig. 5.3. The mixing angles predicted by TBM are given as the minimum of the parabola. All the groups scanned up to order 1536 predict solar mixing angle $\sin^2(\theta_{12}) \geq 1/3$.

Can we classify all those discrete groups that lie on the parabola in a simple systematic way? In Sec. 5.2.1, we had shown that if the Z_3 remnant symmetry in the charged lepton sector is generated by the matrix T_3 given in Eq. (5.16), and the Klein group is generated by the S_3 and U_3 in Eq. (5.18) and Eq. (5.21), the resulting mixing matrix is a TBM as shown in Eq. (5.22). It turns out that all the new mixing patterns in Fig. 5.2 can be parameterized as

$$U_{\text{PMNS}} = U_{\text{HPS}} U_{13}(\theta = \frac{1}{2} \arg(z), \delta = 0), \tag{5.23}$$

with U_{13} defined in Eq. (5.20), i.e. they are all just TBM matrix rotated with certain angle in 1-3 angle plane. This result can be understood as a misalignment between the remnant symmetry T_3 in the charged lepton sector and the "generalized" Klein group generated by S_3 and $U_3(n, k = 1)$ in the neutrino sector, with

$$U_3(n, k) = - \begin{pmatrix} 1 & 0 & 0 \\ 0 & 0 & z_{n,k} \\ 0 & z_{n,k}^* & 0 \end{pmatrix}, \quad \text{with} \quad z_{n,k} = e^{2\pi i k/n}, \ k \leq n \in \mathbb{N}. \tag{5.24}$$

We think of $U_3(n, k = 1)$ as one of a generalized generator for the Klein group. Note that the awkward notation k will be useful for Sec. 5.3.2. It is easy to see that for any $|z| = 1$, we have $[S_3, U_3(n, k = 1)] = 0$ and $U_3(n, k = 1)^2 = \mathbb{1}_3$ and therefore the group generated by S_3 and $U_3(n, k = 1)$ is always a Klein group. The leptonic mixing pattern generated by T_3, S_3, and $U_3(n, k = 1)$ has to be of the form given in Eq. (5.23) with $z_{n,k=1}$ parameterizing the rotation away from TBM. Note that $\langle z_{n,k=1} \rangle \cong Z_n$ is a cyclic group. Different nth root of $z_{n,k}$ will in general generate different leptonic mixing angles according to Eq. (5.23), with the results shown in Fig. 5.2. We list down the names of the groups generated for $n = 4, \ldots, 16$ in Table 5.2. From a first glance one might be tempted to think that all of the interesting groups on the parabola can be classified as $\Delta(6 \cdot n^2)$ [205, 206], however the
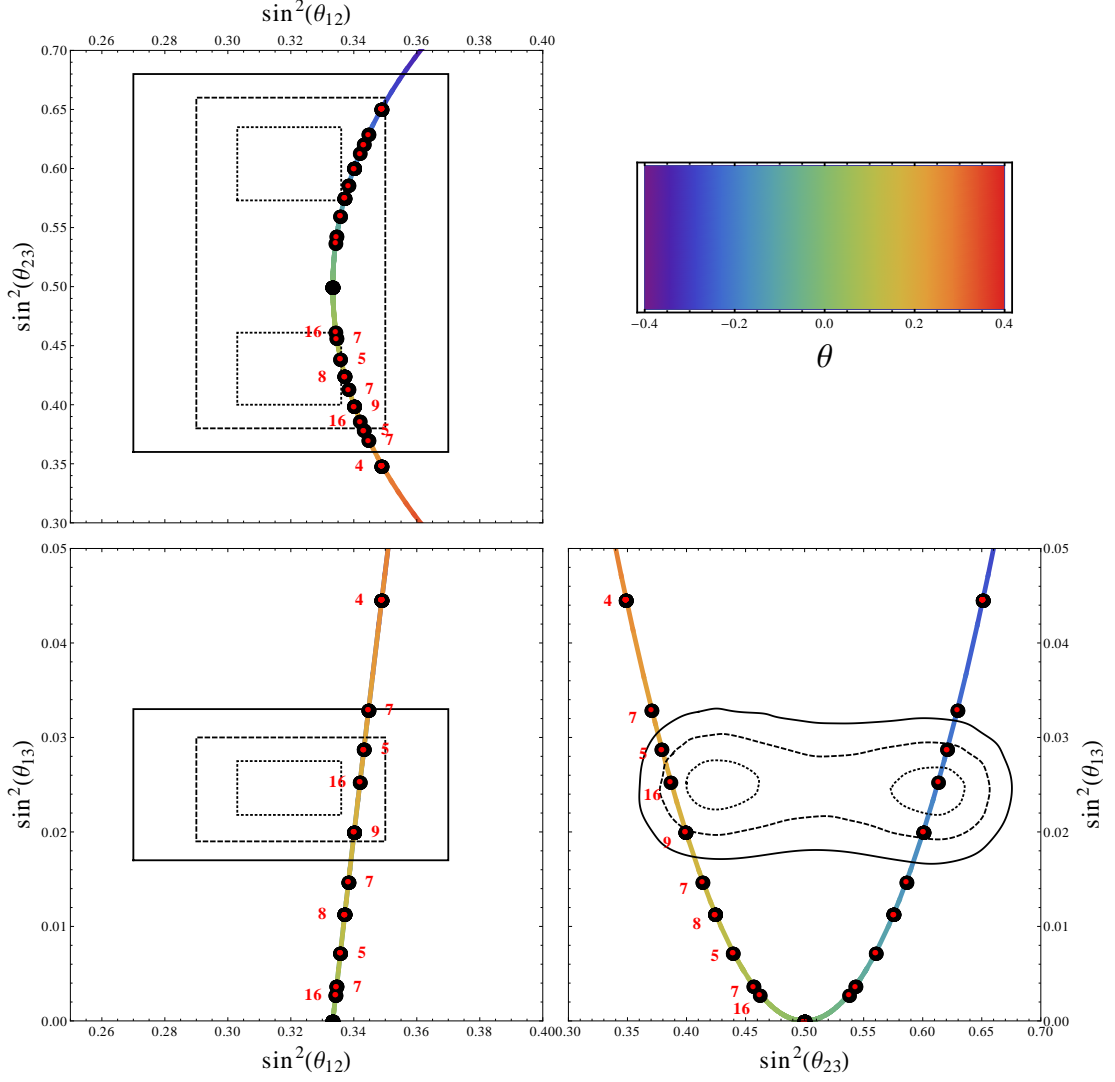
Figure 5.2.: The leptonic mixing angles determined from group scan up to order 1536 are plotted in black circles. The red dots represent the mixing angles determined from the generator S_3, T_3 and $U_3(n, k = 1)$, with the red labels represent the integer n for generator $U_3(n, k = 1)$. The interpolating parabola is colored according to the value of θ as defined in Eq. (5.20).

correct classification should be of the form of $(Z_n \times Z_{n'}) \rtimes \mathcal{S}_3$, which we will discuss shortly. The predictions for mixing angles using our classification are calculated to be

$$|U_{\text{PMNS}}| = \frac{1}{\sqrt{3}} \begin{pmatrix} \sqrt{2}\cos(\frac{\pi}{6} - \frac{\pi}{n}) & 1 & \sqrt{2}\sin(\frac{\pi}{6} - \frac{\pi}{n}) \\ \sqrt{2}\cos(\frac{\pi}{6} + \frac{\pi}{n}) & 1 & \sqrt{2}\sin(\frac{\pi}{6} + \frac{\pi}{n}) \\ \sqrt{2}\sin(\frac{\pi}{n}) & 1 & \sqrt{2}\cos(\frac{\pi}{n}) \end{pmatrix}, \quad \text{for } \sin^2(\theta_{23}) \geq \frac{1}{2}, \quad (5.25)$$

$$\text{or} \quad = \frac{1}{\sqrt{3}} \begin{pmatrix} \sqrt{2}\cos(\frac{\pi}{6} - \frac{\pi}{n}) & 1 & \sqrt{2}\sin(\frac{\pi}{6} - \frac{\pi}{n}) \\ \sqrt{2}\sin(\frac{\pi}{n}) & 1 & \sqrt{2}\cos(\frac{\pi}{n}) \\ \sqrt{2}\cos(\frac{\pi}{6} + \frac{\pi}{n}) & 1 & \sqrt{2}\sin(\frac{\pi}{6} + \frac{\pi}{n}) \end{pmatrix}, \quad \text{for } \sin^2(\theta_{23}) < \frac{1}{2}. \quad (5.26)$$

Note that we consider only the absolute value of the resulting matrices shown in the form above. The result is shown (red dots) in Fig. 5.2 with the relevant result shown in Table

n	G	GAP-Id	$\sin^2(\theta_{12})$	$\sin^2(\theta_{13})$	$\sin^2(\theta_{23})$
5	$\Delta(6 \cdot 10^2)$	$[600, 179]$	0.3432	0.0288	0.3791/0.6209
9	$(Z_{18} \times Z_6) \rtimes \mathcal{S}_3$	$[648, 259]$	0.3402	0.0201	0.3992/0.6008
16	$\Delta(6 \cdot 16^2)$	n.a.	0.3420	0.0254	0.3867/0.6134

Table 5.3.: Mixing angles predicted by interesting groups which are compatible with 3σ experimental results are shown. The group identification function in `SmallGroups` is not available for group with order 1536.

5.3, and all of them agree with our simple classification. Some of the groups such as $\Delta(96)$ ($n = 4$) and $\Delta(384)$ ($n = 8$) have been obtained before in [192], however they do not predict acceptable mixing angles and hence are of no further interest. All the groups restricted to those shown in Fig. 5.2 predict $\delta_{\text{CP}} = \pi$ or 0. The parabola depicted in Fig. 5.2 will be densely covered for groups with arbitrary size. The mixing patterns corresponding to $n = 5$, $n = 9$ and $n = 16$ predict experimentally favored leptonic mixing patterns.

For the case of $G_\nu = Z_2 \times Z_2$, $|G_e| > 3$

We now relax the condition on the charged lepton subgroups by allowing G_e to be any abelian group which is a subgroup of G_f. We keep the Klein group for Majorana neutrino sector. As the number of groups are larger due to the less constraining assumption, a complete search to large order of groups is computationally expensive. Therefore, we have restricted our scanning process of all the discrete finite groups G_f only up to order 511. The result is shown in Fig. 5.3 and to our surprise, only the leptonic mixing patterns predicted by finite modular groups and their subgroups [192] are obtained. Note that in general other groups which lie outside the region shown in Fig. 5.2 do give nontrivial Dirac CP phases, unlike those predicted by $(Z_n \times Z_{n'}) \rtimes \mathcal{S}_3$.

Can we understand heuristically why from all the discrete groups up to order 1536 scanned above, only those with $(Z_n \times Z_{n'}) \rtimes \mathcal{S}_3$ predict acceptable leptonic mixing angles? It turns out that we can naively expect that most of the groups that can yield experimentally favored mixing patterns have the form of TBM, as TBM already provides a relatively good starting point for LO mixing angles compared to other finite modular groups such as A_5, $PSL(2, Z_7)$. From the group structure, the group $(Z_n \times Z_{n'}) \rtimes \mathcal{S}_3$ can be broken into

$$\underbrace{(Z_n \times Z_{n'})}_{\downarrow \atop Z_2 \times Z_2} \rtimes \underbrace{\mathcal{S}_3}_{\downarrow \atop Z_3}, \tag{5.27}$$

where we can observe that the resulting deviation from TBM described by the parabola in Fig. 5.2 stems from the misalignment of the generalized Klein group and Z_3. Of course the actual breaking of $(Z_n \times Z_{n'}) \rtimes \mathcal{S}_3$ is more involved than what we have shown in Eq. (5.27), and the reader should take such a naive argument as an idea on how the discrete groups are broken in such a way that we obtain a deviation pattern from TBM.
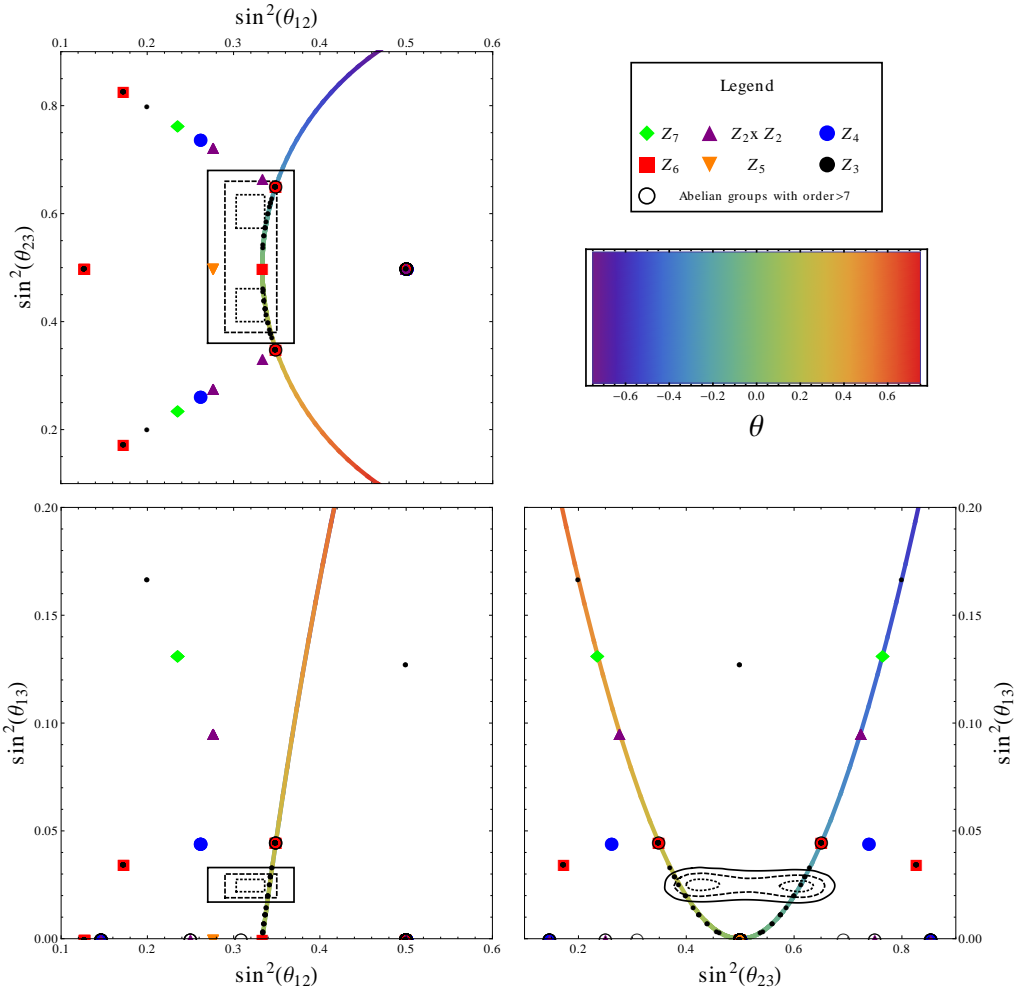
Figure 5.3.: Mixing patterns obtained from G_f up to order 511 by considering all the abelian subgroups for G_e. We also plotted the mixing patterns obtained from groups with $G_e = Z_3$ for the sake of comparison, shown in black dots. Only the mixing patterns predicted by finite modular groups and their subgroups are obtained for $|G_e| > 3$ [192]. The mixing patterns from $G_e = Z_3$ outside the parabola are also generated by finite modular groups (e.g. A_5, $PSL(2, Z_7)$) and their subgroups. Nontrivial Dirac CP-phases are predicted for some of the discrete groups lying outside of the experimentally 3σ range.

5.3.2. Leptonic and Quark Mixing Patterns from Unified Symmetries

In this section we extend our scanning algorithm to search for discrete groups that predict acceptable LO quark mixing angles. The Cabibbo angle θ_c is of similar size as the reactor mixing angle $\theta_{13} \simeq \theta_c/\sqrt{2} \simeq 9.2°$, therefore it would be interesting if all the leptonic and the Cabibbo angle are produced at LO as a result of remnant symmetries from the breaking of a common discrete group. Since other angles in CKM matrix are smaller than the Cabibbo angle, we can assume that they are obtained as a result of NLO corrections. From the finite discrete groups with order less than 1536 in Sec. 5.3.1, only three interesting groups predict LO leptonic mixing patterns within 3σ of current best fit. Since we are looking for discrete groups that can predict both the LO leptonic mixing angles and Cabibbo angle, perhaps these three groups, namely $\Delta(6 \cdot 10^2)$, $(Z_{18} \times Z_6) \rtimes \mathcal{S}_3$ and $\Delta(6 \cdot 16^2)$, could provide a good

n	G_f	GAP-Id	$\sin\tilde\theta$	type
5	$\Delta(6\cdot 10^2)$	$[600, 179]$	0.156	I
			0.309	II
9	$(Z_{18} \times Z_6) \rtimes \mathcal{S}_3$	$[648, 259]$	0.259	I
16	$\Delta(6\cdot 16^2)$	n.a.	0.195	I

Table 5.4.: LO Cabibbo angles $\sin\tilde\theta$ generated by flavor groups up to order 1536 compatible with experimental results are shown. Type I and II refers to different breaking of G_f into residual symmetry groups (see Sec. 5.3.2).

starting point for us to look for their predicted LO Cabibbo angle. By searching all the abelian subgroups contained in these three groups, all the LO CKM matrices obtained are in the following form:

$$
U_{\mathrm{CKM}} = \begin{pmatrix} \cos\tilde\theta & \sin\tilde\theta & 0 \\ -\sin\tilde\theta & \cos\tilde\theta & 0 \\ 0 & 0 & 1 \end{pmatrix}.
\tag{5.28}
$$

The values of $\sin\tilde\theta$ are given in Table 5.4 and the form may be compared to the the CKM experimental values in Eq. (5.2). We also extend our searches to find generic G_Q that can predict three different mixing angles in the quark sector at LO, however no such group has been found. We conclude that no discrete group can predict three distinguished LO CKM mixing angles, as a consequence the Dirac CP phase for the CKM matrix cannot be determined from this approach.

We will now classify our result for the quark mixing patterns in group theory language analogue to the leptonic mixing patterns in Sec. 5.3.1. From the searches, we found two different types of residual subgroups which are relevant. From Eq. (5.28) with the LO CKM matrix, the intersection between G_u and G_d must be nontrivial, otherwise there would be full 3×3 mixing as in the leptonic case. It turns out to be useful to pick S as the generator for the intersection. As a result, we found 2 types of remnant symmetries generated by:

- type I:

$$
G_d = \langle S, U(n, p) \rangle \cong Z_2 \times Z_2,
$$
$$
G_u = \langle (ST)^2 T U(n, m) \rangle \cong Z_4.
$$

- type II:

$$
G_d = \langle S, U(n, p) \rangle \cong Z_2 \times Z_2,
$$
$$
G_u = \langle S, (U(n, m) T^2)^2 (U(n, m) T)^2 U(n, m) \rangle \cong Z_2 \times Z_2.
$$

where the 3-dimensional irreducible representations for S, T and $U(n, p)$ are defined in Eq. (5.18), Eq. (5.16) and Eq. (5.24) respectively. Observe that abelian groups of order 4 play an important role in predicting the acceptable Cabibbo angle.

Let us discuss the case of type I residual symmetries. The LO CKM matrix in Eq. (5.28) is

obtained from the breakdown of G_f down to residual subgroups $G_d = \langle S, U(n,m) \rangle \cong Z_2 \times Z_2$ and $G_u = \langle (ST)^2 TU(n,p) \rangle \cong Z_4$, with $m \neq p$. The element $((ST)^2 TU(n,p))^2 = S$ belongs to both G_d and G_u as it is the generator for the intersection. The generator of the group G_u is given by

$$R_3(n,p) \equiv \rho((ST)^2 TU(n,p)) = \begin{pmatrix} 1 & 0 & 0 \\ 0 & 0 & -z_{n,p} \\ 0 & z_{n,p}^* & 0 \end{pmatrix} \tag{5.29}$$

with $z_{n,p}$ defined in Eq. (5.24). In a same unified group G_f, typically a different nth root in Eq. (5.24) and Eq. (5.29) is required to generate experimentally favored leptonic and quark mixing matrices. For example, if we choose $z_{n,m}$ in Eq. (5.24) and $z_{n,p}$ in Eq. (5.29), the LO CKM matrix

$$U_{\text{CKM}} = \Omega_d^\dagger \Omega_u = \frac{1}{2} \begin{pmatrix} 1 + ie^{-2\pi i(m-p)/n} & 1 - ie^{-2\pi i(m-p)/n} & 0 \\ 1 - ie^{-2\pi i(m-p)/n} & 1 + ie^{-2\pi i(m-p)/n} & 0 \\ 0 & 0 & 2 \end{pmatrix}. \tag{5.30}$$

is generated by

$$\Omega_u = \frac{1}{\sqrt{2}} \begin{pmatrix} 0 & 0 & \sqrt{2} \\ ie^{2\pi ip/n} & -ie^{2\pi ip/n} & 0 \\ 1 & 1 & 0 \end{pmatrix}, \quad \Omega_d = \frac{1}{\sqrt{2}} \begin{pmatrix} 0 & 0 & \sqrt{2} \\ e^{2\pi im/n} & -e^{2\pi im/n} & 0 \\ 1 & 1 & 0 \end{pmatrix}, \tag{5.31}$$

where Ω_u diagonalizes $R_3(n,p)$ while Ω_d diagonalizes S_3 and $U_3(n,m)$. The resulting Cabibbo angle can be expressed as

$$\sin \tilde{\theta} = \frac{1}{2} \sqrt{2 - 2 \sin \left(\frac{2\pi(m-p)}{n} \right)}. \tag{5.32}$$

For case of type I, the interesting cases shown in Table 5.4 correspond to $(n = 5, p = 1, m = 2)$, $(n = 9, p = 1, m = 4)$ and $(n = 16, p = 1, m = 2)$, respectively. Since G_u and G_d have a nontrivial intersection, the full flavor group generated by the elements of G_u and G_d is not G_f, but rather a subgroup of U(2), depending on the values of n, p and m. The three groups generated by $(n = 5, p = 1, m = 2)$, $(n = 9, p = 1, m = 4)$ and $(n = 16, p = 1, m = 2)$ are isomorphic to $(Z_{10} \times Z_2) \rtimes Z_2$, $(Z_6 \times Z_2) \rtimes Z_2$ and QD_{32}[3], respectively. See Ref. [189] for a comprehensive review on the groups described above. For the case of type II, applying the analogous methods and arguments above we find

$$\sin \tilde{\theta} = \left| \cos \left(\frac{\pi(m - 4p)}{n} \right) \right|, \tag{5.33}$$

where only $\Delta(6 \cdot 10^2)$ predicts acceptable Cabibbo angle prediction, shown in Table 5.4. The corresponding subgroup is generated by $(n = 5, p = 1, m = 1)$, which is a D_{20}, dihedral group of size 20 [207].

---

[3] The quasi-dihedral group of order 32.

The structure of the LO CKM mixing (5.28) stems from symmetry breakdown to the remnant symmetry subgroups of type I and type II, which are all abelian groups of order 4. The groups $\Delta(6 \cdot 10^2)$, $(Z_{18} \times Z_6) \rtimes \mathcal{S}_3$ and $\Delta(6 \cdot 16^2)$ are all of the form $(Z_n \times Z_{n'}) \rtimes \mathcal{S}_3$, where they are generated by:

$$Z_n \cong \langle (ST)^2 (U(n,1)T)^4 T \rangle,$$
$$Z_{n'} \cong \langle STSU(n,1)T^2 U(n,1)T^2 U(n,1)TU(n,1) \rangle,$$
$$\mathcal{S}_3 = \langle R', T^2 R'TR' \rangle, \quad \text{with } R' = (U(n,1)T^2)^2 (U(n,1)T)^2 U(n,1). \tag{5.34}$$

Using this structure, one can work out the mathematical structure of the groups. Is there a heuristic way to understand the origin symmetry breaking to type I and II subgroups? It turns out that from the examples we have studied above, the groups of type I and II are subgroups of type $(Z_m \times Z_{m'}) \rtimes Z_2$, which are always subgroups of $(Z_n \times Z_{n'}) \rtimes \mathcal{S}_3$ with $n^{(\prime)} \geq m^{(\prime)}$. One of the Z_m can be trivial, e.g. the dihedral group. Schematically we can understand the flavor symmetry breaking as follows

$$\underbrace{(Z_n \times Z_{n'})}_{\substack{\downarrow \\ Z_m \times Z_{m'}}} \rtimes \underbrace{\mathcal{S}_3}_{\substack{\downarrow \\ Z_2}}. \tag{5.35}$$

We remind the reader that discrete groups that predict acceptable leptonic mixing angles in Sec. 5.3.1 are always in the form of $(Z_n \times Z_{n'}) \rtimes \mathcal{S}_3$, given in Eq. (5.27). Therefore the 1-2 mixing structure of Eq. (5.28) is always a by-product from the leptonic flavor symmetry, i.e. the Cabibbo angle always comes for free in the remnant symmetry approach, provided that we consider group of type $(Z_n \times Z_{n'}) \rtimes \mathcal{S}_3$. Of course we would need to choose a flavor group G_f wisely to find the one that predicts both LO CKM and PMNS closer to the experimental values. One might ask whether it is possible that $G_Q \nsubseteq G_L = \langle G_e, G_\nu \rangle$ but rather as subgroup of yet larger group $G_f = \langle G_Q, G_L \rangle$. However, from all the discrete groups that we have found, G_Q is always a proper subgroup of $G_L \equiv G_f$, and hence an extension to larger group is not necessary. The group generated by G_u and G_d is not G_f but typically a smaller proper subgroup $G_Q \subset G_f$. As all the groups we have scan cannot predict three distinguished quark mixing angles which are experimentally acceptable, it is better to think that the 3-dimensional representation $\mathbf{3}$ of G_f is always decomposable into $\mathbf{3} = \mathbf{2} + \mathbf{1}$, where the doublet $\mathbf{2}$ of G_Q is responsible for generating the Cabibbo angle[4]. This scenario should be kept in mind when we look for quark mixing angles using the remnant symmetry approach.

As we have seen above we can only obtain one mixing angle in the quark sector from our approach. Having Eq. (5.28) as a LO CKM matrix is better than having no mixing angle, i.e. a unit matrix, as we only require small NLO corrections to obtain the correct CKM matrix. NLO corrections of the order of $U_{cb} \sim \lambda_C^2 \sim 0.04$ are needed if we have a LO prediction of the form in Eq. (5.28). Compared to the case of A_4 where only $U_{\text{CKM}} = \mathbb{1}_3$ is predicted at LO, the NLO corrections have to be of the size $U_{cs} \sim \lambda_C \equiv \sin\theta_c \sim 0.22$, which is large.

---

[4]Remember that doublet mixing is described by only an angle.

G_f	GAP-Id	$\{G_e, G_\nu\}$	$\{G_d, G_u\}$	$\sin^2(\theta_{12})$	$\sin^2(\theta_{13})$	$\sin^2(\theta_{23})$	$\sin\tilde{\theta}$
$\Delta(6 \cdot 5^2)$	$[150, 5]$	$\{Z_{10}, Z_3\}$	$\{Z_{10}, Z_{10}\}$	0.3428	0.0289	0.6217	0.309
				0.3428	0.0289	0.3794	
$\Sigma(3 \cdot 3^3) \rtimes Z_2$	$[162, 10]$	$\{Z_6, Z_9\}$	$\{Z_6, Z_6\}$	0.3403	0.0202	0.6013	0.5
$(Z_9 \times Z_3) \rtimes \mathcal{S}_3$	$[162, 12]$	$\{Z_{18}, Z_9\}$	$\{Z_{18}, Z_{18}\}$	0.3403	0.0202	0.3996	
	$[162, 14]$	$\{Z_{18}, Z_3\}$	$\{Z_{18}, Z_{18}\}$				

Table 5.5.: Lepton mixing parameters and LO Cabibbo angles predicted by finite discrete groups of order 150 and 162. We show also the smallest generators for relevant $\{G_e, G_\nu\}$ and $\{G_d, G_u\}$ in the middle columns.

As a quick summary for this section: We systematically scanned for groups that can predict experimentally acceptable leptonic mixing patterns with the assumption of Majorana neutrinos. From over one million groups, only groups of type $(Z_n \times Z_{n'}) \rtimes \mathcal{S}_3$ are interesting and they also predict decent LO Cabibbo angles in the quark sector. Those discrete groups might provide an interesting opportunity for model building.

5.3.3. Leptonic Mixing Patterns for Dirac Neutrinos

In this section we drop the Majorana assumption for neutrinos and assume that they are Dirac particles, as a priori we have no evidence that neutrinos are of Majorana nature. Like previous section, we scan for the smallest finite discrete group that can yield experimentally favored quark and leptonic mixing patterns by assuming that neutrinos are Dirac particles. As we have previously mentioned in Sec. 5.2, the residual symmetry group of neutrino masses may now be an arbitrary abelian group, when we dropped the assumption of Majorana neutrinos. As the amount of group is large and we cannot utilize Lagrange theorem to skip some of the groups, we only perform a scan for all the abelian subgroups of discrete group G_f up to the size of 200. It turns out that the two smallest discrete groups interesting for our purpose are of the order of 150 and 162, with the resulting structure of the relevant remnant groups given in Table 5.5. The 3-dimensional generators for the relevant groups are given in Table 5.6 where we gave the smallest relevant subgroups $\{G_e, G_\nu\}$ and $\{G_u, G_d\}$ that can predict acceptable PMNS and CKM mixing parameters. One can ignore the Cabibbo angle if one is only interested in the smallest discrete flavor group that can yield acceptable leptonic mixing patterns by assuming that neutrinos are Dirac particles. For the first time, the discrete groups that predict acceptable LO leptonic mixing angles with Dirac neutrinos and CKM matrix up to order 200 are completely charted.

Let us discuss some interesting properties of the found groups. To be concrete, we focus on the group $\Delta(6 \times 5^2)$ as an illustrative example[5]. The group $\Delta(6 \times 5^2)$ may be generated by

$$A = (TU(5,1))^4 T^2, \qquad B = (U(5,1)T^2)^2 U(5,1), \tag{5.36}$$

---

[5]Note that the group $\Delta(6 \cdot 5^2)$ is also discussed in Ref. [208], however they only consider a Z_2 as one of the residual subgroup, which will not give full leptonic mixing angle predictions.

G_f [GAP $-$ Id]	Generators of subgroups
$\Delta(6 \cdot 5^2)$ [150, 5]	$\langle G_e, G_\nu \rangle = \left\langle \begin{pmatrix} 0 & -(-1)^{3/5} & 0 \\ 0 & 0 & -\sqrt[5]{-1} \\ -\sqrt[5]{-1} & 0 & 0 \end{pmatrix}, \begin{pmatrix} (-1)^{3/5} & 0 & 0 \\ 0 & 0 & \sqrt[5]{-1} \\ 0 & \sqrt[5]{-1} & 0 \end{pmatrix} \right\rangle$ $\langle G_u, G_d \rangle = \left\langle \begin{pmatrix} (-1)^{3/5} & 0 & 0 \\ 0 & 0 & -(-1)^{2/5} \\ 0 & -1 & 0 \end{pmatrix}, \begin{pmatrix} (-1)^{3/5} & 0 & 0 \\ 0 & 0 & (-1)^{3/5} \\ 0 & -(-1)^{4/5} & 0 \end{pmatrix} \right\rangle$
$\Sigma(3 \cdot 3^3) \rtimes Z_2$ [162, 10]	$\langle G_e, G_\nu \rangle = \left\langle \begin{pmatrix} 0 & 0 & -1 \\ 0 & -\sqrt[3]{-1} & 0 \\ -1 & 0 & 0 \end{pmatrix}, \begin{pmatrix} 0 & 0 & (-1)^{2/3} \\ (-1)^{2/3} & 0 & 0 \\ 0 & -\sqrt[3]{-1} & 0 \end{pmatrix} \right\rangle$ $\langle G_u, G_d \rangle = \left\langle \begin{pmatrix} 0 & 0 & -1 \\ 0 & -\sqrt[3]{-1} & 0 \\ -1 & 0 & 0 \end{pmatrix}, \begin{pmatrix} 0 & 0 & \sqrt[3]{-1} \\ 0 & -1 & 0 \\ -1 & 0 & 0 \end{pmatrix} \right\rangle$
$(Z_9 \times Z_3) \rtimes \mathcal{S}_3$ [162, 12]	$\langle G_e, G_\nu \rangle = \left\langle \begin{pmatrix} 0 & 0 & (-1)^{5/9} \\ 0 & (-1)^{8/9} & -(-1)^{5/9} & 0 \\ (-1)^{5/9} & 0 & 0 \end{pmatrix}, \right.$ $\left. \begin{pmatrix} 0 & 0 & (-1)^{5/9} - (-1)^{8/9} \\ -(-1)^{5/9} & 0 & 0 \\ 0 & -(-1)^{5/9} & 0 \end{pmatrix} \right\rangle$ $\langle G_u, G_d \rangle = \left\langle \begin{pmatrix} 0 & 0 & (-1)^{5/9} \\ 0 & (-1)^{8/9} - (-1)^{5/9} & 0 \\ (-1)^{5/9} & 0 & 0 \end{pmatrix}, \right.$ $\left. \begin{pmatrix} 0 & 0 & (-1)^{8/9} - (-1)^{5/9} \\ 0 & (-1)^{8/9} - (-1)^{5/9} & 0 \\ -(-1)^{8/9} & 0 & 0 \end{pmatrix} \right\rangle$
$(Z_9 \times Z_3) \rtimes \mathcal{S}_3$ [162, 14]	$\langle G_e, G_\nu \rangle = \left\langle \begin{pmatrix} 0 & 0 & (-1)^{5/9} \\ 0 & -(-1)^{8/9} & 0 \\ (-1)^{5/9} & 0 & 0 \end{pmatrix}, \right.$ $\left. \begin{pmatrix} 0 & \sqrt[9]{-1} - (-1)^{4/9} & 0 \\ 0 & 0 & (-1)^{4/9} \\ \sqrt[9]{-1} - (-1)^{4/9} & 0 & 0 \end{pmatrix} \right\rangle$ $\langle G_u, G_d \rangle = \left\langle \begin{pmatrix} 0 & 0 & (-1)^{5/9} \\ 0 & -(-1)^{8/9} & 0 \\ (-1)^{5/9} & 0 & 0 \end{pmatrix}, \right.$ $\left. \begin{pmatrix} 0 & 0 & -(-1)^{8/9} \\ 0 & -(-1)^{8/9} & 0 \\ (-1)^{8/9} - (-1)^{5/9} & 0 & 0 \end{pmatrix} \right\rangle$

Table 5.6.: The relevant group generators for each group listed in Table 5.5 that predicts acceptable mixing patterns with the assumption of Dirac neutrinos are shown.

where again we remind the reader that the 3-dimensional irreducible representations for S, T and $U(n,p)$ are defined in Eq. (5.18), Eq. (5.16) and Eq. (5.24) respectively. After breaking the flavor symmetry to subgroups $G_e = \langle A \rangle \cong Z_3$ and $G_\nu = \langle B \rangle \cong Z_{10}$, the PMNS mixing angles of the first line in Table 5.5 are realized. Analogously the Cabibbo angle can be obtained from the breakdown to $G_d = \langle A^2 B^3 A^2 B^2 \rangle \cong Z_{10}$ and $G_u = \langle ABA^2BA^2B^3A \rangle \cong Z_{10}$. Now comes the interesting part, subgroups of type I and II are constructed from generators of $\Delta(6\cdot10^2)$ (see Sec. 5.3.1), and therefore $\Delta(6\cdot5^2)$ is a subgroup of $\Delta(6\cdot10^2)$. Both discrete flavor groups predict the same PMNS matrix, despite that the remnant symmetries in the mass matrices are different. The only difference is that we have assumed that neutrinos are of Majorana nature in Sec. 5.3.1, and the group $\Delta(6\cdot10^2)$ is the smallest one that predicts

acceptable leptonic mixing patterns in 3σ region. By dropping the Majorana assumption and allowing for Dirac neutrinos, the order of G_f is reduced by a factor of 4, while retaining the same leptonic mixing pattern prediction. This observation indicates that the leptonic mixing pattern does not depend on whether neutrinos are Dirac or Majorana particles (i.e. whether $Z_2 \times Z_2 \subset G_f$ or not), but rather on the representation of the group generators. Our results indicate that different subgroups can give rise to the same mixing patterns, independent of the nature of neutrinos. The same argument also applies for $(Z_9 \times Z_3) \rtimes \mathcal{S}_3$ and $\Sigma(3 \cdot 3^3) \rtimes Z_2$ as these groups are subgroups of $(Z_{18} \times Z_6) \rtimes \mathcal{S}_3$. Interested reader can use the relevant group generators in Table 5.6 for model building. All the interesting groups in Table 5.5 predict a trivial Dirac CP phase in the leptonic sector, as in the case when neutrinos are Majorana particles.

Combining the argument above and the results in Sec. 5.3.2 and Sec. 5.3.1, we conclude that only groups of type $(Z_n \times Z_{n'}) \rtimes \mathcal{S}_3$ can predict LO leptonic mixing patterns which are experimentally favored, if the discrete flavor symmetry group G_f is broken in such a way that remnant symmetries in the leptonic masses are preserved, independent of whether neutrinos are of Dirac or Majorana nature. Additionally we can obtain the LO Cabibbo angle from groups of type $(Z_n \times Z_{n'}) \rtimes \mathcal{S}_3$ as by-product if the size is sufficiently large, as we have pointed out in Sec. 5.3.2. All of the interesting groups predict a trivial Dirac CP phase for the case of lepton mixing, which is already in mild tension with the recent T2K experimental data [209, 210]. Future experiments will shed further light on the fate of discrete symmetry.

5.4. Flavor Symmetry Versus Anarchy

The core of this chapter centered upon the search for new discrete groups that can predict acceptable LO mixing patterns for the lepton and quark sector. So far to be able to explain the experimental results, all the qualified discrete groups are found to be large. As larger flavor groups generically have many different abelian subgroups, very large flavor groups should be able to be reproduce any sort of mixing patterns. From the aesthetical point of view, one should prefer to start from a small flavor group to explain the mixing patterns, which is usually less cumbersome from a model building point of view. However, as we have seen from our scan in Sec. 5.3, only groups with order larger than 100 can predict experimentally favored leptonic and quark mixing pattern at LO. These groups are generally large compared to the simple A_4 or $\mathcal{S}_4$ and one may wonder what is the difference between building models from such a large group and an anarchical [180–182] approach by randomly drawing three angular values from the Haar measure[6].

In this section we aim to compare the predictivity of discrete flavor symmetry approach and the anarchical approach with a quantitative measure, i.e. we want to test the goodness-of-prediction of flavor symmetry against anarchy. We will not provide a mathematically rigorous analysis like Bayesian model selection, but rather we suggest a physically intuitive measure to quantify our test. Essentially we want to reward groups which can predict accurate experimental values, while punish them if their size is getting larger. That is, we do not prefer a large group which can predict everything. We assume that the LO quark and

---

[6]See also Ref. [211, 212] for a critical remark on anarchy approach.

(a) $\mathcal{S}_4$ (b) $(Z_{18} \times Z_6) \rtimes \mathcal{S}_3$
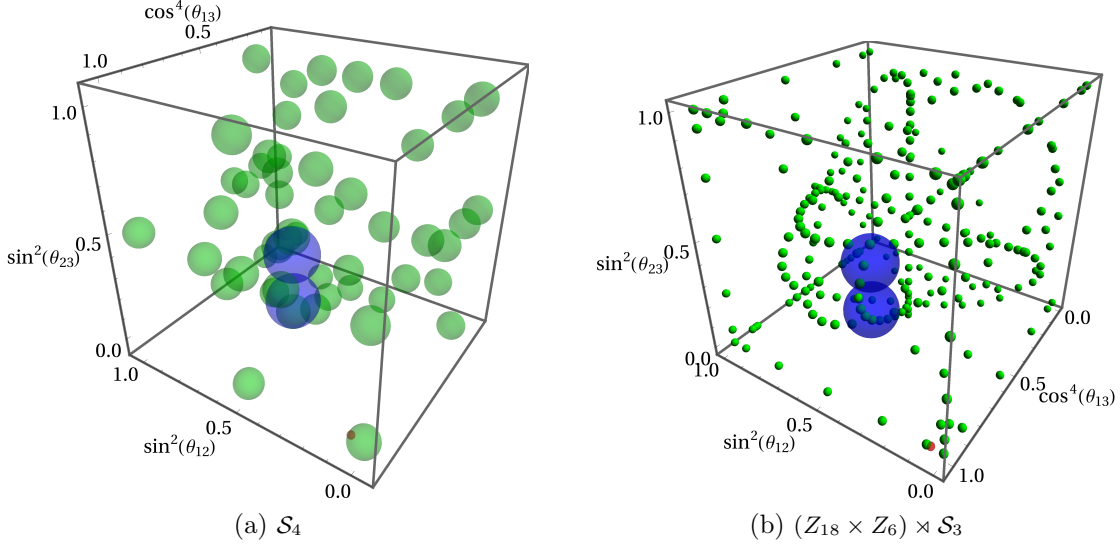
Figure 5.4.: The distribution $\mu(G_f)$ is plotted for groups $\mathcal{S}_4$(left) and $(Z_{18} \times Z_6) \rtimes \mathcal{S}_3$(right). The width of Gaussian Distribution in 1σ deviation is plotted in green. The blue (red) region represents the 3σ global fit region for the leptonic (quark) mixing pattern. The small group $\mathcal{S}_4$ predicts less mixing angles and requires large NLO correction to cover the experimental values, while larger group $(Z_{18} \times Z_6) \rtimes \mathcal{S}_3$ generates more mixing patterns and requires smaller NLO correction.

lepton mixings are determined from mismatched remnant symmetries, where we take each possible LO mixing pattern predicted by a discrete flavor group to be equally probable, i.e. all the predictions of $\Omega_{s_1}^\dagger \Omega_{s_2}$ including all the permutations of rows and columns are equally probable for a chosen discrete group. NLO corrections are assumed to be randomly scattered around the LO values, such that the mixing angle predictions from discrete flavor groups should approach the experimental values at NLO uncertainties. This is well motivated from a model building perspective as typically we have numerous higher-dimensional operators contributing to NLO corrections[7]. The comparison of CP phases is discarded as the leptonic Dirac CP phase is not measured while the CKM CP phase is not predicted in the remnant symmetry approach.

We remind the reader that we work in the coordinates $c_{13}^4 \equiv \cos^4 \theta_{13}$, $s_{12}^2 \equiv \sin^2 \theta_{12}$ and $s_{23}^2 \equiv \sin^2 \theta_{23}$ for which the invariant SU(3) Haar measure is flat, see Eq. (5.5). Under the anarchy hypotheses, each point in the selected angular coordinate space is uniformly distributed:

$$p\mathrm{d}\boldsymbol{V} = \mathbb{1}_{[0,1]^3} \mathrm{d}c_{13}^4 \mathrm{d}s_{12}^2 \mathrm{d}s_{23}^2. \tag{5.37}$$

In this sense, the anarchy hypothesis acts as a flat prior in Bayesian statistics. Let us compare it with the case of flavor symmetry. Without NLO corrections, the discrete flavor group would predict a sum of Dirac delta functions $p_f \mathrm{d}\boldsymbol{V} = \sum_i \delta^{(3)}(\vec{x} - \vec{x}_i) \mathrm{d}c_{13}^4 \mathrm{d}s_{12}^2 \mathrm{d}s_{23}^2$ centered about all the possible LO predictions $\vec{x}_i = (c_{13}^4, s_{12}^2, s_{23}^2)^T$ generated by misalignment of all possible remnant symmetry groups. The LO predictions must either be accepted or rejected

---

[7]In typical models (e.g. [16, 18, 213, 214]), usually these higher-dimensional operators will break the remnant symmetries. However, we stress in some models the structure of NLO corrections are predictive [203, 215], which is usually the case when additional structure such as supersymmetry is included in the theory.

when compared to the experimental values. But since we expect that the NLO corrections exist and they are randomly distributed around the LO predictions, for simplicity we parameterize the NLO corrections as 3-dimensional Gaussian distribution

$$p_f^{(i)} = \exp\left[-\frac{(\vec{x} - \vec{x}_i)^2}{\sigma^2}\right], \tag{5.38}$$

centered around the ith LO mixing, i.e. we have

$$p_f \mathrm{d}\boldsymbol{V} = \sum_i p_f^{(i)} \mathrm{d}c_{13}^4 \mathrm{d}s_{12}^2 \mathrm{d}s_{23}^2 \tag{5.39}$$

as the probability distribution for a discrete group G_f to predict NLO mixing patterns. The variance of the Gaussian distribution is given by

$$\sigma^2 = \mathrm{Min}(\sigma_{\mathrm{CKM}}^2) + \mathrm{Min}(\sigma_{\mathrm{PMNS}}^2), \tag{5.40}$$

i.e. we take the the quadratic sum of the shortest distance

$$\mathrm{Min}(\sigma_{\mathrm{CKM/PMNS}}) \equiv \inf_i |\vec{x}_i - \vec{x}_{\mathrm{CKM/PMNS}}|, \tag{5.41}$$

between the best fit CKM angles $\vec{x}_{\mathrm{CKM}}$ and PMNS angles $\vec{x}_{\mathrm{PMNS}}$ to a LO prediction of the group. We need to normalized the distribution p_f of a discrete group G_f by integrating the sum of $p_f^{(i)}$ and dividing it by the total volume. Let us explain our approach in more details, we assume that for each discrete group, all its mixing angle predictions are generated on the angular coordinate space. Once the points are given, we then look for the shortest distance between one of the points to the experimental points and treat this distance as the NLO corrections. The shorter the distance is, the smaller the NLO corrections should be, such that the LO + NLO prediction of a certain discrete group should be within the error of experimental values. For illustration in Fig. 5.4 we show the p_f distribution for the group $\mathcal{S}_4$ and $(Z_{18} \times Z_6) \rtimes \mathcal{S}_3$ in the angular coordinate space. The small group $\mathcal{S}_4$ predicts less mixing angles and requires large NLO correction (σ) to cover the experimental values, while larger group $(Z_{18} \times Z_6) \rtimes \mathcal{S}_3$ generates more mixing patterns and requires smaller NLO correction. The model building community members who favor large discrete groups usually argue that such large groups are better, as their LO predictions are accurate and the required NLO corrections are smaller (shorter distance); while those who favor small discrete groups will argue the other way round, claiming that such large groups predict better LO value because they simply just "fill up" the angular coordinate space. It is our task to quantify this problem and tackle it in meaningful way.

We introduce a measure of predictivity with the integration of p_f within the 3σ region from global fits of experimental values V_{exp}:

$$\mu(G_f) \equiv \int_{V_{\mathrm{exp}}} p_f(c_{13}^4, s_{12}^2, s_{23}^2) \, \mathrm{d}c_{13}^4 \mathrm{d}s_{12}^2 \mathrm{d}s_{23}^2, \tag{5.42}$$

as a measure for goodness-of-prediction in mixing angles up to the NLO correction by a particular flavor symmetry group. For our example we have calculated $\mu(\mathcal{S}_4) = 1.8 \times 10^{-3}$
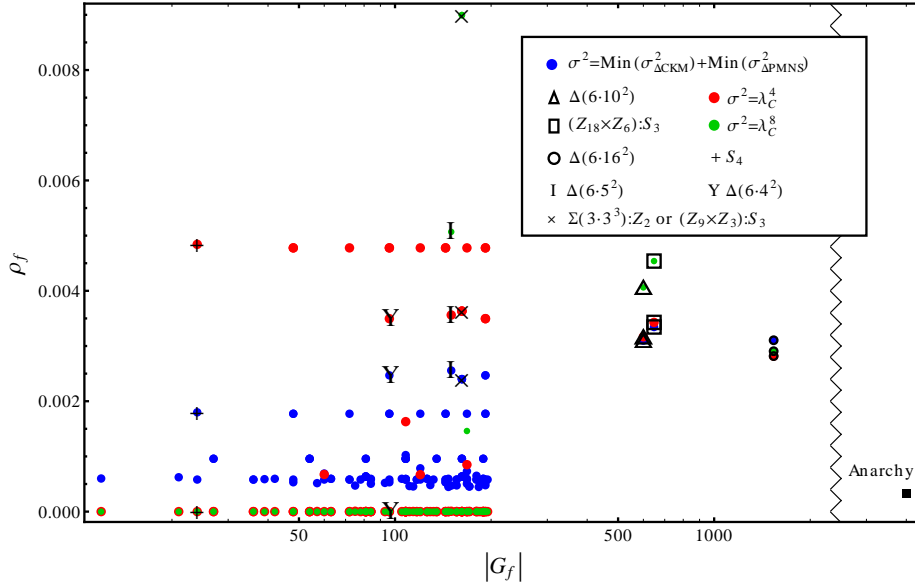
Figure 5.5.: The goodness-of-prediction $\mu(G_f)$ for discrete flavor symmetry groups G_f is plotted. $\mu((Z_{18} \times Z_6) \rtimes \mathcal{S}_3)$ is the discrete group that predict the closest experimental values. $\mu(G_f)$ for anarchy is represented by a black square in the plot. Groups that are relevant for our analysis are highlighted.

and $\mu((Z_{18} \times Z_6) \rtimes \mathcal{S}_3) = 4 \times 10^{-3}$. The larger group that needs smaller NLO corrections beat smaller groups that require larger NLO corrections. The absolute value of $\mu(G_f)$ alone has no intrinsic meaning, rather it serves as a comparison yardstick for the goodness-of-prediction between different flavor groups. Groups that predict values far from the experimental results have smaller values of $\mu(G_f)$. The goodness-of-prediction for each discrete group up to the order 200 and other larger interesting groups identified in Sec. 5.3.1 are plotted with blue points in Fig. 5.5. Some of the groups yield the same $\mu(G_f)$ as the lower order group, this is usually the case when the lower order group is their subgroups. For example $\mathcal{S}_4 \times Z_2$ and $\mathcal{S}_4 \times Z_3$ yield the same value of $\mu(G_f)$ as $\mathcal{S}_4$. From our construction, groups with higher values of $\mu(G_f)$ predict better mixing patterns. However here is the catch, even though larger groups tend to predict better mixing patterns, their larger order would in general reduce or "dilute" the value of $\mu(G_f)$. From Fig. 5.5 we see that $\Delta(6 \cdot 16^2)$ yields a lower value of $\mu(G_f)$ than $(Z_{18} \times Z_6) \rtimes \mathcal{S}_3$ and $\Delta(6 \cdot 10^2)$, even though $\Delta(6 \cdot 16^2)$ predicts better mixing pattern compared to the experiments. Essentially as the group gets too large, it will be punished for every other wrong "prediction" generated. Therefore an optimal discrete group should be predictive (generates the best LO mixing patterns) and simple (small and easy for model building). By this measure the group $(Z_{18} \times Z_6) \rtimes \mathcal{S}_3$ is the most predictive for groups smaller than 1536.

We can now pitch the discrete groups against the predictivity of anarchy

$$\mu(\text{anarchy}) = \int_{V_{\text{exp}}} \mathbb{1}_{[0,1]^3} \, dc_{13}^4 ds_{12}^2 ds_{23}^2 = 3.22 \times 10^{-4}, \tag{5.43}$$

which as our measure has shown, anarchy turns out to be the least predictive theory. Any
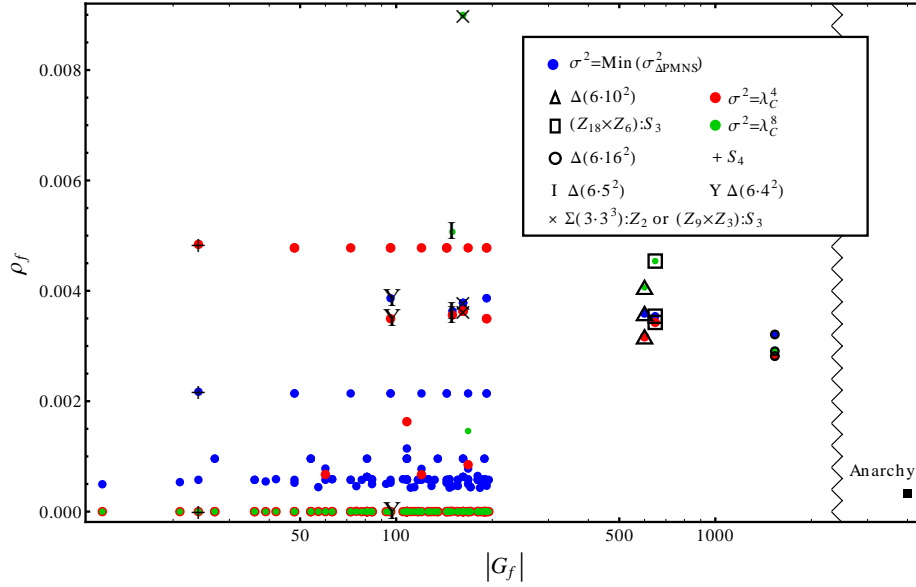
Figure 5.6.: The goodness-of-prediction $\mu(G_f)$ for discrete flavor symmetry groups G_f is plotted, with only the leptonic mixing patterns considered.

flavor theory should certainly be more predictive than anarchy, as anarchy essentially "predicts" every point in the mixing space. Neglecting the CKM contributions, a similar plot in Fig. 5.6 can also be obtained with $\sigma^2 = \text{Min}(\sigma^2_{\text{PMNS}})$, i.e. we only consider the predictivity of discrete groups in the leptonic sector. The resulting $\mu(G_f)$ for each flavor group follows the same trend as in Fig. 5.5. Notice that by combining different subgroups of a fixed G_f in pairs, we essentially give up the information on the nature of neutrinos, otherwise we only restrict the subgroups to Klein group if this additional assumption is made.

One might argue that the our measure of NLO given in Eq. (5.40) is not the best one, as the variance of the Gaussian distribution defined in Eq. (5.40) is arbitrary. Typically the NLO corrections to the leptonic mixing angles are of the order of $\sigma = \lambda_C^2 \equiv \sin^2\theta_c$ or $\sigma = \lambda_C^4$. The result of $\mu(G_f)$ obtained with these assumptions is plotted also for the sake of comparison, and the only significant changes in Fig. 5.5 and Fig. 5.6 stem from the group $\mathcal{S}_4$, $\Delta(6\cdot4^2)$, $\Delta(6\cdot5^2)$, $(Z_9 \times Z_3) \rtimes \mathcal{S}_3$ and $\Sigma(3\cdot3^3) \rtimes Z_2$. The deviations result from larger volume covered by the integration due to narrower Gaussian spread. With $\sigma = \lambda_C^2$, the width of the Gaussian distribution is larger, making smaller groups which predict next-to-best mixing patterns to yield higher values of $\mu(G_f)$. However, the Gaussian spread is too narrow for the case of $\sigma = \lambda_C^4$, hence only groups that predict very accurate LO leptonic mixings will generate higher $\mu(G_f)$ values. In fact, $\mu(G_f)$ for anarchy is higher than certain groups such as $\mathcal{S}_4$ and $\Delta(6\cdot4^2)$ in this case. The decreasing $\mu(G_f)$ w.r.t. the increasing size of the group agrees with our intuition that larger groups tend to generate smaller $\mu(G_f)$ values, as more combinations of the mixing patterns can be generated by larger groups. While we admit that our measure is not unique and not rigorous, it is to our knowledge, the first attempt to quantify such a problem and address it in an intuitive physical way.

5.5. Summary

In conclusion, we have performed a class of systematical searches for finite discrete groups which predict experimentally favored mixing patterns for the leptonic and the quark sector. Our approach only relies on the residual symmetries in the fermionic mass matrices and is model independent. By assuming that neutrinos are Majorana particles, we have scanned all the discrete groups up to the order of 1536 and only three groups, namely $\Delta(6 \cdot 10^2)$, $(Z_{18} \times Z_6) \rtimes \mathcal{S}_3$ and $\Delta(6 \cdot 16^2)$ can generate LO leptonic mixing angles within 3σ region of global fits. Furthermore they can also generate sizable Cabibbo angle which is close to the experimental value. While for the case of Dirac neutrinos, all the discrete groups up to the order of 200 have been surveyed and only three groups listed in Table 5.6 can give rise to acceptable leptonic and quark mixing patterns. Those groups are subgroups of the groups found in the Majorana case, leading us to conclude that mixing patterns predicted by discrete groups are independent of the nature of neutrinos, whether they are Majorana or Dirac particles. All of the interesting groups found predict a trivial Dirac CP phase in the leptonic and quark sector, with the prediction of leptonic case to be the most interesting, as it can be confirmed or ruled out in the future experiments. All the group theoretical classifications have been carried out for our interesting groups, and we conclude that only groups of type $(Z_n \times Z_{n'}) \rtimes \mathcal{S}_3$ are relevant as a new starting point for model building with flavor symmetry. And finally we have provided a measure to test the goodness-of-prediction for flavor symmetry against the anarchy hypothesis, with the relatively unknown group $(Z_{18} \times Z_6) \rtimes \mathcal{S}_3$ stands out to be the most predictive.

Conclusion and Outlook

In this thesis we have focused on the theoretical puzzles in the Standard Model (SM), namely the separation of fundamental scales and the flavor puzzle. We have provided some possible solutions to solve both puzzles, guided by the principle of symmetry. Regarding fundamental scales in high energy physics, the large separation of 17 orders of magnitude between the electroweak (EW) and the Planck scale is known as the hierarchy problem. We have provided two aspects of naturalness, namely the subjective naturalness and technical naturalness, and carefully formulated the hierarchy problem in this context. Given that generic predictions from traditional approaches to solve the hierarchy problem, be it supersymmetry, extra dimension or partial compositeness, have not appeared at the LHC or any other experiment, new ideas and their phenomenologies must be considered.

In the first part of our thesis we have introduced the concept of classical scale symmetry, which could serve as a possible solution to the hierarchy problem. If classical scale symmetry is manifest in nature, its anomalous nature could provide a mechanism to generate the EW scale radiatively. In general there are two ways to generate the EW scale via this anomalous scale symmetry breaking mechanism: either perturbatively with the Coleman-Weinberg mechanism or nonperturbatively through a strongly coupled sector, as we have shown in Sec. 2.6. We have focused on the nonperturbative EW scale generation in this thesis and classified the models which implement this idea into two classes; direct and indirect scale transmission. We have presented a model for each of these approaches.

In Chapter 3 we utilized the *direct* scale transmission approach to explain the EW scale from dimensional transmutation of a strongly coupled sector that is well known, namely the QCD. We have extended QCD minimally by only one scalar particle charged under a higher representation of QCD. Due to the running of the strong coupling, the new scalar particle forms a condensate at the TeV regime and generates a condensation scale which triggers the EW symmetry breaking (EWSB) dynamically. With this minimalistic scenario, the mass of the new scalar particle is bounded from above due to the perturbative renormalization group equation (RGE) constraint. Our model is predictive as the parameter space is constrained by the principle of classical scale invariance. The new QCD scalar particle can be probed by searching for four jets events due to the decay of the condensate pair, while the sizable coupling term for the SM Higgs with the colored scalar can influence the Higgs production cross section in the gluon fusion channel significantly. Furthermore the colored scalar sector in our model possesses an accidental U(1) symmetry, which yields interesting phenomenology particularly in the signal strength of Higgs decaying into two photons, if the accidental

symmetry is identified with the abelian gauge group of electromagnetism. The existence of Landau pole for the colored scalar quartic coupling could signal a need for more realistic models, which could also reconcile the dark matter (DM) problem and explain the origin of neutrino mass. For instance we could introduce additional fermions charged under higher-dimensional representation of QCD to alter ameliorate the Landau pole problem, while providing a good DM candidate. We leave this exciting possibility for future work.

As for the *indirect* scale transmission mechanism to generate the EW scale, we have proposed a model in Chapter 4 with a hidden sector and three flavors of dark fermions charged under the fundamental representation of a new SU(3) gauge group, similar to QCD. A scalar singlet mediator, which couples to the hidden sector via Yukawa interaction with the dark fermion and the SM via the Higgs portal, is introduced. The chiral symmetry of the dark fermion sector is spontaneously broken once the gauge coupling in the hidden strong sector becomes nonperturbative due to RGE. As a consequence mesonic condensates are formed and subsequently the scalar mediator obtains a nontrivial vacuum expectation value (VEV), which triggers EWSB when this VEV is transmitted to the Higgs sector. Due to spontaneous chiral symmetry breaking, dark pions in the form of pseudo Nambu-Goldstone bosons can serve as good DM candidates. We utilized the Nambu-Jona-Lasinio (NJL) approach to calculate the relevant masses and couplings for the scalars and the DM. The advantage of utilizing such a QCD-like model is that we can scale up all the massive NJL couplings from ordinary QCD. As NJL relates the relevant couplings and masses of the theory, the parameter space of our model is very restrictive, where the resulting DM direct detection cross section and the predicted mass can be probed or ruled out by the future XENON1T and LUX experiments. Our model serves as a prototype for model building along the line of indirect scale transmission from a classically scale invariant theory, and further extensions to explain the neutrino mass, or the asymmetry of matter over antimatter have not been charted, which could provide an interesting opportunity for us to investigate further.

In Chapter 5 we tried to provide a solution to the flavor puzzle in the leptonic and quark sector based on the approach of discrete symmetries. With the discovery of a nonzero reactor mixing angle in the leptonic sector, simple discrete groups such as A_4 are strongly disfavored and it is necessary to search for new discrete flavor groups which can yield experimentally compatible mixing patterns. The crucial ingredient for a successful prediction of leading-order (LO) leptonic mixing angles from a discrete flavor symmetry relies on the residual symmetries which remain in the mass matrices of the charged lepton and the neutrino sector. Once the residual symmetries in the mass matrices are identified, the LO leptonic mixing matrix can be obtained without an explicit model. We have systematically searched all the discrete flavor groups up to order 1536 that yield acceptable leptonic mixing angles if neutrinos are Majorana particles. It turns out that from over a million discrete flavor groups, only three can explain the experimental values. The success of these three groups can also be extended to the quark sector, where acceptable LO Cabibbo angle can be obtained. Furthermore we have also perform a group scan for the case when neutrinos are Dirac particles, and all discrete groups up to order 200 are charted. It turns out that those groups which generate mixing patterns compatible with experiments are subgroups of those three interesting groups found for the case of Majorana neutrinos. Our result implies that

the mixing patterns generated by discrete flavor symmetries are independent of whether neutrinos are Dirac or Majorana particles, but rather rely on the representations of the discrete groups. All the interesting discrete groups, which are all of the type $(Z_n \times Z_{n'}) \rtimes \mathcal{S}_3$, and their breaking to residual symmetries, can be classified by simple mathematical reasoning. Combined with the measure of goodness-of-prediction proposed by us, we conclude that discrete flavor symmetry is more predictive than flavor anarchy. All the interesting groups that we have found pave a new model building direction, and indeed several authors have started pursuing this new idea [206, 216].

With no new physics appearing so far, the traditional approach towards naturalness and flavor symmetry should be scrutinized. We should keep an open mind for different possibilities in solving the hierarchy and the flavor puzzle. In this thesis we have proposed several unconventional and interesting new ideas to tackle the two problems. Our ideas are general and can serve as new starting points in model building, whether to solve the hierarchy problem, to explain the origin of the EW scale, to provide a DM stable candidate, or to look for new discrete symmetries for the flavor puzzle. This is not the end of our journey, but only the beginning towards new uncharted territories.

Appendices

Abbreviations and Notations

We list down some of the abbreviations and notations used throughout the thesis. This compilation is useful also in case the reader is feeling a bit rusty with the high energy physics jargons.

BR	Branching ratio
CKM	Cabibbo-Kobayashi-Maskawa
DM	Dark matter
DSE	Dyson-Schwinger equation
EFT	Effective field theory
EOM	Equation of motion
EW	Electroweak
EWSB	Electroweak symmetry breaking
GUT	Grand Unified Theory
IR	Infrared (low energy)
LO	Leading order
NJL	Nambu-Jona-Lasinio
NLO	Next-to-leading order
PCAC	Partially conserved axial current
PCDC	Partially conserved dilatation current
PMNS	Pontecorvo-Maki-Nakagawa-Sakata
PNGB	Pseudo Nambu-Goldstone boson
QCD	Quantum chromodynamics
QFT	Quantum field theory
RGE	Renormalization group equation
SCMF	Self-consistent mean field
SM	Standard Model
TBM	Tri-bimaximal mixing
UV	Ultraviolet (high energy)
VEV	Vacuum expectation value
WIMP	Weakly interacting massive particle
1PI	One-particle irreducible
$0\nu\beta\beta$	Neutrinoless double beta decay

Bosonization and NJL Methods

Bosonization of a fermionic theory provides a description of the transformation of the original Lagrangian into an equivalent description with only bosonic degrees of freedom. This is particularly useful in describing the bound state formed by fermionic pair, and has been extensively used in condensed matter physics. Bosonization provides a relation between physical observables at low energy and the UV parameters, and hence is more predictive than just parameterizing the low energy degrees of freedom such as the linear or nonlinear sigma model. The Nambu-Jona-Lasinio (NJL) approach belongs to one of the bosonization methods, suitable for describing low energy physics of scalar bounded system formed by two underlying fermions. In the NJL model for QCD or strongly coupled theory, nonzero vacuum condensate is formed by such a fermionic pairing, subsequently the Nambu-Goldstone bosons and the chiral partners are formed. The fermion mass is dynamically generated and all of the dynamics described above happen simultaneously in the NJL model. NJL however, does not describe confinement in QCD. For a more complete review we refer the reader to Refs. [111, 136–139].

Let us illustrate the path integral bosonization technique for a free one fermion flavor system. For the NJL approach to work, we introduce the nonrenormalizable operators, say the four fermions operator to our example Lagrangian

$$\mathcal{L} = \bar{\psi}(i\not{\partial} - m)\psi + G\left[(\bar{\psi}\psi)^2 + (\bar{\psi}i\gamma_5\psi)^2\right]. \tag{B.1}$$

One needs to eliminate the heavy fermionic degrees of freedom and this can be achieved by introducing auxiliary bosonic fields, e.g. in our case one scalar σ and a pseudoscalar ϕ which transforms according to

$$\sigma \to \sigma + \frac{\sqrt{2G}}{\mu}\bar{\psi}\psi, \quad \phi \to \phi + \frac{\sqrt{2G}}{\mu}\bar{\psi}i\gamma_5\psi. \tag{B.2}$$

Rearranging and simplifying some terms in the path integral, the functional determinant can be integrated out, resulting in a pure bosonic theory with potential

$$V = \frac{\mu^2}{2}\left(\sigma^2 + \phi^2\right) - 2\int \frac{\mathrm{d}^4 k}{i(2\pi)^4} \ln\left(\sigma^2 + \phi^2 - k^2\right). \tag{B.3}$$

The constituent mass of the fermion is given by $M = m + \mu\sqrt{2G}\langle\sigma\rangle$ the mass of the condensate is given by μ. So far our approach seems easy for a one fermion system. Complications

occur if we consider multi-flavored fermionic system with interactions. To describe the bosonization with interacting system, we will utilize the self-consistent mean field (SCMF) approach, introduced by Kunihiro and Hatsuda [111, 136, 137].

B.1. Bosonization with the SCMF Approximation

In many branches of physics such as solid state physics, many-body physics or high energy physics, the complication of many-body interaction can be usually simplified to mean field approximation. In our case, the fermions are interacting in the background field where chiral symmetry is broken. Although one should think that chiral symmetry is broken dynamically, the mean field approach allows us to investigate the condensates and the fermions in a self-consistent picture at leading-order (LO) approximation. In the NJL approach, we divide the Lagrangian (B.1) into quadratic part $\mathcal{L}_0$ and interacting part $\mathcal{L}_I$. The background vacuum consists of the mesonic spectrum, i.e. $|\text{VAC}\rangle = |[\sigma, \phi]\rangle$ where the interacting $\mathcal{L}_I$ is normal ordered w.r.t. this nontrivial vacuum. The price that we need to pay for such a trick is the necessity to include c-number terms in the quadratic $\mathcal{L}_0$. In our example above, let us try to obtain the time-ordered product of the potential of Lagrangian (B.1)

$$\langle \mathcal{T}\{\bar{\psi}_a\psi_a\bar{\psi}_b\psi_b\}\rangle =: \bar{\psi}_a\psi_a\bar{\psi}_b\psi_b : + 2\widehat{\bar{\psi}_a\psi_a}\bar{\psi}_b\psi_b + \widehat{\bar{\psi}_a\psi_a}\widehat{\bar{\psi}_b\psi_b}, \tag{B.4}$$

where the : represents normal ordering and $\widehat{}$ denotes the contraction w.r.t. the vacuum $|\text{VAC}\rangle$. The spinor index is given by a and b explicitly. The second term contains a factor 2 as there are two pairs of $\bar{\psi}\psi$ that need to be normal ordered. As the second term is quadratic in fermion fields, it should be considered as part of $\mathcal{L}_0$. Adding and subtracting terms

$$2g\varphi\bar{\psi}_b\psi_b - 2g\widehat{\bar{\psi}_a\psi_a}\bar{\psi}_b\psi_b = 2g\varphi\bar{\psi}_b\psi_b - 2g\widehat{\bar{\psi}_a\psi_a} : \bar{\psi}_b\psi_b : -2g\widehat{\bar{\psi}_a\psi_a}\widehat{\bar{\psi}_b\psi_b}, \tag{B.5}$$

to Eq. (B.4) where we have normal ordered the last term in the LHS of the equation, the mean field Lagrangian $\mathcal{L}_0$ is given as

$$\mathcal{L}_0 = \bar{\psi}i\slashed{\partial}\psi + 2g\varphi\bar{\psi}\psi - g\varphi^2, \tag{B.6}$$

with the bosonic field $\varphi = -(\sigma + i\phi)/g$ representing the resulting condensate. The rest of the terms are included in the interacting part $\mathcal{L}_I$ of the total Lagrangian, satisfying $\langle\text{VAC}|\mathcal{L}_I|\text{VAC}\rangle = 0$. Eq. (B.6) serves as a starting point to calculate all the relevant coupling and interaction.

Let us now apply our formalism to our relevant model in Chapter 4. With the given Lagrangian (4.5), the interaction part $2G\,\text{Tr}\,\Phi^\dagger\Phi$ in Eq. (4.5) can be written as

$$2G\,\text{Tr}\,\Phi^\dagger\Phi = G\sum_{a=0}^{8}\left[(\bar{\psi}\lambda^a\psi)^2 + (i\bar{\psi}\gamma_5\lambda^a\psi)^2\right], \tag{B.7}$$

while the second term of the RHS of Eq. (B.7) is given as

$$G\sum_{a=0}^{8}\left(i\bar{\psi}\gamma_5\lambda^a\psi\right)^2 = G\sum_{a=0}^{8}\left(i\bar{\psi}\gamma_5\lambda^a\psi + \frac{1}{2G}\phi_a\right)^2 - \frac{1}{4G}\sum_{a=0}^{8}\phi_a\phi_a - \sum_{a=0}^{8}i\bar{\psi}\gamma_5\lambda^a\psi\phi_a. \quad \text{(B.8)}$$

We regard the first term of Eq. (B.8) as an interaction term and according to the SCMF approximation, it can be rewritten as normal products:

$$G\sum_{a=0}^{8}\left(i\bar{\psi}\gamma_5\lambda^a\psi + \frac{1}{2G}\phi_a\right)^2 = G\sum_{a=0}^{8} : \left(i\bar{\psi}\gamma_5\lambda^a\psi\right)^2 : + G\sum_{a=0}^{8}\left(i\widehat{\bar{\psi}\gamma_5\lambda^a}\psi + \frac{1}{2G}\phi_a\right)^2$$
$$+ 2G\sum_{a=0}^{8} : i\bar{\psi}\gamma_5\lambda^a\psi : \left(i\widehat{\bar{\psi}\gamma_5\lambda^a}\psi + \frac{1}{2G}\phi_a\right). \quad \text{(B.9)}$$

Similarly the scalar part (first term of Eq. (B.7)) can be rewritten in the same way. Like Eq. (B.6), we can package the bosonic fields as a condensate of fermionic pair

$$\widehat{\Phi} = \varphi = -\frac{1}{4G}\left(\text{diag}(\sigma,\sigma,\sigma) + i(\lambda^a)^T\phi_a\right). \quad \text{(B.10)}$$

The axial anomaly term can also be treated in a similar manner. Using the result of Cayley-Hamilton theorem for operator

$$\det\Phi = \frac{1}{3}\text{Tr}\,\Phi^3 - \frac{1}{2}\text{Tr}\,\Phi^2\ \text{Tr}\,\Phi + \frac{1}{6}(\text{Tr}\,\Phi)^3, \quad \text{(B.11)}$$

we obtain

$$G_D\left(\text{Tr}\,\varphi^2\Phi - \text{Tr}\,\varphi\Phi\,\text{Tr}\,\varphi - \frac{1}{2}\text{Tr}\,\varphi^2\,\text{Tr}\,\Phi + \frac{1}{2}(\text{Tr}\,\varphi)^2\,\text{Tr}\,\Phi\right) - 2G_D(\det\varphi) + h.c., \quad \text{(B.12)}$$

and this term should be added to the quadratic part $\mathcal{L}_0$ of the Lagrangian. Adding all the relevant terms together yields the quadratic part $\mathcal{L}_0$ of the Lagrangian

$$\mathcal{L}_0 = \text{Tr}\,\bar{\psi}(i\gamma^\mu\partial_\mu - yS)\psi + 2G\,\text{Tr}(\varphi^\dagger\Phi + h.c) - 2G\,\text{Tr}\,\varphi^\dagger\varphi - 2G_D(\det\varphi + h.c.)$$
$$+ G_D\left(\text{Tr}\,\varphi^2\Phi - \text{Tr}\,\varphi\Phi\,\text{Tr}\,\varphi - \frac{1}{2}\text{Tr}\,\varphi^2\,\text{Tr}\,\Phi + \frac{1}{2}(\text{Tr}\,\varphi)^2\,\text{Tr}\,\Phi + h.c.\right), \quad \text{(B.13)}$$

while $\langle\text{VAC}|\mathcal{L}_I|\text{VAC}\rangle = 0$, as required.

Useful Passarino-Veltman Integrals for NJL

All the relevant messy integrals found in Chapter 4 can be cast into some basic integral functions, known as the Passarino-Veltman integrals [140]. Typically the Passarino-Veltman functions are expressed with dimensional regularization already been carried out, which are not that useful in the NJL approach. We follow the `FeynCalc` [217] notations and recast some of the relevant integrals with a cutoff here.

The one-point function is given as

$$
\begin{aligned}
\mathrm{A}_0(m^2) =& \frac{1}{i\pi^2} \int \frac{\mathrm{d}^4 k}{k^2 - m^2} = -\int_0^{\Lambda^2} dk_E^2 \frac{k_E^2}{k_E^2 + m^2} \\
=& -\Lambda^2 + m^2 \ln\left(1 + \frac{\Lambda^2}{m^2}\right).
\end{aligned}
\tag{C.1}
$$

The relevant two-point function is calculated to be

$$
\begin{aligned}
\mathrm{B}_0(p^2, m^2, m^2) =& \frac{1}{i\pi^2} \int \frac{\mathrm{d}^4 k}{(k^2 - m^2)((k+p)^2 - m^2)} \\
=& \int_0^1 \mathrm{d}x \ln\left(1 + \frac{\Lambda^2}{\Delta_\mathrm{B}^2}\right) - \frac{\Lambda^2}{\Lambda^2 + \Delta_\mathrm{B}} \\
=& \ln\left(1 + \frac{\Lambda^2}{m^2}\right) - 2\sqrt{\frac{m^2}{p^2} - 1} \tan^{-1}\left(\sqrt{\frac{p^2}{m^2 - p^2}}\right) \\
& + \frac{(\Lambda^2 - 2p^2 + 2m^2)}{p^2\sqrt{\Lambda^2 - p^2 + m^2}} \tan^{-1}\left(\sqrt{\frac{p^2}{\Lambda^2 - p^2 + m^2}}\right),
\end{aligned}
\tag{C.2}
$$

where $\Delta_\mathrm{B} = m^2 - x(1-x)p^2$.

The interesting three-point function related to our model is given as

$$
\begin{aligned}
\mathrm{C}_0(p_1^2, p_1 \cdot p_2, p_2^2, m^2, m^2, m^2) =& \frac{1}{i\pi^2} \int \frac{\mathrm{d}^4 k}{(k^2 - m^2)((k+p_1)^2 - m^2)((k+p_2)^2 - m^2)} \\
=& -\int_0^1 \mathrm{d}x \int_0^{1-x} \mathrm{d}y \frac{\Lambda^4}{\Delta_\mathrm{C}(\Delta_\mathrm{C} + \Lambda^2)^2},
\end{aligned}
\tag{C.3}
$$

with $\Delta_\mathrm{C} = m^2 + x(x-1)p_1^2 + y(y-1)p_2^2 + 2xyp_1 \cdot p_2$.

Lastly the important four-point function is given as

$$
D_0(p_1^2, p_2^2, p_3^2, p_1 \cdot p_2, p_2 \cdot p_3, p_1 \cdot p_3, m^2, m^2, m^2)
$$

$$
= \frac{1}{i\pi^2} \int \frac{\mathrm{d}^4 k}{(k^2 - m^2)((k + p_1)^2 - m^2)((k + p_2)^2 - m^2)((k + p_3)^2 - m^2)}
$$

$$
= \int_0^1 \mathrm{d}x \int_{1-x}^1 \mathrm{d}y \int_{1-x-y}^0 \mathrm{d}z \frac{\Lambda^4 (3\Delta_{\mathrm{D}} + \Lambda^2)}{\Delta_{\mathrm{D}}^2 (\Delta_{\mathrm{D}} + \Lambda^2)^3}, \tag{C.4}
$$

where $\Delta_{\mathrm{D}} = m^2 + (xp_1 + yp_2 + zp_3)^2 - xp_1^2 - yp_2^2 - zp_3^2$.

Acknowledgements

Bibliography

[1] S. Glashow, Nucl.Phys. **22**, 579 (1961).

[2] S. Weinberg, Phys.Rev.Lett. **19**, 1264 (1967).

[3] D. Gross and F. Wilczek, Phys.Rev. **D8**, 3633 (1973).

[4] D. Gross and F. Wilczek, Phys.Rev. **D9**, 980 (1974).

[5] H. Politzer, Phys.Rept. **14**, 129 (1974).

[6] G. Aad *et al.* (ATLAS Collaboration), Phys.Lett. **B716**, 1 (2012), arXiv:1207.7214 [hep-ex].

[7] S. Chatrchyan *et al.* (CMS Collaboration), Phys.Lett. **B716**, 30 (2012), arXiv:1207.7235 [hep-ex].

[8] J. Beringer *et al.* (Particle Data Group), Phys.Rev. **D86**, 010001 (2012).

[9] F. An *et al.* (DAYA-BAY Collaboration), Phys.Rev.Lett. **108**, 171803 (2012), arXiv:1203.1669 [hep-ex].

[10] J. Ahn *et al.* (RENO collaboration), Phys.Rev.Lett. **108**, 191802 (2012), arXiv:1204.0626 [hep-ex].

[11] Y. Abe *et al.* (DOUBLE-CHOOZ Collaboration), Phys.Rev.Lett. **108**, 131801 (2012), arXiv:1112.6353 [hep-ex].

[12] E. Ma and G. Rajasekaran, Phys. Rev. D **64**, 113012 (2001), hep-ph/0106291.

[13] K. S. Babu, E. Ma, and J. W. F. Valle, Physics Letters B **552**, 207 (Jan. 2003), hep-ph/0206292.

[14] E. Ma, Phys. Rev. D **70**, 031901 (2004), hep-ph/0404199.

[15] K. Babu and X.-G. He(2005), arXiv:hep-ph/0507217 [hep-ph].

[16] G. Altarelli and F. Feruglio, Nuclear Physics B **720**, 64 (Aug. 2005), hep-ph/0504165.

[17] X.-G. He, Y.-Y. Keum, and R. R. Volkas, JHEP **04**, 039 (2006), hep-ph/0601001.

[18] G. Altarelli and F. Feruglio, Nuclear Physics B **741**, 215 (2006), hep-ph/0512103.

[19] A. Duncan, *The Conceptual Framework of Quantum Field Theory* (Oxford University Press, USA, 2012) ISBN 0199573263.

[20] B. Kosyakov, *Introduction to the Classical Theory of Particles and Fields* (Springer, 2007) ISBN 3540409335.

[21] K. Brading and H. R. Brown(2000), arXiv:hep-th/0009058 [hep-th].

[22] *The Quantum Theory of Fields, Volume II: Modern Applications* (Cambridge University Press, 2005) ISBN 0521670543.

[23] F. Englert and R. Brout, Phys.Rev.Lett. **13**, 321 (1964).

[24] P. W. Higgs, Phys.Lett. **12**, 132 (1964).

[25] P. W. Higgs, Phys.Rev.Lett. **13**, 508 (1964).

[26] M. Kobayashi and T. Maskawa, Prog.Theor.Phys. **49**, 652 (1973).

[27] M. Apollonio *et al.* (CHOOZ Collaboration), Phys.Lett. **B466**, 415 (1999), arXiv:hep-ex/9907037 [hep-ex].

[28] Q. R. Ahmad *et al.* (SNO), Phys. Rev. Lett. **89**, 011301 (2002), arXiv:nucl-ex/0204008.

[29] P. Ade *et al.* (Planck Collaboration)(2013), arXiv:1303.5076 [astro-ph.CO].

[30] A. Osipowicz *et al.* (KATRIN Collaboration)(2001), arXiv:hep-ex/0109033 [hep-ex].

[31] M. Agostini *et al.* (GERDA Collaboration), Phys.Rev.Lett. **111**, 122503 (2013), arXiv:1307.4720 [nucl-ex].

[32] A. Y. Smirnov, Nucl.Phys.Proc.Suppl. **235-236**, 431 (2013), arXiv:1210.4061 [hep-ph].

[33] S. F. King, A. Merle, S. Morisi, Y. Shimizu, and M. Tanimoto, New J.Phys. **16**, 045018 (2014), arXiv:1402.4271 [hep-ph].

[34] M. Tegmark *et al.* (SDSS Collaboration), Phys.Rev. **D69**, 103501 (2004), arXiv:astro-ph/0310723 [astro-ph].

[35] V. C. Rubin and J. Ford, W. Kent, Astrophys.J. **159**, 379 (1970).

[36] M. Bartelmann and P. Schneider, Phys.Rept. **340**, 291 (2001), arXiv:astro-ph/9912508 [astro-ph].

[37] G. Bertone, D. Hooper, and J. Silk, Phys.Rept. **405**, 279 (2005), arXiv:hep-ph/0404175 [hep-ph].

[38] A. Sakharov, JETP Lett. **5**, 32 (1967).

[39] I. Affleck and M. Dine, Nucl.Phys. **B249**, 361 (1985).

[40] G. R. Farrar and M. Shaposhnikov, Phys.Rev.Lett. **70**, 2833 (1993), arXiv:hep-ph/9305274 [hep-ph].

[41] M. Fukugita and T. Yanagida, Phys.Lett. **B174**, 45 (1986).

[42] R. Crewther, P. Di Vecchia, G. Veneziano, and E. Witten, Phys.Lett. **B88**, 123 (1979).

[43] R. Peccei and H. R. Quinn, Phys.Rev.Lett. **38**, 1440 (1977).

[44] S. Antusch, M. Holthausen, M. A. Schmidt, and M. Spinrath, Nucl.Phys. **B877**, 752 (2013), arXiv:1307.0710 [hep-ph].

[45] S. Perlmutter *et al.* (Supernova Cosmology Project), Astrophys.J. **517**, 565 (1999), arXiv:astro-ph/9812133 [astro-ph].

[46] A. G. Riess *et al.* (Supernova Search Team), Astron.J. **116**, 1009 (1998), arXiv:astro-ph/9805201 [astro-ph].

[47] J. Frieman, M. Turner, and D. Huterer, Ann.Rev.Astron.Astrophys. **46**, 385 (2008), arXiv:0803.0982 [astro-ph].

[48] N. Arkani-Hamed, S. Dimopoulos, and G. R. Dvali, Phys. Lett. **B429**, 263 (1998), arXiv:hep-ph/9803315.

[49] L. Randall and R. Sundrum, Phys. Rev. Lett. **83**, 3370 (1999), arXiv:hep-ph/9905221.

[50] M. Lindner, Zeit. Phys. **C31**, 295 (1986).

[51] M. Lindner, M. Sher, and H. W. Zaglauer, Phys. Lett. **B228**, 139 (1989).

[52] M. Holthausen, K. S. Lim, and M. Lindner, JHEP **1202**, 037 (2012), arXiv:1112.2415 [hep-ph].

[53] G. Degrassi, S. Di Vita, J. Elias-Miro, J. R. Espinosa, G. F. Giudice, *et al.*, JHEP **1208**, 098 (2012), arXiv:1205.6497 [hep-ph].

[54] D. Buttazzo, G. Degrassi, P. P. Giardino, G. F. Giudice, F. Sala, *et al.*, JHEP **1312**, 089 (2013), arXiv:1307.3536.

[55] S. Alekhin, A. Djouadi, and S. Moch, Phys.Lett. **B716**, 214 (2012), arXiv:1207.0980 [hep-ph].

[56] G. F. Giudice(2008), arXiv:0801.2562 [hep-ph].

[57] D. Baumann and L. McAllister(2014), arXiv:1404.2601 [hep-th].

[58] G. 't Hooft, NATO Sci.Ser.B **59**, 135 (1980).

[59] P. Fayet and S. Ferrara, Phys.Rept. **32**, 249 (1977).

[60] L. Susskind, Phys.Rev. **D20**, 2619 (1979).

[61] S. Weinberg, Phys.Rev. **D13**, 974 (1976).

[62] W. A. Bardeen, C. T. Hill, and M. Lindner, Phys.Rev. **D41**, 1647 (1990).

[63] K. Agashe, R. Contino, and A. Pomarol, Nucl.Phys. **B719**, 165 (2005), arXiv:hep-ph/0412089 [hep-ph].

[64] M. Holthausen, K. S. Lim, and M. Lindner, JHEP **1202**, 037 (2012), arXiv:1112.2415 [hep-ph].

[65] W. A. Bardeen, FERMILAB-CONF-95-391-T, C95-08-27.3(1995).

[66] C. G. J. Callan, S. R. Coleman, and R. Jackiw, Ann. Phys. **59**, 42 (1970).

[67] A. Zamolodchikov, JETP Lett. **43**, 730 (1986).

[68] J. Polchinski, Nucl.Phys. **B303**, 226 (1988).

[69] Y. Nakayama(2013), arXiv:1302.0884 [hep-th].

[70] M. Shaposhnikov and D. Zenhausern, Phys. Lett. **B671**, 162 (2009), arXiv:0809.3406 [hep-th].

[71] J. C. Collins, A. Duncan, and S. D. Joglekar, Phys.Rev. **D16**, 438 (1977).

[72] H. Osborn, Nucl.Phys. **B363**, 486 (1991).

[73] J. M. Maldacena, Int.J.Theor.Phys. **38**, 1113 (1999), arXiv:hep-th/9711200 [hep-th].

[74] M. Shaposhnikov and C. Wetterich, Phys.Lett. **B683**, 196 (2010), arXiv:0912.0208 [hep-th].

[75] G. Marques Tavares, M. Schmaltz, and W. Skiba, Phys.Rev. **D89**, 015009 (2014), arXiv:1308.0025 [hep-ph].

[76] S. R. Coleman and E. J. Weinberg, Phys.Rev. **D7**, 1888 (1973).

[77] J. Fatelo, J. Gerard, T. Hambye, and J. Weyers, Phys.Rev.Lett. **74**, 492 (1995).

[78] R. Hempfling, Phys.Lett. **B379**, 153 (1996), arXiv:hep-ph/9604278 [hep-ph].

[79] K. A. Meissner and H. Nicolai, Phys.Lett. **B648**, 312 (2007), arXiv:hep-th/0612165 [hep-th].

[80] R. Foot, A. Kobakhidze, and R. R. Volkas, Phys. Lett. **B655**, 156 (2007), arXiv:0704.1165 [hep-ph].

[81] R. Foot, A. Kobakhidze, K. L. McDonald, and R. R. Volkas, Phys. Rev. **D77**, 035006 (2008), arXiv:0709.2750 [hep-ph].

[82] W.-F. Chang, J. N. Ng, and J. M. Wu, Phys.Rev. **D75**, 115016 (2007), arXiv:hep-ph/0701254 [HEP-PH].

[83] M. Holthausen, M. Lindner, and M. A. Schmidt, Phys.Rev. **D82**, 055002 (2010), arXiv:0911.0710 [hep-ph].

[84] S. Iso, N. Okada, and Y. Orikasa, Phys. Lett. **B676**, 81 (2009), arXiv:0902.4050 [hep-ph].

[85] S. Iso, N. Okada, and Y. Orikasa, Phys.Rev. **D80**, 115007 (2009), arXiv:0909.0128 [hep-ph].

[86] S. Iso and Y. Orikasa, PTEP **2013**, 023B08 (2013), arXiv:1210.2848 [hep-ph].

[87] V. V. Khoze, JHEP **1311**, 215 (2013), arXiv:1308.6338 [hep-ph].

[88] Y. Kawamura, PTEP **2013**, 113B04 (2013), arXiv:1308.5069 [hep-ph].

[89] C. Englert, J. Jaeckel, V. Khoze, and M. Spannowsky, JHEP **1304**, 060 (2013), arXiv:1301.4224 [hep-ph].

[90] A. Farzinnia, H.-J. He, and J. Ren, Phys.Lett. **B727**, 141 (2013), arXiv:1308.0295 [hep-ph].

[91] R. Dermisek, T. H. Jung, and H. D. Kim, Phys.Rev.Lett. **113**, 051801 (2014), arXiv:1308.0891 [hep-ph].

[92] C. D. Carone and R. Ramos, Phys.Rev. **D88**, 055020 (2013), arXiv:1307.8428 [hep-ph].

[93] S. Benic and B. Radovcic, Phys.Lett. **B732**, 91 (2014), arXiv:1401.8183 [hep-ph].

[94] C. T. Hill, Phys.Rev. **D89**, 073003 (2014), arXiv:1401.4185 [hep-ph].

[95] T. Hambye and M. H. Tytgat, Phys.Lett. **B659**, 651 (2008), arXiv:0707.0633 [hep-ph].

[96] T. Hur, D.-W. Jung, P. Ko, and J. Y. Lee, Phys.Lett. **B696**, 262 (2011), arXiv:0709.1218 [hep-ph].

[97] T. Hur and P. Ko, Phys.Rev.Lett. **106**, 141802 (2011), arXiv:1103.2571 [hep-ph].

[98] M. Heikinheimo, A. Racioppi, M. Raidal, C. Spethmann, and K. Tuominen(2013), arXiv:1304.7006 [hep-ph].

[99] T. Hambye and A. Strumia, Phys.Rev. **D88**, 055022 (2013), arXiv:1306.2329 [hep-ph].

[100] M. Holthausen, J. Kubo, K. S. Lim, and M. Lindner, JHEP **1312**, 076 (2013), arXiv:1310.4423 [hep-ph].

[101] J. Kubo, K. S. Lim, and M. Lindner(2014), arXiv:1405.1052 [hep-ph].

[102] J. Kubo, K. S. Lim, and M. Lindner(2014), arXiv:1403.4262 [hep-ph].

[103] V. Miransky, Nuovo Cim. **A90**, 149 (1985).

[104] R. Alkofer and L. von Smekal, Phys.Rept. **353**, 281 (2001), arXiv:hep-ph/0007355 [hep-ph].

[105] V. Gribov, Eur.Phys.J. **C10**, 91 (1999), arXiv:hep-ph/9902279 [hep-ph].

[106] W. J. Marciano, Phys.Rev. **D21**, 2425 (1980).

[107] D. Lust, E. Papantonopoulos, K. Streng, and G. Zoupanos, Nucl.Phys. **B268**, 49 (1986).

[108] R. Slansky, Phys.Rept. **79**, 1 (1981).

[109] R. Feger and T. W. Kephart(2012), arXiv:1206.6379 [math-ph].

[110] T. Cheng, E. Eichten, and L.-F. Li, Phys.Rev. **D9**, 2259 (1974).

[111] T. Kunihiro and T. Hatsuda, Prog.Theor.Phys. **71**, 1332 (1984).

[112] Tech. Rep. ATLAS-CONF-2014-009 (CERN, Geneva, 2014).

[113] Tech. Rep. CMS-PAS-HIG-14-009 (CERN, Geneva, 2014).

[114] R. Bonciani, G. Degrassi, and A. Vicini, JHEP **0711**, 095 (2007), arXiv:0709.4227 [hep-ph].

[115] A. Djouadi, J. Kalinowski, and M. Spira, Comput.Phys.Commun. **108**, 56 (1998), arXiv:hep-ph/9704448 [hep-ph].

[116] M. Spira(1995), arXiv:hep-ph/9510347 [hep-ph].

[117] C. Anastasiou, S. Buehler, F. Herzog, and A. Lazopoulos, JHEP **1112**, 058 (2011), arXiv:1107.0683 [hep-ph].

[118] A. Martin, W. Stirling, R. Thorne, and G. Watt, Eur.Phys.J. **C63**, 189 (2009), arXiv:0901.0002 [hep-ph].

[119] M. Whalley, D. Bourilkov, and R. Group(2005), arXiv:hep-ph/0508110 [hep-ph].

[120] M. Carena, I. Low, and C. E. Wagner, JHEP **1208**, 060 (2012), arXiv:1206.1082 [hep-ph].

[121] M. Martynov and A. Smirnov, Mod.Phys.Lett. **A23**, 2907 (2008), arXiv:0807.4486 [hep-ph].

[122] T. Plehn and T. M. Tait, J.Phys. **G36**, 075001 (2009), arXiv:0810.3919 [hep-ph].

[123] Y. Bai and B. A. Dobrescu, JHEP **1107**, 100 (2011), arXiv:1012.5814 [hep-ph].

[124] A. Idilbi, C. Kim, and T. Mehen, Phys.Rev. **D82**, 075017 (2010), arXiv:1007.0865 [hep-ph].

[125] D. Goncalves-Netto, D. Lopez-Val, K. Mawatari, T. Plehn, and I. Wigmore, Phys.Rev. **D85**, 114024 (2012), arXiv:1203.6358 [hep-ph].

[126] G. Aad *et al.* (ATLAS Collaboration), Eur.Phys.J. **C73**, 2263 (2013), arXiv:1210.4826 [hep-ex].

[127] A. V. Manohar and M. B. Wise, Phys.Lett. **B636**, 107 (2006), arXiv:hep-ph/0601212 [hep-ph].

[128] A. G. Cohen and H. Georgi, Nucl.Phys. **B314**, 7 (1989).

[129] C. N. Leung, S. Love, and W. A. Bardeen, Nucl.Phys. **B323**, 493 (1989).

[130] L. Fister, R. Alkofer, and K. Schwenzer, Phys.Lett. **B688**, 237 (2010), arXiv:1003.1668 [hep-th].

[131] C. Wetterich, Phys.Lett. **B301**, 90 (1993).

[132] Y. Nambu and G. Jona-Lasinio, Phys.Rev. **124**, 246 (1961).

[133] M. Kobayashi, H. Kondo, and T. Maskawa, Prog.Theor.Phys. **45**, 1955 (1971).

[134] M. Kobayashi and T. Maskawa, Prog.Theor.Phys. **44**, 1422 (1970).

[135] G. 't Hooft, Phys.Rev.Lett. **37**, 8 (1976).

[136] T. Kunihiro and T. Hatsuda, Phys.Lett. **B206**, 385 (1988).

[137] T. Hatsuda and T. Kunihiro, Phys.Rept. **247**, 221 (1994), arXiv:hep-ph/9401310 [hep-ph].

[138] U. Vogl and W. Weise, Prog.Part.Nucl.Phys. **27**, 195 (1991).

[139] S. Klevansky, Rev.Mod.Phys. **64**, 649 (1992).

[140] G. Passarino and M. Veltman, Nucl.Phys. **B160**, 151 (1979).

[141] K. Griest and M. Kamionkowski, Phys.Rev.Lett. **64**, 615 (1990).

[142] M. R. Buckley and E. T. Neil, Phys.Rev. **D87**, 043510 (2013), arXiv:1209.6054 [hep-ph].

[143] K. Griest, Phys.Rev. **D38**, 2357 (1988).

[144] L. Baudis, Phys.Dark Univ. **1**, 94 (2012), arXiv:1211.7222 [astro-ph.IM].

[145] R. Barbieri, L. J. Hall, and V. S. Rychkov, Phys.Rev. **D74**, 015007 (2006), arXiv:hep-ph/0603188 [hep-ph].

[146] J. R. Ellis, A. Ferstl, and K. A. Olive, Phys.Lett. **B481**, 304 (2000), arXiv:hep-ph/0001005 [hep-ph].

[147] E. Aprile *et al.* (XENON100 Collaboration), Phys.Rev.Lett. **109**, 181301 (2012), arXiv:1207.5988 [astro-ph.CO].

[148] D. Akerib *et al.* (LUX Collaboration), Phys.Rev.Lett. **112**, 091303 (2014), arXiv:1310.8214 [astro-ph.CO].

[149] E. Aprile (XENON1T collaboration)(2012), arXiv:1206.6288 [astro-ph.IM].

[150] D. McKinsey and R. Gaitskell, "First science results from the lux dark matter experiment," http://lux.brown.edu/talks/20131030_LUX_First_Results.pdf.

[151] M. Gustafsson (collaboration for the Fermi-LAT)(2013), arXiv:1310.2953 [astro-ph.HE].

[152] M. Ackermann *et al.* (LAT Collaboration), Phys.Rev. **D86**, 022002 (2012), arXiv:1205.2739 [astro-ph.HE].

[153] G. Bertone, C. Jackson, G. Shaughnessy, T. M. Tait, and A. Vallinotto, Phys.Rev. **D80**, 023512 (2009), arXiv:0904.1442 [astro-ph.HE].

[154] R. Laha, K. C. Y. Ng, B. Dasgupta, and S. Horiuchi, Phys.Rev. **D87**, 043516 (2013), arXiv:1208.5488 [astro-ph.CO].

[155] D. Kirzhnits and A. D. Linde, Phys.Lett. **B42**, 471 (1972).

[156] V. Kuzmin, V. Rubakov, and M. Shaposhnikov, Phys.Lett. **B155**, 36 (1985).

[157] F. R. Klinkhamer and N. Manton, Phys.Rev. **D30**, 2212 (1984).

[158] P. B. Arnold and L. D. McLerran, Phys.Rev. **D36**, 581 (1987).

[159] M. Shaposhnikov, JETP Lett. **44**, 465 (1986).

[160] G. W. Anderson and L. J. Hall, Phys.Rev. **D45**, 2685 (1992).

[161] M. Carrington, Phys.Rev. **D45**, 2933 (1992).

[162] M. Dine, P. Huet, and J. Singleton, Robert L., Nucl.Phys. **B375**, 625 (1992).

[163] M. Dine, R. G. Leigh, P. Y. Huet, A. D. Linde, and D. A. Linde, Phys.Rev. **D46**, 550 (1992), arXiv:hep-ph/9203203 [hep-ph].

[164] A. Ahriche, Phys.Rev. **D75**, 083522 (2007), arXiv:hep-ph/0701192 [hep-ph].

[165] The GAP Group, *GAP – Groups, Algorithms, and Programming, Version 4.4.12* (2008), `http://www.gap-system.org`.

[166] V. Dabbaghian, *REPSN - for constructing representations of finite groups, GAP package, Version 3.0.2*, The GAP Group (2011), `http://www.gap-system.org/Packages/repsn.html`.

[167] H.U.Besche, B.Eick, and E.O'Brien, *SmallGroups - library of all 'small' groups, GAP package, Version included in GAP 4.4.12*, The GAP Group (2002), `http://www.gap-system.org/Packages/sgl.html`.

[168] E. Aichinger, F. Binder, J. Ecker, P. Mayr, and C. Nöbauer, *SONATA - system of near-rings and their applications, GAP package, Version 2* (2003), `http://www.algebra.uni-linz.ac.at/Sonata/`.

[169] M. Holthausen, K. S. Lim, and M. Lindner, Phys.Lett. **B721**, 61 (2013), arXiv:1212.2411 [hep-ph].

[170] M. Holthausen and K. S. Lim, Phys.Rev. **D88**, 033018 (2013), arXiv:1306.4356 [hep-ph].

[171] D. Forero, M. Tortola, and J. Valle, Phys.Rev. **D86**, 073012 (2012), arXiv:1205.4018 [hep-ph].

[172] G. Fogli, E. Lisi, A. Marrone, D. Montanino, A. Palazzo, *et al.*, Phys.Rev. **D86**, 013012 (2012), arXiv:1205.5254 [hep-ph].

[173] M. Gonzalez-Garcia, M. Maltoni, J. Salvado, and T. Schwetz, JHEP **1212**, 123 (2012), arXiv:1209.3023 [hep-ph].

[174] Y. Fukuda *et al.* (Super-Kamiokande Collaboration), Phys.Rev.Lett. **81**, 1562 (1998), arXiv:hep-ex/9807003 [hep-ex].

[175] C. S. Lam, Physics Letters B **656**, 193 (Nov. 2007), arXiv:0708.3665 [hep-ph].

[176] C. Lam, Phys.Rev.Lett. **101**, 121602 (2008), arXiv:0804.2622 [hep-ph].

[177] C. S. Lam, Phys. Rev. **D78**, 073015 (2008), 0809.1185 [hep-ph].

[178] P. F. Harrison, D. H. Perkins, and W. G. Scott, Phys. Lett. **B530**, 167 (2002), hep-ph/0202074.

[179] P. F. Harrison and W. G. Scott, Phys. Lett. **B535**, 163 (2002), hep-ph/0203209.

[180] L. Hall, H. Murayama, and N. Weiner, Physical Review Letters **84**, 2572 (Mar. 2000), arXiv:hep-ph/9911341.

[181] A. de Gouvêa and H. Murayama, Physics Letters B **573**, 94 (Oct. 2003), arXiv:hep-ph/0301050.

[182] A. de Gouvea and H. Murayama, ArXiv e-prints(Apr. 2012), arXiv:1204.1249 [hep-ph].

[183] K. Babu arXiv:0910.2948 [hep-ph].

[184] C. Froggatt and H. B. Nielsen, Nucl.Phys. **B147**, 277 (1979).

[185] R. Barbieri, L. J. Hall, S. Raby, and A. Romanino, Nucl.Phys. **B493**, 3 (1997), arXiv:hep-ph/9610449 [hep-ph].

[186] S. King, JHEP **0508**, 105 (2005), arXiv:hep-ph/0506297 [hep-ph].

[187] S. King and G. G. Ross, Phys.Lett. **B520**, 243 (2001), arXiv:hep-ph/0108112 [hep-ph].

[188] G. Altarelli and F. Feruglio, Reviews of Modern Physics **82**, 2701 (Jul. 2010), arXiv:1002.0211 [hep-ph].

[189] H. Ishimori, T. Kobayashi, H. Ohki, Y. Shimizu, H. Okada, and M. Tanimoto, Progress of Theoretical Physics Supplement **183**, 1 (2010), arXiv:1003.3552 [hep-th].

[190] W. Grimus and P. O. Ludl, Journal of Physics A Mathematical General **45**, 233001 (Jun. 2012), arXiv:1110.6376 [hep-ph].

[191] R. d. A. Toorop, F. Feruglio, and C. Hagedorn, Phys.Lett. **B703**, 447 (2011), 1107.3486 [hep-ph].

[192] R. de Adelhart Toorop, F. Feruglio, and C. Hagedorn, Nuclear Physics B **858**, 437 (May 2012), arXiv:1112.1340 [hep-ph].

[193] C. Lam, Phys.Rev. **D87**, 013001 (2013), arXiv:1208.5527 [hep-ph].

[194] P. Ramond, *Group Theory: A Physicist's Survey*, 1st ed. (Cambridge University Press, 2010) ISBN 0521896037, http://www.worldcat.org/isbn/0521896037.

[195] W. Grimus and L. Lavoura, JHEP **9**, 106 (2008), 0809.0226 [hep-ph].

[196] C. H. Albright and W. Rodejohann, Eur.Phys.J. **C62**, 599 (2009), arXiv:0812.0436 [hep-ph].

[197] S.-F. Ge, D. A. Dicus, and W. W. Repko, Phys.Rev.Lett. **108**, 041801 (2012), arXiv:1108.0964 [hep-ph].

[198] S.-F. Ge, D. A. Dicus, and W. W. Repko, Phys.Lett. **B702**, 220 (2011), arXiv:1104.0602 [hep-ph].

[199] D. Hernandez and A. Y. Smirnov, Phys.Rev. **D86**, 053014 (2012), arXiv:1204.0445 [hep-ph].

[200] F. Feruglio, C. Hagedorn, and R. Ziegler(2012), arXiv:1211.5560 [hep-ph].

[201] S. F. King and C. Luhn, Rept.Prog.Phys. **76**, 056201 (2013), arXiv:1301.1340 [hep-ph].

[202] I. K. Cooper, S. F. King, and C. Luhn, JHEP **1206**, 130 (2012), arXiv:1203.1324 [hep-ph].

[203] S. F. King and C. Luhn, JHEP **1109**, 042 (2011), arXiv:1107.5332 [hep-ph].

[204] S. Antusch, S. F. King, C. Luhn, and M. Spinrath, Nucl.Phys. **B856**, 328 (2012), arXiv:1108.4278 [hep-ph].

[205] J. A. Escobar and C. Luhn, Journal of Mathematical Physics **50**, 013524 (2009), arXiv:0809.0639 [hep-th].

[206] S. F. King, T. Neder, and A. J. Stuart, Phys.Lett. **B726**, 312 (2013), arXiv:1305.3200 [hep-ph].

[207] A. Blum and C. Hagedorn, Nucl.Phys. **B821**, 327 (2009), arXiv:0902.4885 [hep-ph].

[208] C. Lam, Phys.Rev. **D87**, 053012 (2013), arXiv:1301.1736 [hep-ph].

[209] K. Abe *et al.* (T2K Collaboration), Phys.Rev.Lett. **112**, 061802 (2014), arXiv:1311.4750 [hep-ex].

[210] K. Abe *et al.* (T2K Collaboration), Phys.Rev.Lett. **112**, 181801 (2014), arXiv:1403.1532 [hep-ex].

[211] M. Hirsch, ArXiv High Energy Physics - Phenomenology e-prints(Feb. 2001), arXiv:hep-ph/0102102.

[212] J. R. Espinosa, ArXiv High Energy Physics - Phenomenology e-prints(Jun. 2003), arXiv:hep-ph/0306019.

[213] M. Holthausen and M. A. Schmidt, JHEP **1201**, 126 (2012), arXiv:1111.1730 [hep-ph].

[214] C. Luhn, K. M. Parattu, and A. Wingerter, JHEP **1212**, 096 (2012), arXiv:1210.1197 [hep-ph].

[215] M.-C. Chen, M. Fallbacher, Y. Omura, M. Ratz, and C. Staudt, Nucl.Phys. **B873**, 343 (2013), arXiv:1302.5576 [hep-ph].

[216] S. F. King and T. Neder(2014), arXiv:1403.1758 [hep-ph].

[217] R. Mertig, M. Bohm, and A. Denner, Comput.Phys.Commun. **64**, 345 (1991).

Letting go,
is the biggest accomplishment...